CHALMERS
UNIVERSITY OF TECHNOLOGY

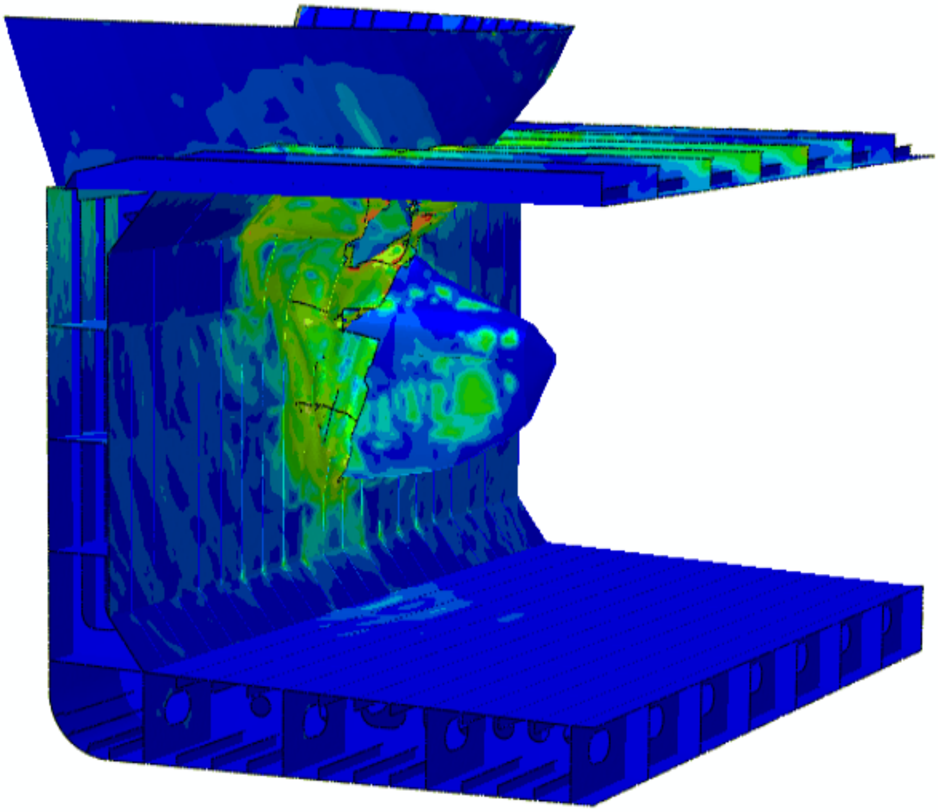

Residual strength assessment of corroded ships involved in ship-to-ship collisions

Master's thesis in the International Master´s Programme Naval Architecture and Ocean Engineering

DIMITRIOS BAXEVANIS

Department of Mechanics and Maritime Sciences
CHALMERS UNIVERSITY OF TECHNOLOGY
Gothenburg, Sweden 2019
Master's Thesis 2019/85

MASTER’S THESIS IN THE INTERNATIONAL MASTER’S PROGRAMME IN NAVAL ARCHITECTURE AND OCEAN ENGINEERING

Residual strength assessment of corroded ships involved in ship-to-ship collisions

DIMITRIOS BAXEVANIS

Department of Mechanics and Maritime Sciences

Division of Marine Technology

CHALMERS UNIVERSITY OF TECHNOLOGY

Göteborg, Sweden 2019

Residual strength assessment of corroded ships involved in ship-to-ship collisions
DIMITRIOS BAXEVANIS

Master's Thesis 2019/85
Department of Mechanics and Maritime Sciences
Division of Marine Technology
Chalmers University of Technology
SE - 412 96 Göteborg
Sweden
Telephone: + 46 (0)31-772 1000

Cover: Ship-ship collision simulation conducted in Abaqus

Printed by Chalmers Reproservice

Göteborg, Sweden 2019

Residual strength assessment of corroded ships involved in ship-to-ship collisions
Master's Thesis in the International Master's Program in Naval Architecture and Ocean Engineering
DIMITRIOS BAXEVANIS
Department of Mechanics and Maritime Sciences
Division of Marine Technology
Chalmers University of Technology

Abstract

Ships and marine structures are forced to operate in a very complex environment with corrosion to be regarded as one of its main features. Another crucial aspect of shipping operation is the ship collisions. The possibility of an accidental collision can't be ignored due to the increase of traffic density. The objective of the present study is to estimate the ultimate strength of damaged ships considering the effects of material degradation due to corrosion. A review of the corrosion models, which can be used for the prediction of the thickness reduction of the hull, is included. The structural damage of non-corroded and corroded ships involved in ship collisions are calculated by nonlinear FEA. The Smith-Fujikubo method is applied for the residual strength assessment of the damaged ship under biaxial loading conditions. The largest reduction of the ultimate strength is observed when the most severe structural damage appears in a corroded hull showing a correlation between residual strength and corrosion presence. The most significant ultimate strength decrease is found in loading directions, which do not correspond to hogging and sagging conditions concluding the importace of the biaxial loading in the residual strength assessment.

Keywords: Biaxial loading, corrosion, corrosion models, material degradation, residual strength, ship collisions, ultimate strength.

Table of Contents

Preface

The current thesis is part of the requirements for the master's degree at Chalmers University of Technology, Göteborg, and has been carried out at the Division of Marine Technology, Department of Mechanics and Maritime Sciences, Chalmers University of Technology between January and June of 2019.

I would like to thank my supervisor and examiner Professor Jonas Ringsberg at the Department of Mechanics and Maritime Sciences, Chalmers University of Technology for his knowledge, comments and overall contribution to the completion of this work. I would also like to thank my supervisor Zhiyuan Li at Department of Mechanics and Maritime Sciences, Chalmers University of Technology for his support in the Thesis.

Special thanks to Artjoms Kuznecovs at Department of Mechanics and Maritime Sciences, Chalmers University of Technology for his guidance and assistance in the preparation of the simulations and analysis of the results.

Göteborg, June 2019

Dimitrios Baxevanis

Abbreviations

CPS	Corrosion Protection System
CSR-H	Harmonized Common Structural Rules
DE	Damage Evolution
DI	Damage Initiation
DNV GL	Det Norske Veritas Germanischer Lloyd
DOP	Degree of Pitting
FEA	Finite Element Analysis
GBS	Goal Based Standards
IACS	International Association of Classification Societies
IMO	International Maritime Organization
ISSC	International Ship Security Certificate
ISUM	Idealized Structural Unit Method
PSM	Primary Supporting Member
LOA	Length Overall
MSC	Maritime Safety Committee
RoPax	Roll-on/roll-off passenger vessel is a RORO vessel built for freight vehicle transport along with passenger accommodation
SDG	Sustainable Development Goals
SRB	Sulphate Reducing Bacteria
ULS	Ultimate Limit State
UN	United Nations

Notations

α	Inverse of the mean of the time T_r [years^{-1}], Corrosion control parameter [-], Shape parameter [-], Corrosion rate constant [-]
β	Model parameter [-], Shape parameter [-], Corrosion depth constant [-]
γ_M	Partial safety factor [-]
γ_S	Partial safety factor [-]
γ_W	Partial safety factor [-]
δ	Diffusion layer thickness [mm]
$\dot{\varepsilon}$	Material strain rate [-]
ε_f	Fracture strain [-]
ε_n	Necking strain [-]
ε_{true}	True strain [-]
$\varepsilon(t, E)$	Zero mean uncertainty function
η	Model parameter [-], Scale parameter [-]
λ	Scale parameter [-]
μ	Mean value, Moisture availability coefficient [-]
ν	Poisson's ratio [-]
σ	Standard deviation, Axial stress [N/m^2]
σ_b	Maximum value of the bending stress [N/m^2]
$\sigma_{y,d}$	Dynamic yield stress [MPa]
$\sigma_{y,s}$	Yield stress [MPa]
σ_{true}	True stress [MPa]
τ	Time interval after the appearance of progressive pitting points [years]
τ_c	Life of coating [years]
τ_t	Transition time [years]
A	Cross-sectional area [m^2], Power law model empirical constant [-]
B	Power law model empirical constant [-]
b	Corrosion control parameter [-]
$b(t, E)$	Bias function
C	Cowper-Symonds constant [-], Oxygen concentration [mg/L]
c_a	Melcher model parameter for general corrosion [mm]
c_{ap}	Melcher model parameter for pitting corrosion [mm]
C_i	Oxygen concentration in the boundary between the surface of the material and the layer of corrosion [mg/L]
C_0	Oxygen concentration in the seawater volume away from the area of corrosion activity [mg/L]
c_s	Melcher model parameter for general corrosion [mm]
c_{sp}	Melcher model parameter for pitting corrosion [mm]
$c(t)$	Material loss as a function of time for uniform corrosion
$c(t, E)$	Function of material loss due to corrosion activity
C_1	Corrosion rate coefficient [-]
C_2	Corrosion pattern coefficient [-]
d_o	Initial plate thickness [mm]
d_∞	Long-term corrosion wastage [mm]
$d(t)$	Corrosion wastage thickness [mm]

$\dot{d(t)}$	Corrosion rate [mm/year]
$d(t_j)$	Model estimated wear [mm/year]
$d_p(t)$	Maximum value of the pit depth as a function of time
D	Degree of corrosion [%], Oxygen diffusion coefficient [-]
D_{cp}	Oxidized steel diffusion coefficient [-]
D_i	Tangential axial stiffness of i-th element [-]
$D_i(t_j)$	Measured corrosion wastage of a plate [mm/year]
E	Young's modulus [GPa], Mean value, Vector of environmental and material factors
F	Faraday constant [-]
$fn(t, E)$	Mean value function
h	Plate thickness [mm]
i	Corrosion current [A]
K	Hardening coefficient [MPa]
k	Corrosion rate [mm/years], Coefficient [-]
L	Pit diameter [mm]
M_S	Maximum still water vertical bending moment [Nm]
M_{u}	Ultimate bending moment [Nm]
M_W	Wave action vertical bending moment [Nm]
n	Hardening exponent [-], Number of electrons [-]
P	Cowper-Symonds constant [-], Perimeter of exposed area to corrosive medium [m]
r_a	Melcher model parameter for general corrosion [mm/year]
r_{ap}	Melcher model parameter for pitting corrosion [mm/year]
r_o	Melcher model parameter for general corrosion [mm/year]
r_s	Melcher model parameter for general corrosion [mm/year]
r_{sp}	Melcher model parameter for pitting corrosion [mm/year]
$R(t)$	Structural strength as a function of time
S	Standard deviation
t	Initial plate thickness [mm]
t_a	Melcher model parameter for general and pitting corrosion [years]
$t_{as\ built}$	Actual thickness [m]
t_c	Corrosion addition [m]
t_k	Plate thickness [m]
t_{off}	Net thickness [m]
t_r	Plate thickness reduction [mm]
t_{res}	Reserved thickness [m]
t_t	Anaerobic corrosion transition time [years]
$t_{vol\ add}$	Voluntary addition thickness [m]
t_*	Exposure time [years]
T	Age of ship [years]
T_A	Time point of maximum corrosion rate [years]
T_c	Coating's life [years]
T_{cl}	General corrosion initiation time [years]
T_L	Lifespan of structure [years]
T_t	Transition time [years]

T_r	Time interval between active and progressive pitting points [years]
T_{st}	Pitting corrosion initiation time [years]
T_o	Life of protective layer [years]
Z	Hull's section modulus [m^3]
z	Pitting depth [mm]
z_p	Thickness reduction [mm]

1 Introduction

This section deals with the global importance of shipping operations while focusing on subjects that will be further discussed in the current study such as the possibility of accidental collisions between ships, the corrosion influence in the structural degradation of marine structures, the ultimate strength assessment of a ship and the existing regulatory framework. A description of the objectives is followed with the possible limitations and assumptions that strengthen the feasibility of the study while the chosen methodology is presented completing this section.

1.1 Background and motivation of study

Maritime shipping constitutes one of the most important pillars of global economy with constant presence during the evolution of civilization. The use of ships for the transportation of goods has an essential contribution in the international trade since over 80 per cent by weight and 70 per cent by value of them are transferred by sea (Lister, 2015). These figures clarify the contribution of shipping in the financial growth and the preservation of the modern way of living. The Sustainable Development Goals (SDGs) constitute a global effort that aims to the protection of the planet, the promotion of dignity as an unquestionable feature of human lives, the economic growth and the constant pursuit of peace and prosperity. Their introduction is attributed to the United Nations with the intention to serve as guidance for governments to integrate these goals in to their national policies. Non-state actors such as business are not excluded but also encouraged to adjust their activities towards the achievement of the SDGs. The importance of shipping in the world's economy ensures its role in fulfilling the framework of targets set by the United Nations (UN, 2016).

The proper function of the shipping operations is ensured by the implementation of a series of mandatory regulations with the objective to strengthen the maritime sector's safety and quality framework (Karakasnaki et al., 2018). However, safety in sea transportation can't be regarded as an absolute notion since the risk of accidents is always present (Uğurlu et al., 2015). Incidents such as collisions are not unusual especially when statistical analysis has shown a small increase of events involving collision between ships in the last decade (Hogström and Ringsberg 2013). Although there is no clear explanation for this trend, the causes can be considered as a combination of factors such as the higher traffic density because of the large number of ships at sea together with the constant effort for bigger profit leading to tighter schedules of the operations (Hogström and Ringsberg, 2013). The significance of safety in the maritime activities is promoted by the International Maritime Organization (IMO) the decisions of which combined with the active participation of the shipbuilding industry has led to a different approach of how ship's safety should be regarded. According to this new way of thinking, accidents were no longer the starting point for the decision-making process relating safety issues with probabilistic assessment methods and goal-based standards (GBS) (Boulougouris and Papanikolaou 2013).The introduction of the Common Structural Rules (CSR) by the International Association of Classification Societies (IACS) was also motivated by the change in the safety standards. The GBS has been arranged in five Tiers according to Figure 1.1 starting with the specification of the goals concerning the design and building of new vessels, followed by Tier II with the definition of the requirements that are needed for these goals to be fulfilled. Lastly, Tier III is used to verify Tier IV based on the existing regulations provided by IMO and classification societies (ISSC, 2015).

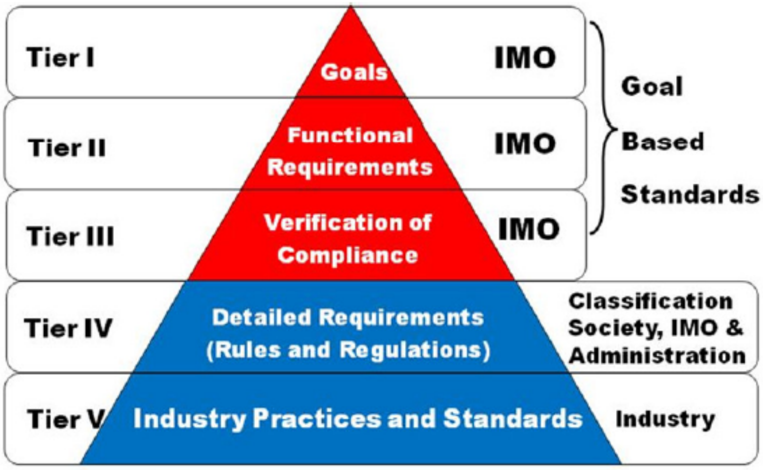

Figure 1.1 Goal Based Standards arrangement (Peng, 2011)

The assessment of a ship's strength includes the consideration of the longitudinal, transverse and local strength. The safety of the vessel depends on the longitudinal term, which defines the hull girder strength (Yao, 2003). Forces that are generated by the cargo, buoyancy, wave loads, and the weight of the ship's structure are acting on the hull girder resulting in a combination of shear force, bending and torsional moment exerting on its cross section. The ability of the hull girder to withstand the numerous loads is of fundamental importance and a crucial design parameter, which can affect the expected service life (ISSC, 2015). The significance of hull girder strength is acknowledged by IACS with the adoption of the hull girder section modulus as a measure of its strength. According to the regulation framework established by IACS, 90 per cent of the section modulus as it is defined for a newbuilt vessel should be maintained during the lifespan of a ship. IMO has also implemented this requirement for tankers and bulk carriers with Resolutions MSC.105(73) and MSC.145(77) (Wang et al., 2008a).

Corrosion is considered the most crucial degrading process with serious implications regarding safety and efficiency of any vessel operating in marine environment. The gradual material loss will eventually undermine the load capacity of the structure and can promote the propagation of fatigue cracks resulting in uncontrolled failure with losses both in human lives and financial expenses (Yang et al., 2016). Examples where structural degradation due to corrosion was the main cause of failure can be seen in the accidents of Erika in 1999 and Prestige in 2002, see Figures 1.2 and 1.3. The former resulted in 20000 tons of oil being spilled and the pollution of 400 Km of Brittany's coastal area while destroying the marine life and affecting the local tourism economy. In the case of Prestige more than 35000 tons of HFO were spilled while equal amount remained in the ship's tanks creating environmental issues in several kilometers of coast between Spain and France (Tscheliesnig, 2006). These possible consequences forced regulatory agencies to a more active involvement to the design, operation and maintenance of ships and other structures affected by marine corrosion. Classification societies under the supervision of IACS perform periodic surveys in vessels to establish that the existing rules are followed, and the maintenance is kept in an acceptable level. In addition, IMO through its international presence promotes the constant safety upgrade on a global scale. The possible reduction of the plating thickness is controlled by adopting a corrosion addition to the ship scantlings during the design phase. The level of the addition varies with the type of the ship and the location in the hull since corrosion wastage can be influenced by the different conditions defined by the vessel's operational profile. The amount of material that is allowed to be lost due to corrosion is regulated by classification societies along with the suitable repair solutions. The net scantling approach has been adopted by IACS to deal with the strength degradation caused by corrosion and uses the net thickness for the local strength assessment while half of the corrosion addition is deducted for the calculation of the hull girder ultimate strength (Wang et al., 2014).

Figure 1.2 Accident of Prestige (Incaz and Özdemir, 2018)

Figure 1.3 Accident of Erika (Tscheliesnig, 2006)

1.2 Objectives and goals

The operational environment of marine structures will lead to the generation of corrosion regardless of any protective measure. The implications of this fact affect the hull girder strength through the gradual reduction of its cross section and limits the ship's service life. Furthermore, the existing regulations as they are described in the Common Structural Rules (IACS, 2019) are focusing on the thickness reduction due to uniform corrosion disregarding any change of the material features. Research in ship collisions seems to adopt this approach for reasons of simplicity or because of the limited knowledge regarding the impact of corrosion in the constitutive material properties. The current thesis serves as a continuation of a previous thesis of Kuznecovs and Shafieisabet (2017) in which the material loss due to corrosion and the change of its properties were regarded in cases of ship collisions involving a RoPax and a tanker. The results were used to examine the contribution of corrosion in the ship's ultimate strength. The objective of the present work is to investigate the residual strength of both corroded and non-corroded ships in a series of collision simulations by varying the point of impact between the struck and striking ship. In addition, the following topics will also be included:

- Research of existing corrosion models that are suitable for marine applications.
- Recommendation of a practical approach of modelling corrosion.
- Calculation of the hull girder strength for intact and damage conditions under biaxial loading.

1.3 Limitations and assumptions

The process of producing useful results in a study includes certain assumptions and simplifications that might narrow the range of applications of the conclusions, but they are considered necessary to overcome certain matters whose limited knowledge can cause problems and introduce uncertainties. To begin with, the collision simulations involve two coastal oil tankers as a striking and struck ship and their design data were used as a starting point for calculations such as the corrosion margin of the various structural members of the hull. As a result, safe predictions about other type of vessels with different arrangements can't be made using the conclusions of this study.

The thickness reduction caused by corrosion activity is based on the model developed by Paik et al (2003) with the assumptions that there is no transition time after the loss of coating effectiveness and the ship is expected to exceed the 25 years of service with a coating life of 7.5 years. The outcome is a linear relationship between corrosion wastage and time leading in this way to a constant annual corrosion rate (Paik et al., 2003a).

The change of material properties due to corrosion uses the experimental results from the work of Garbatov et al. (2014). However, the constructed stress strain curves provide little information about the necking strain or the post-necking behavior of the material. Therefore, it is assumed that failure will occur after the material has reached a certain value of strain and the plastic hardening follows a linear relation.

During the ship collision simulation, the struck ship is regarded as fixed, and any motion is prevented. The influence from any external dynamic mechanism is not considered while the focus is given on the structure's response during the collision. The variation of parameters such as the angle of collision and the speed of the striking ship would have resulted in many simulated cases. For practical reasons only right-angle collisions were chosen maintaining the speed at 5 knots. The location of the impact point is altered corresponding in three different draft values.

The residual strength assessment of the damaged ship is based on the Smith-Fujikubo method as it is described in the work of Fujikubo et al.- (2013), which considers loading in both vertical and horizontal directions. Finite Element Analysis was not included in the process of the residual strength estimation. The parameters that are considered for the residual strength evaluations are limited in the location and size of the damage opening. Any possible influence from plastic deformations of structural members are excluded. The damage progression and the effect of strain hardening is not regarded in the calculation process with any residual stress to be treated in a similar manner.

1.4 Methodology and outline of the study

The description of the methodology starts with the choice of the collision scenarios based on parameters such as ship type, degree of corrosion, collision angle and point of impact. The geometry of the chosen vessels is modelled by considering the scantlings and the corrosion margin. The influence of corrosion activity, which appears with the thickness reduction, is expressed by the selected corrosion model. Once the loss of thickness has been determined, the change in the material properties due to corrosion is provided by the constitutive material models. Both above models are combined in a finite element analysis to simulate the selected ship collisions with the use of the software ABAQUS (Dassault Systèmes, 2014). The results from the FE simulations such as the shape, size and location of the opening of the damaged ship together with the geometry model and the simplified constitutive model, which represents elastic-perfectly plastic models, are combined in a MATLAB script for the calculation of the ultimate and residual strength based on the Smith-Fujikubo method (Fujikubo et al., 2013). The representation of the procedure can be observed in Figure 1.4.

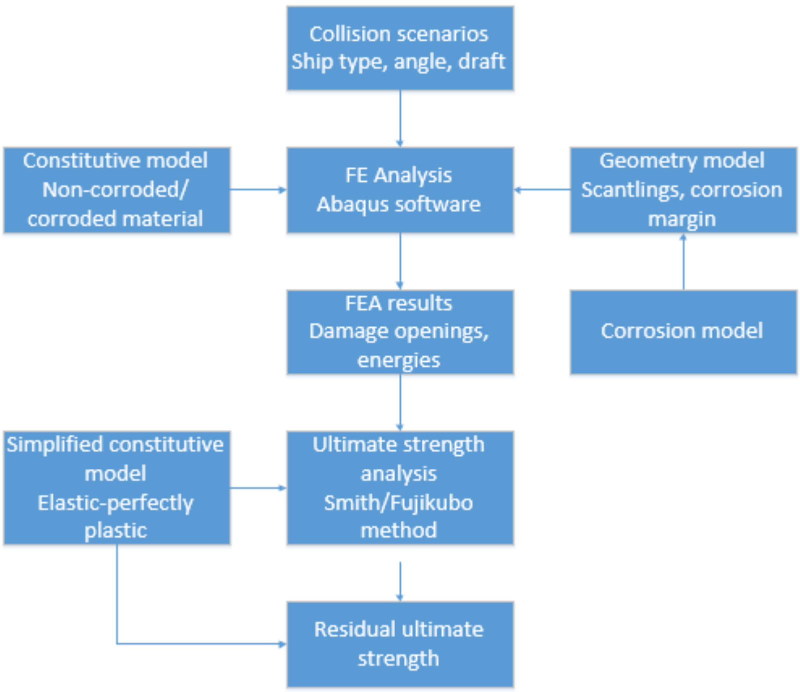

Figure 1.4: Methodology flowchart

The structure of the thesis consists of a literature study with focus on existing corrosion models followed by a description of ship collision simulations and the assessment of the hull girder ultimate strength. The selection of the corrosion model that satisfies the needs of the current study leads to the case study where the procedure of the finite element simulations is presented. The results of the simulations and the calculation of the residual ultimate strength are discussed, and specific conclusions are reached.

2 Literature study

The effect of corrosion in marine structures, how and where it usually appears in a ship's hull together with the available protective measures are discussed in section 2.1. The necessity of the accurate prediction of the thickness reduction in the form of corrosion models and the division they follow is presented in section 2.2. The influence of corrosion in the material properties through the existing literature is investigated in section 2.3. The last two sections 2.4 and 2.5 aim to describe the collision between ships and the ways their ultimate strength can be evaluated respectively.

2.1 Examples of corrosion problems in marine structures

The lifespan of ships and offshore structures is heavily affected by the presence of corrosion. The appearance and development of any corrosive activity in a structure cannot be avoided and generate problems, which are crucial for its safety during its operational life. According to statistics corrosion together with corrosion fatigue are responsible for nearly 90% of ship failures. Poor maintenance and corrosion action are the two most important factors that led to many accidents of bulk carriers and oil tankers with severe environmental consequences (Qin and Cui 2003).

Mild and low alloy steels are affected by several types of corrosion with the general form to be observed more frequently leading to a uniform loss of the structure's thickness, see Figure 2.1. Pitting or grooving corrosion constitutes a localized type of material degradation, which also appears in marine structures, see Figure 2.2 (Paik et al., 2003a). Locations where general corrosion is more likely to be seen are the ullage space in cargo oil holds and the lower stools of bulk carriers due to absence of coating. Crude oil is the source of many gases such as sulphur trioxide (SO_3), sulphur dioxide (SO_2) and carbon dioxide (CO_2) that under specific conditions can influence the corrosion activity. The dissolution of these gases into the layer of water that is created because of humidity and temperature variations results in the formation of an acidic medium. Furthermore, hydrogen ions because of the presence of hydrogen sulfide (H_2S) in the crude oil are combined with iron producing sulphide compounds. The process continues with the reaction of these compounds with oxygen to form sulphur and iron oxides. The corrosion process may be accelerated by the removal of the oxidized material due to the presence of rust and sulphur, exposing cleaner parts of the metal. In the case of bulk carriers, steel degradation is governed by the pH level of water in the cargo holds and determined by the supply rate of pyrite (FeS_2) and carbonates provided by coal. Iron ore may cause corrosion of the structure mainly because of the small presence of sulphur but it is water, which remains after cleaning of the surfaces that can create the suitable conditions for corrosion to initiate and progress (Wang et al., 2014).

Figure 2.1: General corrosion (IACS, 2015)

Pitting constitutes a localized form of corrosion that can be observed on structural members of a vessel that are in direct contact with the seawater such as the bottom and side shell plating or the parts that can be affected by the combination of water presence and wind. Pitting corrosion can naturally be found in tanks, which are used for the transportation of liquid cargoes and in the ship's ballast tanks. Parts of the hull affected by water in the form of spray and without immersion conditions are less likely to be attacked by pitting corrosion. Perforation of the steel plate is the result of the pitting activity with severe consequences for the marine environment and the performance of the ship (Daidola et al., 1997). The lower part of cargo oil tanks is occupied by water, which can reach up to 20 % of the tanks volume as the result of both condensation and crude oil's production process. Normally bottom plating is protected by oil, which forms a thin layer above the surface of the plate preventing any influence from the volume of water. However, corrosion in the form of pits may start in locations where the layer of oil disappears or damaged. In such confined spaces the combination of humidity, low levels of oxygen and chemical nutrients create the suitable anaerobic environment for the growth of sulphate-reducing bacteria (SRB). Heating installations to assist the transfer operations of oil create the ideal temperature conditions for the metabolism of the bacterial life and the increase of their corrosion activity. In the horizontal areas of ballast tanks, the formation of blisters in the surface of the organic coating is indicative of corrosion initiation. The blisters are caused by the penetration of oxygen and water through the protective coating creating a buildup of materials in the boundary between the coating and the steel's surface. They can be either alkaline or neutral with the former to be associated with the generation of pitting corrosion while the latter allow the formation of pits if mechanical damage of the blisters occurs (Wang et al., 2014).

Figure 2.2:Pitting corrosion (IACS, 2015)

Grooving corrosion is more likely to be found in locations where the longitudinal and the deck are connected by weld while edge corrosion affects the free ends of parts such as stiffeners where the geometry doesn't allow the proper application of coating making corrosion more possible to appear. Both forms of corrosion are presented in Figure 2.3 (Wang et al., 2014).

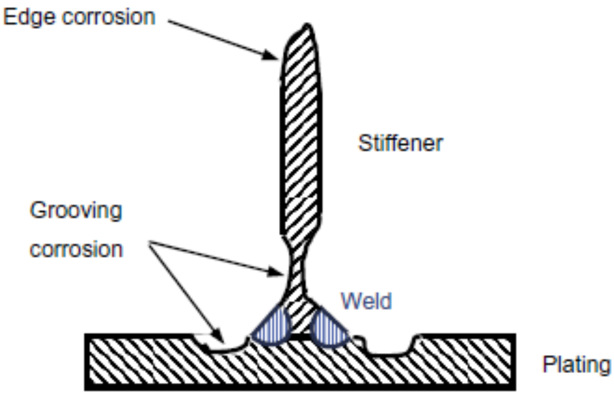

Figure 2.3: Grooving and edge corrosion in a stiffened panel (Wang et al.,2014)

Coatings and cathodic protection are the most common options for corrosion prevention in marine structures. The use of paint coatings usually involves the application of several coats that can be distinguished in a primer that aims to provide corrosion protection and enough adhesion to the steel's surface, followed by one or more intermediate coats and a topcoat to complete the process. The level of protection that coating is supposed to provide is ensured by certain features such as resistance to ultraviolet radiation and ability to withstand the weather elements as well as mechanical damage. Its lifetime is limited by the combined action of humidity, temperature and ultraviolet radiation while its failure can be attributed to several reasons, which are summarized in the following: (1) Insufficient surface preparation, (2) False selection of coating, (3) Wrong application method, (4) Inability to use the specified times for drying, curing and over-coating, (5) Absence of protection against moisture, (6) Impact damage (Bhandari et al., 2015).

Cathodic protection systems are based on the external supply of electrons to the protected material forcing it to act as a cathode. The cathodic reaction involves the flow of electrons from the anode to the cathode. If an external source of electrons is chosen, the anodic reaction is unable to provide more electrons while the rate of cathodic reaction starts to increase. The result is that the anodic reactions can be limited in the surface of another material, which acts as a cathode protecting the other parts of the structure. Sacrificial anode protecting system is used in seagoing vessels by adopting an electrical connection between the metal that intends to protect and another more reactive metal. Oxidation of the reactive part of the couple results in the protection of the less active. The application in a ship's structure includes its connection with a more active metal, which concentrates all corrosion activity and protects the rest of the structure (Cicek, 2017).

Field observations have shown that the combination of measures such as coatings and anodic protection systems can't ensure the complete absence of corrosion in a ship's structure. The solution to the inevitable material loss is the adoption of a corrosion allowance as a compensation to the expected thickness reduction during the service life of the vessel. The level of the corrosion margin must be accurately estimated because of the serious financial consequences that a false value can have. The need to efficiently predict the material loss has led to the development of time-variant corrosion models (Yang et al., 2016).

Generally, problems regarding corrosion are quantified by the introduction of a margin and an allowed level of corrosion. These two terms are determined by considering past collection of data and their necessity stems from the complexity of corrosion phenomena. The ratio of the thickness reduction of an aged and worn structural member to the age of the ship at a specific time provides the annual corrosion rate and serves as the basic criteria mainly because of the accessibility it offers. However, this method is not completely effective since it doesn't consider the time during of which the corrosion is formed and the fact that the rate of corrosion doesn't remain stable. Also, it doesn't provide any information about the pattern that the mechanism of corrosion follows from its beginning and gradual progression. These deficiencies originate mostly from the probabilistic behavior that the corrosion process exhibits. It becomes clear that another type of criteria is necessary in the form of a probabilistic model to describe more accurately the phenomena of corrosion including the time of their generation and how they advance. Empirical data are supposed to be used for the identification of such a model (Yamamoto and Ikegami, 1998).

Beyond the thickness reduction of the various structural members of the hull and the degradation of the ship's ultimate strength, corrosion activity can affect other aspects of a component such as its surface roughness and its mechanical properties (Garbatov et al., 2014). The presence of steel in a wet hydrogen sulfide (H_2S) environment leads to the generation of hydrogen atoms during the oxidation reaction of iron. Production of molecular gaseous hydrogen is more likely to happen if the hydrogen atoms are combined. However, the hydrogen sulfide (H_2S) tends to decelerate the formation of the molecular hydrogen forcing several hydrogen atoms to be diffused into the steel decreasing the local atomic cohesive force and increasing the possibility of a crack initiation. This process is known as hydrogen embrittlement and can affect the steel's material properties by diminishing its ductility and strength. Moreover, the damage caused by hydrogen can be further enhanced by the presence of inclusions in the steel that can act as hydrogen traps (Zheng et al., 2012).The degradation of the steel's material properties because of hydrogen embrittlement can possibly cause problems in locations where considerable quantities of hydrogen sulfide (H_2S) are observed such as the deck plates of oil tankers (Garbatov et al., 2014).

Pitting corrosion along with the uniform loss of material also affects marine structures and threatens their structural integrity not only due to the perforation of the plating that they can cause but also because of the surface defects they can introduce resulting in local stress concentrations (Garbatov et al., 2014). Corrosion pits act as stress intensifiers and may lead to fracture, fatigue crack initiation and rupture regardless of their small size. Research has shown that the value of the stress concentration factor depends on the aspect ratio of the pit, which is the ratio between the depth of the pit and its opening (Bertin et al., 2019).

The description of the corrosion process makes clear its complex influence in the service life of marine structures. The thickness reduction of the various structural parts can undermine the ship's ultimate strength while the mechanical properties of the corroded material may be also affected, which is not considered during the strength assessment. Moreover, pitting corrosion increases the likelihood of plating penetration but also allows the generation of local stress concentrations. Any attempt to predict how corrosion will progress and its impact in structural integrity of a vessel should be focused on the three aspects of material loss, degradation of its properties and presence of pitting corrosion.

The development of corrosion models can be approached by three different methods. The first simply assumes that corrosion growth shows a linear behavior, which leads to very crude results. The second method focuses on experimental data under precise conditions that indicate certain laws of corrosion growth with a dependency on specific parameters. Taking these laws into account forms the basis in the derivation of a corrosion model. A disadvantage of this process has to do with the difficulty in extrapolating the data from coupons in costal test facilities to conditions that are expected in real structures. Another drawback is associated with the limited knowledge in the way that environment affects the corrosion process in full-scale conditions. The third method suggests that a corrosion model should indicate the pattern, which is determined by the general corrosion mechanism and this pattern should be compared to the field data. In this way the model doesn't try to describe the overall form of corrosion progression but focuses on the part that seems to prevail over the others. Data from real operational conditions in marine structures are used to derive the parameters of the prevailing mechanism instead of experimental figures that the second method relies on. By fitting the curve to the real data, the possible errors that derive from excluding less important corrosion processes is reduced. This fact also provides a more realistic perspective to the model although it doesn't represent the exact corrosion mechanism (Garbatov and Guedes Soares, 2008).

According to literature many time-dependent corrosion models have been developed as an effort to quantify the effect of corrosive activity in structures in marine environments. The three approaches that have been previously described simply indicate the way that research has tried to describe corrosion modelling. In general, the models that has been suggested can be divided in two categories: plausible empirical models and physical models. Data that have been recorded in past measurements of material loss due to corrosion are the basis for the formation of empirical models while physical models use the physical mechanism as a starting point to simulate the corrosion wastage. For corrosion problems in ships and marine structures the adoption of empirical models is more likely to happen (Paik and Kim, 2012).

2.1.1 Pitting corrosion

Pitting corrosion is a form of localized corrosion that appears in certain points or small areas of the surface of a metal and results in the gradual formation of cavities. Its initiation is associated with the damage of the surface film that allows the material to be exposed to the corrosive medium. During the progression of pitting corrosion, a pattern of concentrated attack on the material is observed while the surface in the proximity of the attack point seems to be relatively unaffected. The factors that influence the growth of pitting can be summarized in the following (Bhandari et al., 2015):

- Breakdown of the protective oxide film because of chemical or mechanical action.
- Instability of the oxide film due to presence of acids, low oxygen and high chloride concentrations that favors the pit initiation.
- Improper application or damage of the paint coating.
- Presence of non-metallic inclusions in the material that disturbs its uniformity.

The pits can appear as uncovered or covered with a thin layer of oxidized material that doesn't isolate the interior of the pit from the surrounding environment. Their shape can be hemispherical, conical, flat-walled or completely irregular. An example of the shape variation can be seen in Figure 2.4.

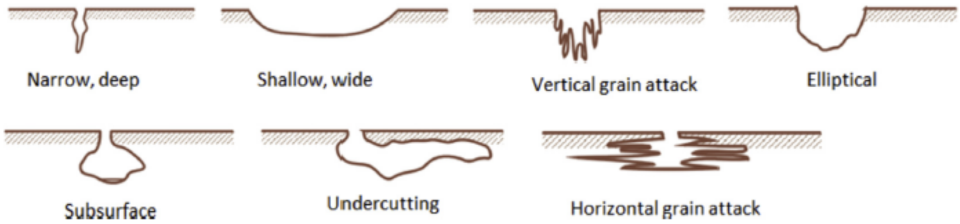

Figure 2.4:Pit shape variation -trough pits (upper),sideway pits (lower) (Bhandari et al., 2015)

The process of pit formation shows an increased degree of complexity and can be divided in four stages for the case of a single pit as it can be seen in Figure 2.5 (Bhandari et al., 2015):

- Stage 0. The metallic surface has not yet been affected by corrosion and is under the protection of passive films.
- Stage 1. The thin layer of oxidized products tends to break, allowing the electrolyte to meet the material through a small patch while the rest of the substrate remains protected. The size of the patch can be less or equal to the passive film's thickness. Progressively the substrate starts to be dissolved by the electrolyte.
- Stage 2. The conditions allow the pit to grow.
- Stage 3. Increase of the substrate's dissolution process while the size of the hemispherical or polyhedral pit is between 1-10 µm, which means that microscopic observation is possible.
- Stage 4. The final stage involves the growth of the pits at a size that allows them to be visible with irregular shapes or partially hidden by corrosion products.

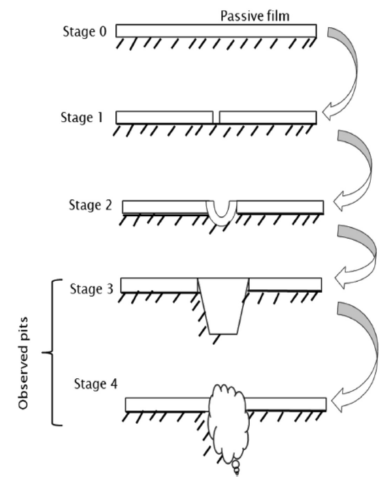

Figure 2.5:Pit formation stages (Bhandari et al., 2015)

Modelling of pitting corrosion is considered a difficult task mainly because of the small scale that the processes of initiation and growth takes place, which can be in the range of nanometers. Furthermore, it can be affected by several factors such as temperature , oxygen concentration, pH, velocity , bacterial presence (Bhandari et al., 2015). Its initiation is followed by a rapid generation, which is concentrated in small areas of the surface, causing failure due to perforation. Because of the randomness of the pitting corrosion process, there are significant difficulties in the prediction of its growth pattern. Mechanistic models are associated with a degree of uncertainty despite the knowledge of the internal function of pitting corrosion that has been gained. An alternative option is the use of statistical and stochastic models such as extreme value distribution models, which are applicable for the estimation of the largest pit depth (Yuan et al., 2009). According to Melchers (2010), pitting corrosion is not regarded as a design-critical issue for materials such as mild and low-alloy steels. Its influence on the strength assessment of well-maintained marine structure can be considered small while the focus is given in the thickness reduction due to uniform corrosion. The possibility of plate perforation due to pitting is more crucial in situations where containment is important such as ships and pipelines. However, the load carrying capacity of a structure may be influenced by the change on the ultimate strength caused by pitting geometric parameters (Wang et al., 2008b). It has been found that in the case of pitted plate elements subjected to axial compressive loading, there is a strong dependency of the ultimate strength on the most corroded section of the plate (Paik et al., 2003b). Another study led to the conclusion that the presence of pitting corrosion in plate elements under edge shear, shifts the dependency of the ultimate strength on the degree of pit corrosion intensity (DOP), which is defined as the ratio percentage of the corroded surface area to the original plate surface area (Paik, 2004).The tensile strength and buckling behavior of hold frames in bulk carriers affected by pitting corrosion was investigated by evaluating the results of several tensile and buckling tests. The decrease of the tensile strength was found to be larger compare to members with uniform material loss. Also the compressive buckling strength of the pitted members appeared to have a smaller or equal value with the members affected by uniform corrosion (Nakai et al., 2004). It is reasonable to conclude that pitting corrosion can't be neglected during the ship's ultimate strength assessment.

For the purposes of the present study the choice of considering the influence of pitting corrosion in the ultimate strength estimation is not practical. The contribution of pitted structural members in the load carrying capacity is included in the change of the material properties since the reduction of the strength as it will be further described in section 2.3 can be also attributed in the presence of pitting corrosion, which acts as a stress raiser in the surface of the material.

2.2 Corrosion models

The division of the corrosion models in linear and non-linear is presented in subsection 2.2.1 and 2.2.2 respectively. The two last subsections 2.2.3 and 2.2.4 aim to summarize the basic features of the described models and the select the corrosion model that fulfills the requirements of the current study.

2.2.1 Linear corrosion models

Linear corrosion models assume that the thickness reduction of the structural member shows a linear relationship with time when the structure is attacked by a corrosive environment. An example of linear model can be found in Guedes Soares (1988) where the initial thickness t of a plate is reduced at a rate of k mm per unit of time according to the following equation:

$$t_k = t - kt_* \tag{1}$$

where t_k represents the thickness of the plate after a time t_* .

Corrosion damages of military equipment operating in tropic climate during WW2 initiated a large-scale corrosion project in the Panama Canal Zone (PMZ). For a period of 16 years coupons with dimensions 225x225x6 mm were sampled after they were subjected to the corrosive attack of seawater and atmospheric conditions for a certain time. This project provided a realistic source of data that could be used in corrosion related problems. Examination of the data led Southwell et al. (1965) to the conclusion that the long-term corrosion behavior is governed by sulfate reducing bacteria (SRB). The short-term corrosion wastage cannot represent the long-term loss of material and the latter seems to become linear after a period of rapid corrosive action, see Figure 2.6. The initial non-linear period of corrosion development was estimated to 2-5 years after of which the layer of oxidized material prohibits the contact of the coupon with the corrosive medium protecting in this way the rest of the material. A linear and bilinear model was proposed, which can be used for design purposes although they tend to overestimate the material loss in the early stages of exposure (Garbatov and Guedes Soares, 2008,1999; Melchers, 2008):

$$d = 0.076 + 0.038t, \tag{2}$$

$$d = \begin{cases} 0.090t & 0.00 \leq t < 1.46 \\ 0.076 + 0.038t & 1.46 \leq t < 16.00 \end{cases} \tag{3}$$

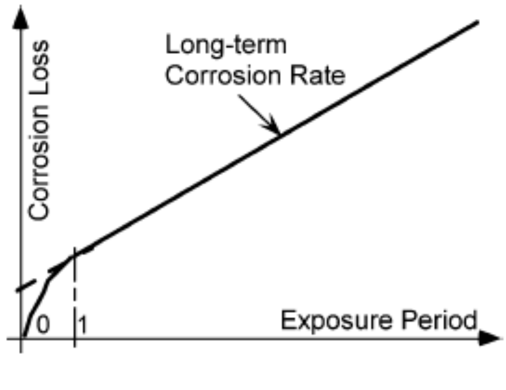

Figure 2.6: Southwell model (Melchers, 2008)

The linear model has been extended in Melchers (1999) by expressing it as a mean value model with the loss of thickness to be given by $\mu_d(t)=d(t)$. Data analysis lead to the calculation of the second statistical moment of the nominal corrosion depth about the mean, which is found to be 0.67. The function of the standard deviation for the corrosion depth that can be expected is:

$$\sigma_d(t) = 0.051 + 0.025t \tag{4}$$

A refinement of the model is possible by adopting a bilinear model in the early stage of the corrosion process. The second statistical moment about the mean is estimated to be 0.69 and 0.67 for the early and stable stage of the model respectively. The most appropriate fit for the changeover point is found to be 1.46 years. Therefore:

$$\mu_d(t) = \begin{cases} 0.09t & 0 < t < 1.46\,years \\ 0.076 + 0.038t & 1.46 < t < 16\,years \end{cases} \tag{5}$$

$$\sigma_d(t) = \begin{cases} 0.062t & 0 < t < 1.46\,years \\ 0.035 + 0.017t & 1.46 < t < 16\,years \end{cases} \tag{6}$$

Both the above linear and bilinear models are considered conservative because of their tendency to over-estimate the loss of material due to corrosive activity at the early stage of its initiation and more specific in the time interval between 1-3 years.

When the data are attempted to be fitted using a non-linear function the result is described by the following function:

$$d(t) = \mu_d(t) = 0.084t^{0.823} \tag{7}$$

$$\sigma_d(t) = 0.056t^{0.823} \tag{8}$$

A trilinear and a power function was also proposed to describe the corrosion wastage in the following way:

$$d(t) = \begin{cases} 0.170t & 0 \le t < 1 \\ 0.152 + 0.0186t & 1 \le t < 8 \\ -0.364 + 0.083t & 8 \le t \le 16 \end{cases} \tag{9}$$

$$d(t) = 0.1207t^{0.6257} \tag{10}$$

2.2.2 Nonlinear Corrosion Models

2.2.2.1 The Yamamoto and Ikegami model

The corrosion model that was developed by Yamamoto and Ikegami (1998) used data of plate thickness, which were conducted on several different vessels affected by pitting corrosion. The model regards the loss of material as the product of the progressive growth of a large number of pitting points (Garbatov and Guedes Soares, 2008). According to Yamamoto and Ikegami (1998) the development of the model was based on the following assumptions :

a) During the time the protective layer of paint remains effective, no corrosion activity takes place. When the paint coating loses its effectiveness, pitting points start to appear in the surface of the material.
b) The process of the appearance of the active pitting points and their evolution to progressive pitting points is associated with the general corrosion over time.
c) In areas where the progression of pitting points occurs each point grows individually.

The three processes are probabilistic leading to the introduction of the following probabilistic models:

- Anti-corrosive paint coating effectiveness probabilistic model.

The life of the protective layer T_o is defined as the period before the appearance of active pitting points. By adopting the assumption of a log-normal distribution the following equation can be used:

$$f_{T_o}(t) = \frac{1}{\sqrt{2\pi}} \frac{1}{\sigma_o t} exp\left[-\frac{(\ln t - \mu_o)^2}{2\sigma_o^2}\right] \tag{11}$$

where μ_o represents the mean of $\ln T_o$ and σ_o the standard deviation of $\ln T_o$.

The mean and standard deviation of $\ln T_o$ are regarded as unknowns during the analysis due to fact that their values can't be determined. Because of the inability to fully understand the relation between the stages when the paint layer loses its efficiency and the formation of active pitting points, a different approach was considered. Empirical observations have determined the following expression:

$$cov = \frac{\sqrt{V(T_O)}}{E(T_O)} = \sqrt{\exp(\sigma_o) - 1} \approx 0.4 \tag{12}$$

where cov is the coefficient of covariance of the duration of the coating effectiveness.

- Pitting point generation probabilistic model

It is assumed that an exponential distribution is more appropriate to describe the time that is needed for the active pitting points to transform to progressive pitting points. If T_r refers to this time, then it is given by the equation below:

$$g_{T_r}(t) = a * \exp(-at) \tag{13}$$

where the parameter α represents the inverse of the mean of the time T_r and since its value cannot be determined beforehand it will be treated as an unknown during the analysis.

- Pitting points progression probabilistic model

The growth pattern of the pitting points after their generation can expressed by the following equation:

$$z(t) = a\tau^b \tag{14}$$

where α and b are parameters that control the corrosion process, z represents the depth that the pitting has reached while τ gives the time that has passed since the progressive pits started to appear. The term α is described by log-normal distribution:

$$h_\alpha(x) = \frac{1}{\sqrt{2\pi}\sigma_\alpha x} \; exp\left(-\frac{(\ln x - \mu_\alpha)^2}{2\sigma_\alpha^2}\right) \tag{15}$$

In the previous equation μ_α and σ_α are the mean and the standard deviation of $\ln\alpha$ and are regarded as unknowns. The values of coefficient b can vary between 1 and 1/3 depending on factors such as material and environmental conditions.

In the suggested model the shape of the pit was considered an important factor in the estimation of the general corrosion as the results of generation and progression of pitting corrosion. Measurements of the shape of the pit in the corroded surfaces of ordinary hulls led to the assumption of a pit size with a ratio of diameter to depth equal to 5:1 or $\frac{z_0}{L} = 0.4$ according to Figure 2.7.

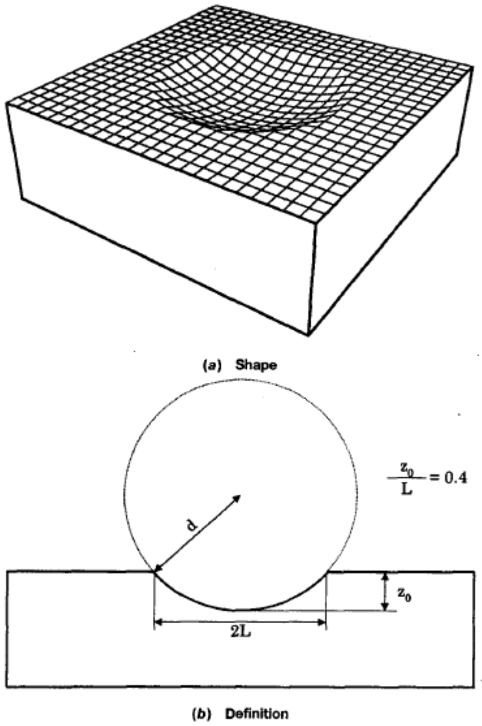

Figure 2.7: Shape of pit (Yamamoto and Ikegami, 1998)

The combination of Eq. (14) and Eq. (15) provides the mathematical expression of the probability of the pitting corrosion depth with the requirement that time τ is known:

$$p_z(z|\tau) = \frac{1}{\sqrt{2\pi}\sigma_\alpha z} \; exp\left(-\frac{(lnz - bln\tau - \mu_\alpha)^2}{2\sigma_\alpha^2}\right) \tag{16}$$

The analysis of the data obtained by measurements of the plate thickness reduction due to corrosion, makes possible the estimation of the unknown parameters in the previously described probabilistic models. Considering those models, the decrease of thickness z_p because of corrosion activity can be calculated as the value that satisfies the following equation in which the term $P(t)$ is used to describe the cumulative probability at a certain time t:

$$P(t) = \int_t^\infty f_{T_o}(t_o) G_{T_r}(t - t_o) dt_o + \int_0^{z_p} p_z(z|t) dz \tag{17}$$

2.2.2.2 The Garbatov and Guedes Soares model

A nonlinear model that demonstrates more flexibility was developed by Garbatov and Guedes Soares (1999). The model aims to improve the models that are independent of time with a constant corrosion rate by introducing a nonlinear function of time in which the corrosion growth is divided in three different stages:

1. The first phase is defined by the absence of corrosive activity due to fact that the protective coating hasn't lost its efficiency. Many factors can affect this stage and the evaluation of statistical data shows that it can vary between 1.5-5.5 years for structures such as ships ([O′, O] in Figure 2.8).
2. The second stage starts when the paint loses its ability to protect the surface of the plate and corrosion starts to act with the subsequent reduction of the plate's thickness. For structural members found in a ship this period lasts about 1-4 years ((O, B] in Figure 2.8).
3. The third phase is associated with the end of the corrosion process in which the value of corrosion rate becomes equal to zero. This fact is justified by the presence of oxidized material that remains in the surface acting protectively to the rest of the plate. Removing the corroded material by cleaning or by any other way will result in the initiation of a new nonlinear corrosion activity (t>B in Figure 2.8).

According to Garbatov and Guedes Soares (1999), the proposed model is derived as the solution of a differential equation, which is used to describe the corrosion wastage:

$$d_\infty \dot{d}(t) + d(t) = d_\infty \tag{18}$$

The general form of solution of the above equation is:

$$d(t) = d_\infty(1 - e^{-\frac{t}{\tau_t}}) \tag{19}$$

The particular solution is given by:

$$d(t) = \begin{cases} d_\infty\left(1 - e^{-\frac{(t-\tau_c)}{\tau_t}}\right), & t > \tau_c \\ 0, & t \leq \tau_c \end{cases} \tag{20}$$

where d_∞ expresses the long-term corrosion wastage, $d(t)$ is the corrosion wastage thickness at a specific time t and $\dot{d}(t)$ is the rate of corrosion. The terms τ_c represents the life of the coating, which is defined as the time between any appliance of paint and the time when the coating can no longer protect the plate from the action of the corrosive medium while τ_t is the transition time. The latter can be found as:

$$\tau_t = \frac{d_\infty}{tga} \tag{21}$$

with α is the angle, which is formed by OA and OB, see Figure 2.8.

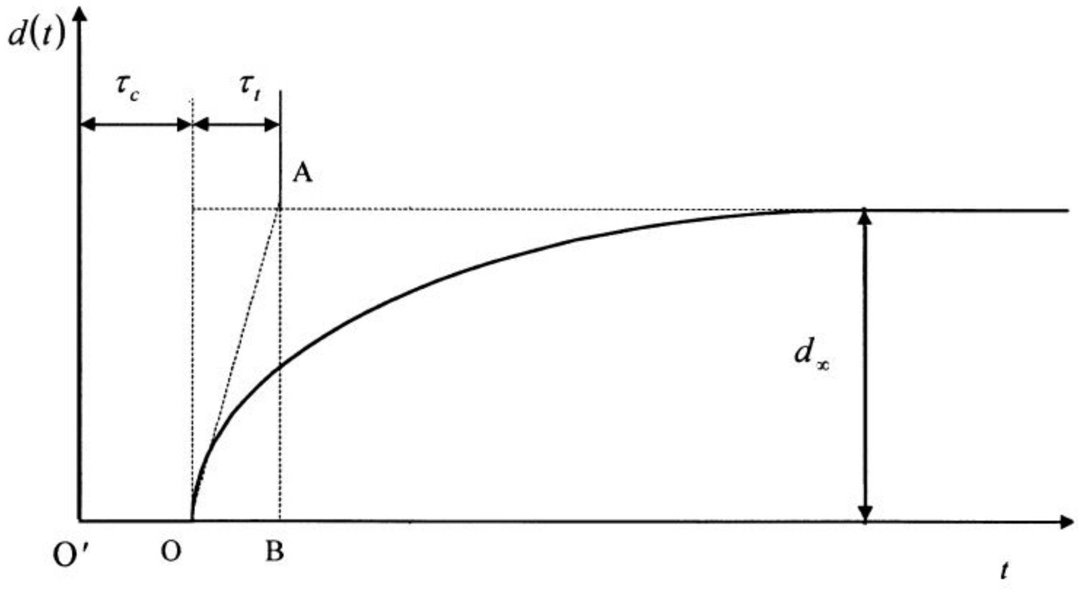

Figure 2.8: Corrosion wastage thickness as a function of time (Garbatov and Guedes Soares, 1999)

Data obtained from measurements in plates with different stages of corrosion activity were successfully fitted to the model. There are two boundary conditions that ensure the function of the model with the first to be related with the absence of any corrosion process in the interval $0 < t < \tau_c$ while the second requires that the corrosion depth will not exceed the thickness h of the plate when the structure reaches the end of its service life $h \geq d_\infty \geq d(t)$. The latter is fulfilled if the corrosion rate seizes when the thickness reduction approaches the long-term corrosion wastage for the case of a plate with unclean surface or the as built thickness when the structure reaches its useful life. Certain features of the maintenance process such as the cleaning of the steel surfaces and the application of new coating can be represented by the model contributing in its increased flexibility (Garbatov and Guedes Soares, 2008).

2.2.2.3 The Paik model

The progress of the corrosion process in a coated part of a marine steel structure can be described by the following three phases:

- Coating life
- Transition
- Corrosion progression

The corrosion progression can be represented by a convex or concave curve, which can be seen by the dotted line in Figure 2.9. The former curve is an indication of an increased corrosion rate at the beginning of the exposure, which tends to decrease as the corrosion process advances. This kind of curve can be observed in non-immersion conditions at sea because the products of corrosion that are accumulated in the steel's surface can influence the initiation of the corrosion progression phase. Conversely, an acceleration of the corrosion rate is indicative of the concave version of the curve and it is more possible to be seen in dynamic loading cases where the motion of the structural members results in cleaner part of the surface to be exposed to the corrosive medium. There is also the choice of a linear approximation between those two cases (Paik et al., 2003a).

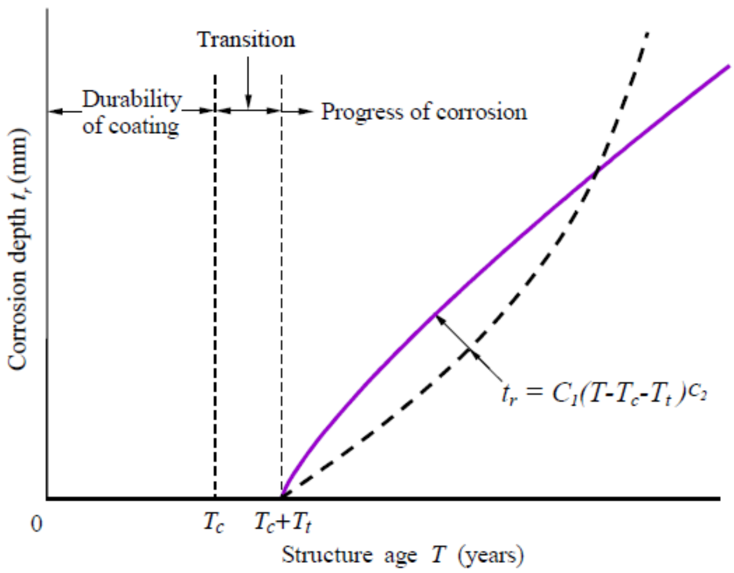

Figure 2.9:Paik et al. model (Paik et al., 2003a)

The life of the paint layer is defined by the time any corrosion activity starts to appear in a new-built vessel. It can be assumed that the coating's life is described by normal distribution according to the equation below:

$$f(t) = \frac{1}{\sqrt{2\pi}\ \sigma_{cl}}\, exp\left(-\frac{(t-\mu_{cl})^2}{2\sigma_{cl}^2}\right) \tag{22}$$

where μ_{cl} and σ_{cl} represent the mean value and the standard deviation of coating life respectively. It has been found that 5-10 years can be regarded as a normal figure for the mean value of the coating life with 5 years to be a relative undesirable possibility while 10 years seems to describe a more advantageous situation. Also, research has concluded that the coefficient of variation (COV) of coating life is approximately equal to 0.4 (Paik et al., 1998).

The loss of coating effectiveness is followed by a transition time, which is defined as the interval between the moment the coating loses its ability to protect the surface of the hull and the moment corrosion can be observed in a measurable scale. It can be regarded as a random variable described by exponential distribution. A zero value of the transition time is translated to the instant initiation of the corrosion activity after the loss of coating effectiveness (Paik et al., 2003).

After the deterioration of the paint layer, the corrosion growth leads to gradual loss of material of the ship's structural members. The reduction of the plate thickness can be regarded as a function of time after the initiation of the corrosion process:

$$t_r = C_1(T - T_c - T_t)^{C_2} \tag{23}$$

where t_r is the reduction of the plate thickness, T is the ship's age, T_c is the duration of the coating, T_t is the transition time and C_1, C_2 are coefficients. The coefficient C_1 acts as an indication of the corrosion rate while the coefficient C_2 defines the pattern that corrosion process progresses. The determination of the two coefficients can be achieved by the analysis of selected corrosion data from ships and other marine structures, which is not regarded as a straightforward procedure mainly because of the scatter those data usually exhibit. Another option, which doesn't eliminate the problems of the data collection, is to calculate C_1 as a function of a specific value of C_2.The latter has been observed to obtain values between 0.3-1.5, which correspond to a corrosion trend where the rate tends to become constant after a certain time. However, if corrosion seems to accelerate over time, which is indicative for a dynamic loaded component the above range of values can't be used. For practical reasons the coefficient C_2 =1 accepting in this way a constant annual corrosion rate. Following the choice of C_2 the coefficient C_1 can be determined which means calculation of its mean, variance and type of probability density. This is possible by using Eq. (24) for a sampling point assuming zero transition time (Paik et al., 2003a):

$$C_1 = \frac{t_r}{(T - T_c)^{C_2}} \tag{24}$$

It has been found that the cumulative density function of the corrosion rate can be described by the Weibull distribution and as a result the function of the coefficient c_1 is expressed by:

$$F_{C_1}(x) = 1 - \exp\left(-\left(\frac{x}{a}\right)^{\lambda}\right) \tag{25}$$

Combining the Eq. (23) and Eq. (25) the probability density function of the plate thickness reduction is:

$$f_{C_1} = \frac{\lambda}{\alpha}\left(\frac{x}{a}\right)^{\lambda-1} exp\left(-\left(\frac{x}{a}\right)^{\lambda}\right) \tag{26}$$

where α and λ represent the shape and scale parameter.

In order to estimate the probabilistic behavior of corrosion the mean and standard deviation of c_1 are needed to be determined. For this reason, the least square method is chosen forcing Eq. (25) to be rewritten in the following form:

$$Y = \lambda X - \lambda \ln x \tag{27}$$

where $X = \ln x$ and $Y = \ln$ [-ln (1-$F_{C_1}(x)$)]. Using this method, the shape and scale parameter can be calculated form the gathered corrosion data. Once they are determined the Gamma function can be used to obtain the standard deviation and mean of the coefficient C_1 according to (Paik et al., 1998):

$$\mu_{C_1} = \int_0^{\infty} x f_{c_1}(x)dx = a\Gamma\left(1 + \frac{1}{\lambda}\right) \tag{28}$$

$$\sigma_{C_1}^2 = \int_0^{\infty} (x-\mu)^2 f_{c_1}(x)dx = a^2\left[\Gamma\left(1+\frac{2}{\lambda}\right) - \left\{\Gamma\left(1+\frac{1}{\lambda}\right)\right\}^2\right] \tag{29}$$

2.2.2.4 The Qin and Cui model

In the previously described models, the corrosion protection system (CPS) was ignored or considered by interpreting the loss of its effectiveness as the start of the corrosion process.

There was no effort in analyzing the possible interaction between the coating and the environment. In the model suggested by Qin and Cui (2003) an attempt was made to include the role that the Corrosion Protection System (CPS) might have in the mechanism of corrosion. In actual conditions the coating will not instantly lose the ability to protect the material, but a progressive degradation is more likely to happen allowing the appearance of pitting corrosion before it is completely unable to stop the attack from the corrosive medium. It is necessary to adopt two parameters T_{st} and T_{cl} that describe the function of the Corrosion Protection System. T_{st} represents the measurable quantity that indicates the beginning of the pitting corrosion while T_{cl} is determined by the time when the general corrosion appears. It is advisable that both T_{st} and T_{cl} are treated as random variables since the coating life can be affected by several factors that have to do with stress level, location and the environment. The introduction of the life T_{st} when corrosion actually starts and the coating life T_{cl} makes clear the influence of the CPS and any environmental factor in the corrosion rate during the progression phase of pitting corrosion. The corrosion rate can be specified by associating the magnitude of pitting corrosion to general corrosion. While pitting corrosion continues the rate of corrosion tends to increase and when this acceleration period ends with the loss of coating's effectiveness, the general corrosion begins along with a reduction of the corrosion rate due to amount of oxidized material that has been produced (Qin and Cui, 2003)

It becomes obvious that the process of corrosion can be described in three phases according to Figure 2.10:

1. Absence of corrosion due to the effectiveness of the CPS ($[0, T_{st}]$).
2. Generation and gradual progression of pitting corrosion leading to the acceleration of the uniform corrosion ($[T_{st}\ , T_A]$).
3. Deceleration of corrosion ($[T_A\ , T_L\ ]$).

The point T_L defines the structural lifespan or the time when repair or maintenance is scheduled. For simplicity reasons it is assumed that T_A=T_{cl} .

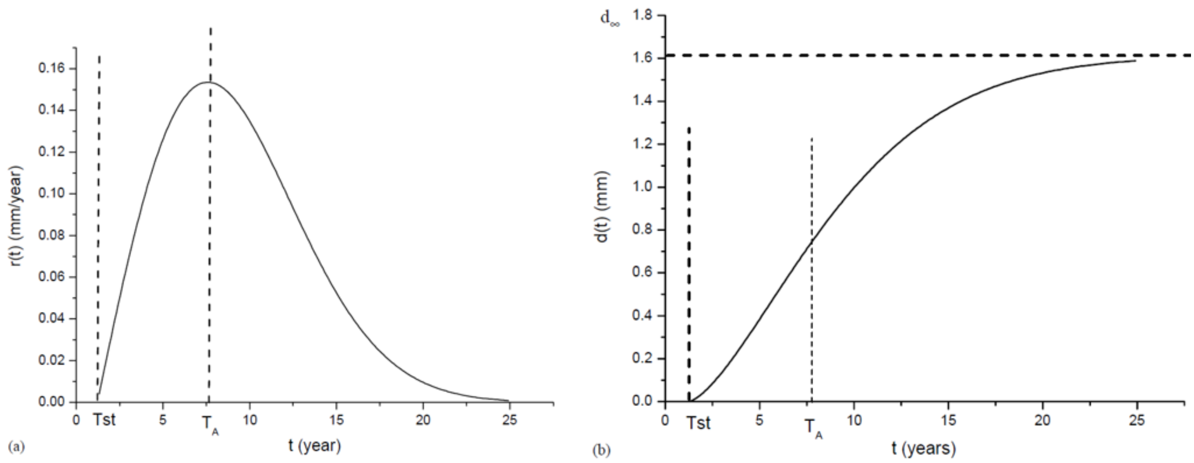

Figure 2.10: Qin and Cui model a) Corrosion rate b) Corrosion wear (Qin and Cui, 2003)

The representation of the corrosion rate in Figure 2.10 shows that a Weibull distribution is more applicable and mathematically is expressed by:

$$r(t) = \begin{cases} 0\,, & 0 \le t \le T_{st} \\ d_\infty \dfrac{\beta}{\eta}\left(\dfrac{t - T_{st}}{\eta}\right)^2 exp\left\{-\left(\dfrac{t - T_{st}}{\eta}\right)^\beta\right\}, & T_{st} \le t \le T_L \end{cases} \tag{30}$$

The corrosion rate will reach its maximum value at the time point T_A:

$$T_A = \begin{cases} T_{cl} = T_{st} + \eta\left(\dfrac{\beta - 1}{\beta}\right)^{1/\beta} & ,\beta > 1 \\ T_{st}, & \beta \le 1 \end{cases} \tag{31}$$

The maximum value of the corrosion rate is given by:

$$r_{max} = \begin{cases} d_\infty \dfrac{\beta}{\eta}\left(\dfrac{\beta - 1}{\beta}\right)^{(\beta-1)/\beta} exp\left(\dfrac{\beta - 1}{\beta}\right), & \beta > 1 \\ \dfrac{d_\infty \beta}{\eta}, & \beta = 1 \\ \to \infty, & \beta < 1 \end{cases} \tag{32}$$

The corrosion wastage according to previously described model is:

$$d(t) = \begin{cases} 0, & 0 \le t \le T_{st} \\ d_\infty \left(1 - exp\left[-\left(\dfrac{t - T_{st}}{\eta}\right)^\beta\right]\right), & T_{st} \le t \le T_L \end{cases} \tag{33}$$

where $d_\infty, \beta, \eta, T_{st}$ are parameters that it is necessary to be determined in order to fully define the corrosion model. Its flexibility can be seen in Figure 2.1, which shows the time points of maximum corrosion rate under variation of the values of the above parameters.

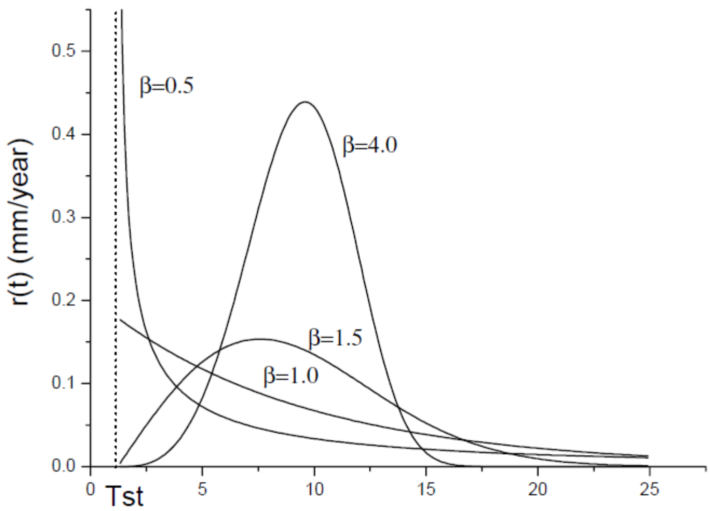

Figure 2.11: Corrosion model flexibility (Qin and Cui, 2003)

The model can transform its mathematical expression by choosing specific values of the parameters $d_\infty, \beta, \eta, T_{st}$ describing several of the existing corrosion models. This can be seen in the analysis below.

- For $\beta = 1$ Eq. (33) becomes:

$$d(t) = d_\infty \left(1 - exp\left[-\left(\frac{t - T_{st}}{\eta}\right)\right]\right) \tag{34}$$

which corresponds to the model developed by Garbatov and Guedes Soares (1999) described by Eq. (20) in section 2.2.2.2.

- For $\eta = 1$ Eq. (33) after application of the Taylor expansion series and by keeping the linear part the following equation is obtained:

$$d(t) = d_\infty \left(\frac{t - T_{st}}{\eta}\right)^\beta = d_\infty (t - T_{st})^\beta \tag{35}$$

resulting in an expression similar to Eq. (23), which describes the model suggested by Paik et al., (2003a)

- For $d_\infty = 0.1207, \beta = 0.6257, \eta = 1, T_{st}$=0 Eq. (35) becomes:

$$d(t) = 0.1207t^{0.6257} \tag{36}$$

The Eq. (36) is identical to Eq. (10) of the corrosion model developed by Melchers (1999) as it is described in section 2.2.1.

Two methods were suggested for the determination of the parameters $d_\infty, \beta, \eta, T_{st}$. One method assumes that the nature of these parameters is deterministic while the second method treats them as random variables. According to Qin and Cui (2003) these methods are:

Method 1

For values of time according to the inequality $T_{st} \le t \le T_L$ Eq. (33) can be rewritten in the following way:

$$-\ln\left(-\ln\left(1 - \frac{d(t)}{d_\infty}\right)\right) = \beta \ln \eta - \beta \ln(t - T_{st}) \tag{37}$$

It is assumed that

$$Y = -\ln\left(-\ln\left(1 - \frac{d(t)}{d_\infty}\right)\right), \quad X = \ln(t - T_{st})$$
$$A = \beta \ln \eta, \text{B=}-\beta \tag{38}$$

The Eq. (37) has the linear form

$$Y = A + BX \tag{39}$$

Least square method can be used to calculate the values of A and B provided that d_∞ and T_{st} are known. Therefore:

$$B = \frac{L_{xy}}{L_{xx}}, \quad A = \bar{Y} - B\bar{X} \tag{40}$$

The coefficient R of linear regression is calculated by:

$$R = \frac{L_{xy}}{\sqrt{L_{xx}\, L_{yy}}} \tag{41}$$

The terms of Eq. (40) and Eq. (41) are given by the set of equations:

$$\begin{gathered} L_{xy} = U_{xy} - \bar{X}\,\bar{Y}, L_{xx} = U_{xx} - \bar{X}^2, L_{yy} = U_{yy} - \bar{Y}^2 \\ U_{xy} = \frac{1}{n}\sum X_i Y_i\,, U_{xx} = \frac{1}{n}\sum X_i^2\,, U_{yy} = \frac{1}{n}\sum Y_i^2 \\ \bar{X} = \frac{1}{n}\sum X_i\,, \bar{Y} = \frac{1}{n}\sum Y_i \end{gathered} \tag{42}$$

The terms β and η are calculated by:

$$\beta = -B, \eta = exp\left(\frac{A}{\beta}\right) \tag{43}$$

The values of T_{st} and d_∞ can be derived by adopting an iterative process. The following assumption is made:

$$d_\infty = d_{\max} + \Delta d \tag{44}$$

where $d_{\max}$ represents the maximum corrosion wastage that exists in a database and Δd is an increment chosen to be relatively small and according to the judgement of the user. For example, it could be chosen to satisfy the relation $\Delta d = d_{\max}/100$. For every value of d_∞ defined by Eq. (44) the value of T_{st} can be calculated as long as the condition $\frac{dR}{dt} = 0$ is fulfilled. The term T_{st} is determined in the following way:

$$\frac{\left(\Sigma\frac{X_i}{t_i - T_{st}} - \Sigma\frac{\overline{X_i}}{t_i - T_{st}}\right)}{L_{xx}} - \frac{\left(\Sigma\frac{Y_i}{t_i - T_{st}} - \Sigma\frac{\overline{Y_i}}{t_i - T_{st}}\right)}{L_{xy}} = 0 \tag{45}$$

Considering the assumption:

$$d_\infty(i+1) = d_\infty(i) + \Delta d \tag{46}$$

the terms $T_{st}(i+1)$ and $R(i+1)$ can be obtained. The condition $R(i) > R(i+1)$ must be satisfied, which means that Eq. (46) must be applied until this condition is reached allowing the derivation of the other two unknown parameters according to the Eq. (40) - Eq. (43).

Method 2

The parameters d_∞, β, η, T_{st} can be regarded as random variables to deal with the large uncertainties of the corrosion databases. The statistical features of these parameters can be obtained by using a method in which a function is formulated to demonstrate the error between the observed corrosion wastage in a specific plate and the wear due to corrosion according to the suggested model. This is expressed by:

$$Error1 = \sum \left(D_i(t_j) - d(t_j)\right)^2$$
$$= \sum \left(D_i(t_j) - d_\infty \left(1 - exp\left(-\left(\frac{t_j - T_{st}}{\eta}\right)^\beta\right)\right)\right)^2 \quad (47)$$

The application of the previous equation to minimize the error cannot be performed easily and as a result another function is preferred:

$$Error2 = \sum \left(\left(\left(E\left(D_i(t_j)\right) - E\left(d_\infty\left(1 - exp\left(-\left(\frac{t_j - T_{st}}{\eta}\right)^\beta\right)\right)\right)\right)\right)^2 + \left(\left(S\left(D_i(t_j)\right) - S\left(d_\infty\left(1 - exp\left(-\left(\frac{t_j - T_{st}}{\eta}\right)^\beta\right)\right)\right)\right)^2\right)\right) \quad (48)$$

where $D_i(t_j)$ is the measured corrosion wastage of a plate, $d(t_j)$ is the model estimated wear while E and S are the mean and the standard deviation of the variables inside the brackets respectively.

2.2.2.5 The Melchers model

The starting point of most of the corrosion wastage models is the acceptance that the corrosion process is difficult to comprehend, and it can be influenced by a number of factors. As a result, the development of corrosion models was based on the collection of data that are gathered during periodic surveys conducted by classification societies. The gathering of these data follows a certain pattern, which includes measurements of thickness reduction on specific locations of the vessel's hull without considering the size of the structure or operational and environmental factors that might have affected the corrosion activity. These facts lead to set of data that show a large degree of heterogeneity and scattering (Melchers and Jeffrey, 2008)

The estimation of the lifespan of a structure in most cases uses the assumption that loss of material is provided by a constant rate of corrosion as a function of time. The latter is usually derived from the corrosion current by using Faraday's law in tests under laboratory conditions or by extrapolating the measured wear on steel coupons for no longer than one-year exposure in a marine environment. Both approaches can't entirely simulate the corrosion process that takes place in the actual structures under specific environmental and operational conditions. The average corrosion rates that are found in handbooks tend to promote the idea of constant over time corrosion rates without providing any information regarding how or when the data were gathered. In this way the theoretical notion of the reduction over time of the momentary corrosion rate seems to be ignored. The perception of nonlinearity has been integrated in certain corrosion models while the introduction of a model based on the principles of corrosion science has only in the recent years attempted (Melchers and Jeffrey, 2008).

The ability of a structure to carry loads is heavily affected by the corrosion activity, which appears in the form of uniform loss of material over the surface of the structure or in the forms of pits. According to Melchers and Jeffrey (2008) the structural strength is related to the material loss $c(t)$ for certain typical cases as follows:

- In an axial member, which is subjected to axial stress while is submerged in seawater the structural strength is given by:

$$R(t) = \sigma[A - Pc(t)] \tag{49}$$

where $R(t)$ is the structural strength, σ is the stress, A is the area of the member's cross-section, P is the perimeter of the exposed area to corrosive medium and $c(t)$ is the material loss in the case of uniform corrosion.

- In steel plates under bending loading with the presence of corrosion on both sides of the plate the structural capacity is:

$$R(t) = k\sigma_b[d(t)]^2 = k\sigma_b[d_o - 2c(t)]^2 \tag{50}$$

where k is a coefficient with values $k = 0.25$ for ductile materials and $k = 0.167$ for brittle materials, σ_b is the maximum value of the bending stress, $d(t)$ is thickness after any corrosive action and d_o is the initial thickness of the plate. The estimation of the quantity $c(t)$ for materials that show a ductile response can be obtained by measurements of the reduction of their weight or by calculation of the average corrosion depth. In brittle materials the point where the maximum local stress appears defines the maximum value of $c(t)$ that should be used.

In the case of pitting corrosion, the quantity $d(t)$ is calculated by:

$$d(t) = d_o - d_p(t) \tag{51}$$

with the term $d_p(t)$ to represent the maximum value of the pit depth as a function of time, which is considered important in structures such as pipelines and ships since the pit with the largest depth will result to the first penetration and possible failure. The above cases are presented in Figure 2.12.

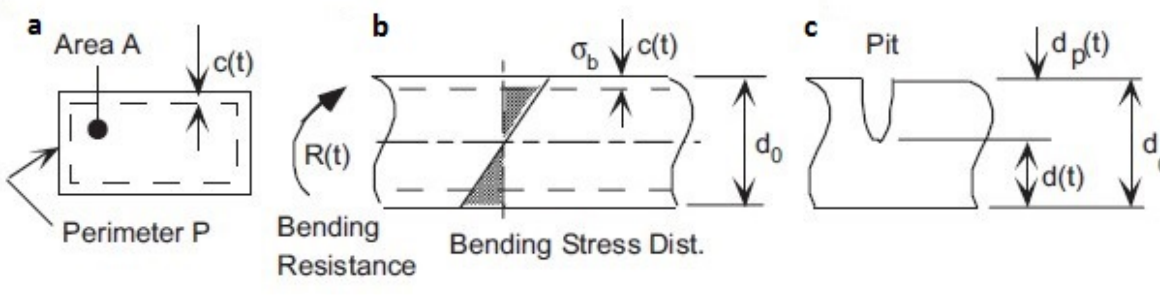

Figure 2.12: a) Bar member under axial loading with material loss due to corrosion b) plate under bending with effects from corrosion c) one side pitting of a plate (Melchers and Jeffrey, 2008)

The loss of material $c(t)$ in the case of uniform corrosion and the remaining thickness $d_p(t)$ in the case of pitting corrosion show a noticeable variation from the average corrosion rates, which are defined as the ratio of the above quantities to the exposure time t.Therefore it is recommended to be treated as random variables with terms that are function of time. This can be expressed for the loss of material $c(t)$ in the following way:

$$c(t, E) = b(t, E)fn(t, E) + \varepsilon(t, E) \tag{52}$$

where $c(t, E)$ is the material loss due to corrosion activity, $b(t, E)$ is a bias function that indicates the difference between the actual results and those predicted by the model, $fn(t, E)$ is a mean value function, $\varepsilon(t, E)$ is a zero mean uncertainty function while E is a vector of factors that define the environment the structural member needs to operate and certain characteristics of the material that has been used such as exact composition and content of carbon. The environmental factors are summarized in Table 2.1.

Table 2.1: Influence of environmental factor in marine corrosion (Melchers, 1999)

Factor	Effect on initial corrosion rate	Effect on steady state corrosion rate	Influenced by
Biological			
Bacterial	None	Reduces and probably controls rate	Temperature of seawater
Biomass/plant life			NaCl concentration
Animal life			Water velocity Suspended solids Pollutant type and level Percentage wetting
Chemical			
O_2	Directly proportional	None, if corrosion controlled by O_2 transfer rate	Seawater temperature
CO_2	Little effect	Little effect	
NaCl	Inversely proportional	Proportional	Unimportant in open oceans Fresh water inflows Effect of biological activity
pH	Little effect	Little effect	
Carbonate solubility	Little effect	Little effect	
Pollutants	Varies	Varies	Geographical location
Physical			
Temperature	Directly proportional	Proportional	Geographical location
Pressure			Not significant for shallow waters
Water velocity	Little effect	Little effect	Geographical location
Suspended solids		Little effect, if any	Geographical location
Percentage wetting	Proportional for tidal and splash zones	Proportional for tidal and splash zones	Location, weather patterns

The average amount of material that has been lost due to corrosion and the resulting reduction of thickness are important for the derivation of the structural capacity. This the reason why Eq. (52) is ideal for this purpose since it calculates the average value of the total material loss and its deviation around the mean. For pitting corrosion in which the emphasis is given in identifying the pit with the largest depth a relation similar to Eq. (52) can be used.

The term $\varepsilon(t, E)$ of Eq. (52) defines the quality of the model and its decrease will have positive impact to the performance of the model. That can be achieved by producing a high-quality model for the mean value function $fn(t, E)$, which requires similar level of quality regarding the measured data and knowledge of the corrosion mechanisms. On the other hand, a mean value model of inferior quality will lead to high irregularity of the error term $\varepsilon(t, E)$.

Principles form corrosion science and marine bacteriology were used for to develop corrosion models for the prediction of material loss and crucial pit depth in marine environments. During the first stages of exposure to seawater, corrosion activity is controlled by the rate the metal is oxidized by oxygen. For longer periods of exposure, the metabolism rate of anaerobic bacteria controls the corrosion process. Because the models are based on a combination of physical and chemical concepts, there is the need of calibration to the field data. This has been completed by using data that are available in literature, which are also used for a prediction of the error term $\varepsilon(t, E)$ and several parameters of the vector E . Both models for general corrosion and pitting corrosion can be seen in Figure 2.13. It is assumed that no removal of corrosion products takes place since little evidence exist to support the notion that waves, or water motion can wash away parts of the corroded material. The two models demonstrate certain similarities except for the larger pit growth after the metal is exposed to seawater. Also, the term r_o,which represents the corrosion rate at early stages doesn’t exist in the pitting depth model since several days of exposure are required for any substantial pit to grow (Melchers and Jeffrey, 2008).

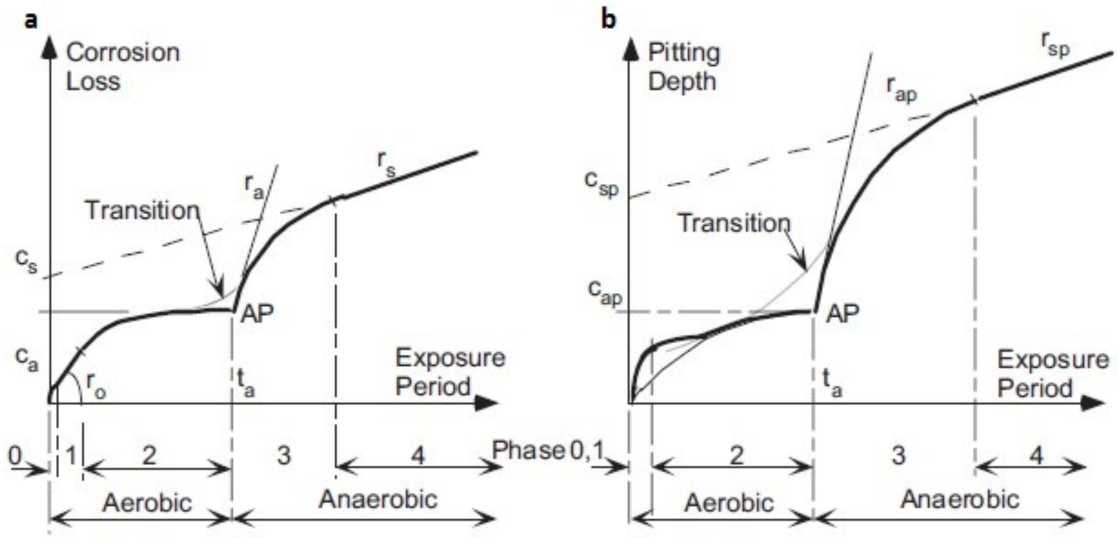

Figure 2.13: Mean value function model a) General corrosion b) Pitting corrosion (Melchers and Jeffrey, 2008)

Both models demonstrate several phases, which evolve along with the exposure period and are associated with the different mechanisms of the corrosion rate. According to Melchers (2003), Melchers and Jeffrey (2008) these phases are:

- Phase 0

Marine life such as bacteria and other organisms are starting to develop on the surface of the steel specimen shortly after immersion. The rate of corrosion is controlled by several local chemical reactions, which are not largely affected by any external factor.

- Phase 1

During immersion of the steel specimen in seawater the ions of iron (Fe) are dissolved and diffused from its surface to the electrolyte while the corroded surface is provided with oxygen (O_2) and it receives the electrons, which are formed during the dissolution of the iron (Fe). Both reactions result in a cathodic and anodic polarization according to the equations:

$$Fe \longrightarrow Fe^{++} + 2e^{-} \tag{53}$$

$$O_2 + 2H_2O + 4e^{-} \longrightarrow 4OH^{-} \tag{54}$$

This state of polarization is temporary and seizes in short time after equilibrium has been reached and a steady flow of current i is observed. In theory the process described by the above equations could control the corrosion activity. The usage of oxygen in the area near to the corroded surface of the material results in the local decrease of oxygen forcing it to start moving towards the surface where corrosion occurs. By controlling the concentration of oxygen, the regulation of corrosion is achieved according to the relationship:

$$i = \frac{nFDC}{\delta} \tag{55}$$

where i is current during corrosion of the material, n is the number of electrons that take part in the reaction described by Eq. (54), F is the Faraday constant, D is the oxygen diffusion coefficient, C is the oxygen concentration in the volume of the electrolyte and δ is the thickness of the diffusion layer, which is the area close to corrosion surface, where the oxygen flux takes place.

Stagnant waters show a slow rate of corrosion because the water layer near the corroded surface is saturated by oxygen making its flow from the atmosphere to the surface and finally to the points of corrosion a constricting factor.

The corrosion current i is affected by several parameters with an increase of its value to be observed when the diffusion layer thickness δ is reduced in tests under laboratory conditions because of the action of water velocity and turbulence. These conditions correspond in sea states where waves and currents have a strong presence in the early period of exposure to seawater. The diffusion coefficient D shows a dependency on temperature and an increase of the latter will lead to an increase of the current i.However, temperature also controls the ability of the oxygen to be dissolved in the seawater, which diminishes with temperature increase. The most direct relation to the corrosion current i must be attributed to the provision of oxygen in the seawater close to the corroded surface. Conditions that permit the solubility of the oxygen are expected mostly at sea due to the increased turbulence and mixing.

Marine life is another feature that can be seen in the surface of a material immersed in seawater and starts as a layer of bacteria and other microorganisms with the form of a biofilm. As the corrosion activity progresses this biofilm together with other kinds of biological coating increases in size and can create problems in the sufficient flux of oxygen to the surface underneath. At this point corrosion rate begins to be controlled by oxygen diffusion.

- Phase 2

The most important feature of this phase is the dependence of corrosion rate on the oxygen's ability to penetrate the layer of the oxidized material and marine life. The diffusion of the oxygen through a penetrable layer with an increased thickness over time can be expressed by:

$$\frac{dO_2}{dt} = \frac{k(C_0 - C_i)}{D_{cp}} \tag{56}$$

where O_2 is the mass of the oxygen flow, C_0 is the oxygen concentration in the seawater volume away from the area of corrosion activity, C_i is the oxygen concentration in the boundary between the surface of the material and the layer of corrosion and biological products, D_{cp} is the diffusion coefficient for the oxidized part of steel and k is a constant.

Theoretical approach and field measurements have concluded that oxygen consumption and corrosion show a linear behavior and it is reasonable to assume that a linear relation exists between the process of corrosion and the quantity C_0. Based on the previous assumption the amount of material loss due to corrosion is:

$$c = \sqrt{at + b} \tag{57}$$

with a, b to be constants. It must also be noted that the thickness of the corroded product shows a uniform density. If the corrosion rate is controlled by the diffusion of oxygen at the first stages of exposure, which is rejected by the theoretical analysis or for small values of the constant b, Eq. (57) becomes:

$$c = dt^{0.5} + e \tag{58}$$

where d and e are constants.

- Phases 3-4

As the growth of the biological coating and the oxidized material continues, the amount of oxygen that can penetrate the layer of these products is reduced. Months or years are required for the layer to create these conditions. At this point anaerobic bacteria are starting to appear if the food supply is sufficient enough to support them. Since their survival is not related to the presence of oxygen, other factors can contribute to their growth such as chemical composition of the material and temperature of the surrounding environment. Corrosion in these phases appears mostly in the form of pitting with the concentration of oxygen in the pits to be very low even close to zero (Melchers, 2018). The amount of corrosion that corresponds to the anaerobic activity is estimated by:

$$c_{an} = \mu\alpha(t - t_a) + \beta \tag{59}$$

with μ to represent the availability of moisture, α is a constant relevant to corrosion rate and β is a constant that defines the corrosion depth at the time t_t, which signifies the transition to the anaerobic stage of the corrosion activity.

The calibration of the model is achieved by using corrosion data from swallow coastal test sites with low water velocity and insignificant degree of pollution. This fact has allowed the term E of Eq. (52) to be reduced to the mean value of the seawater temperature T with a small error margin. In this way the parameters that are described in Table 2.2 can use available data in literature as a source of calibration having only the temperature T as the main variable (Melchers and Jeffrey, 2008).

Table 2.2: Model parameters calibration for general and pitting corrosion (Melchers and Jeffrey, 2008)

Model parameter	General corrosion	At 10^oC	Pitting corrosion	At 10^oC
r_o(mm/year)	$r_o = 0.076\exp(0.054T)$	0.13	-	
c_a (mm)	$c_a = 0.32\exp(-0.038T)$	0.22	$c_{ap} = 0.99\exp(-0.052T)$	0.59
t_a (year)	$t_a = 6.61\exp(-0.088T)$	2.75	$t_a = 6.61\exp(-0.088T)$	2.75
r_a(mm/year)	$r_a = 0.066\exp(0.061T)$	0.12	$r_{ap} = 0.596\exp(0.0526T)$	1.01
c_s (mm)	$c_s = 0.141 - 0.00133T$	0.13	$c_{sp} = 0.641\exp(0.00613T)$	0.68
r_s(mm/year)	$r_s = 0.039\exp(0.0254T)$	0.05	$r_{sp} = 0.353\exp(-0.0436T)$	0.23

As it was noted in Melchers (2018) the criticism about this bimodal model is focused on its seeming complexity. However, if only long-term corrosion is of interest phases 0 to 3 can be neglected resulting in a simplification of the phase 4, which can be expressed by a linear function in the form of:

$$c(t) = a + bt \tag{60}$$

with the coefficients a and b to be equal to the model parameters c_s and r_s respectively.

In the case of pitting corrosion, the pit with the largest depth appears to be most important because it can lead to the perforation of the plate and the loss of functionality of the structure such as pipes, tanks or vessels. Therefore, it is sensible to seek the maximum value of the pit depth as a function of its occurrence probability. Gumbel distribution is applied for this purpose to obtain the largest extreme value from an extreme value distribution. Traditionally a simple power law model is adopted as a starting point for a maximum pit depth analysis, which can have the form of $d_p = At^B$, where the maximum pit depth is expressed as a function of time with A and B to be empirical constants. This makes possible the collection of data from different times of exposure to be used in the extreme value analysis. Figure 2.14 shows the distribution of the largest value of pit depth as well as the average of six deepest pits with the period of exposure. It becomes clear that the power law doesn't seem to follow the distribution pattern of these two quantities and it is safe to conclude that the choice of the power law model will result in an extreme value analysis with an increased degree of inaccuracy (Melchers and Jeffrey, 2008).

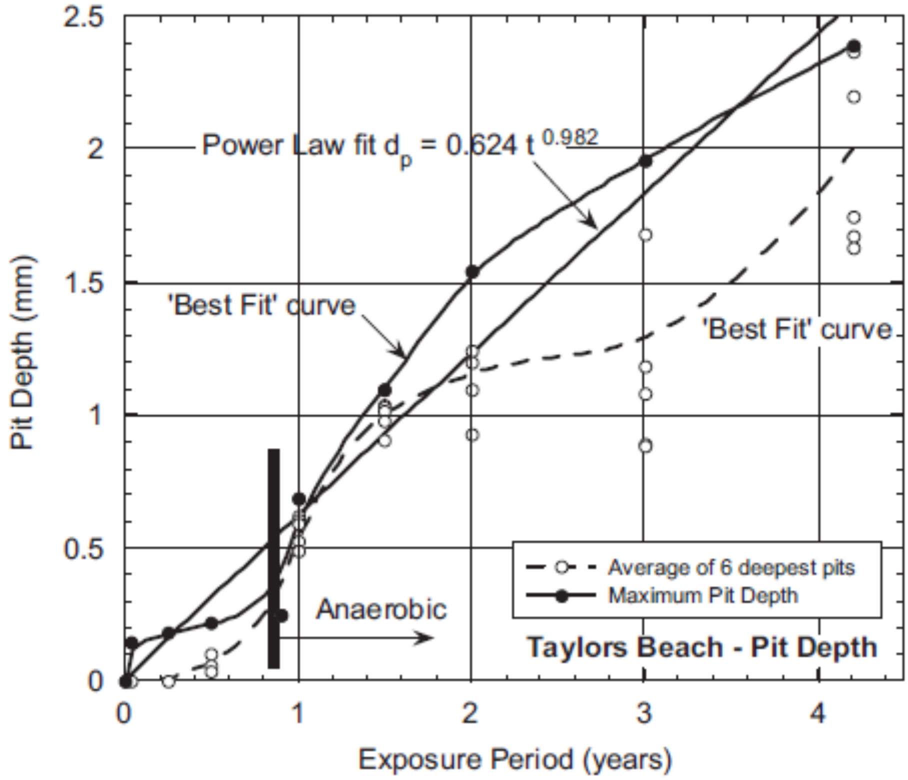

Figure 2.14: Maximum pit depth as a function of exposure time (Melchers and Jeffrey, 2008)

The inefficiency of the power law model can be explained by the incoherent nature of the corrosion mechanism. The pitting activity results in two types of pits, the stable pits whose depth continues to grow with time after their initiation and the metastable pits that tend to delay their start or their growth seizes after a period of time (Paik and Melchers, 2008). Both of these types exist during phase 1 and 2 of the pitting corrosion process but only stable pits is assumed to produce extreme values of depth. The latter are also known as super-stable since they start to generate when the opportunity is provided while their rate of growth depends on the environmental and material conditions. After a period of time a change in the pattern of pitting is observed with the appearance of broad pits, which are formed from the fusion of smaller pits in anaerobic conditions (Melchers and Jeffrey, 2008). This change means that the population of pits becomes different with consequences in the way is treated by statistics. During phases 3 and 4 extreme depth of pits can be more precisely represent by Frechet distribution rather than Gumbel.

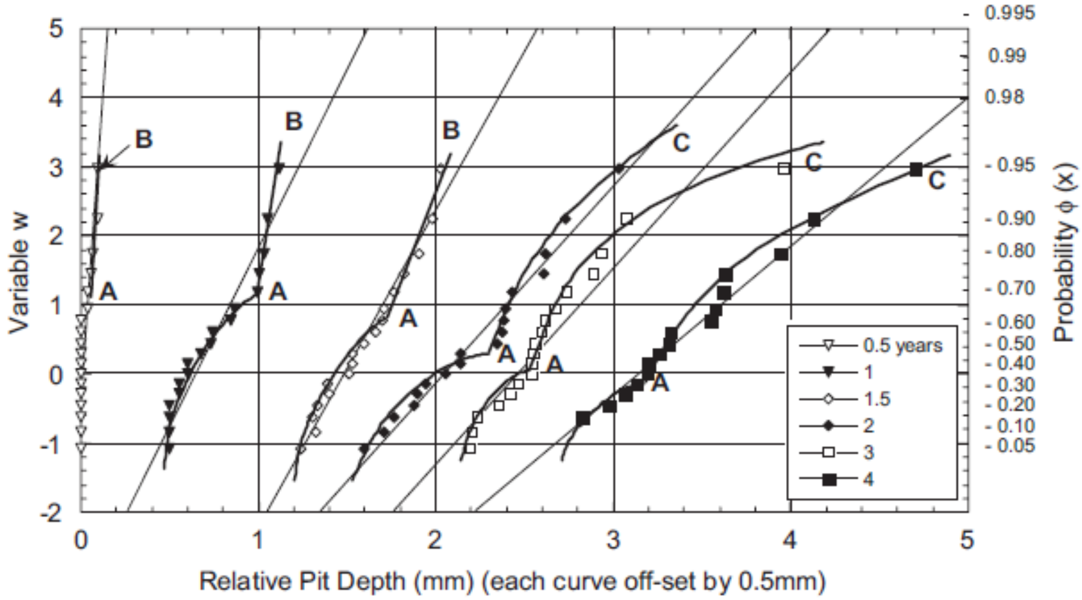

Figure 2.15: Maximum pit depth in a Gumbel plot from mild steel coupon data(Melchers and Jeffrey, 2008)

By observing Figure 2.15 the data show a significant deviation from the linear pattern of a Gumbel distribution. In order to determine the maximum pit depth during all phases of exposure, all data below the point A, which defines the transition from metastable to stable pit growth under aerobic conditions, should not be considered. For short periods of exposure such as phase 1 and 2 Gumbel distribution seems to be appropriate for the data above point A, which leads to lower occurrence probabilities for a specific extreme depth. The obvious feature of the data in phases 3 and 4 is non-linearity that is described better by Frechet distribution and results in higher occurrence probabilities for a given extreme depth, which can lead to serious implications, when the probability of perforation is required to be calculated (Paik and Melchers, 2008).

2.2.3 Corrosion model summary

The thickness reduction of a structural member, which assumes a constant corrosion rate, results in a linear expression between loss of material and time, which is a crude approach of the corrosion wastage. A nonlinear model seems to be more suitable as it has proven by experimental corrosion data provided by several authors (Garbatov and Guedes Soares, 2008).

Corrosion data obtained by field tests resulted in the corrosion wastage representation as a function of exposure time of Figure 2.16. It can be observed that after 2-5 years the rate of corrosion becomes approximately uniform, which has led to the linear expression of the Southwell et al. (1965) model. It can also be seen that the models suggested by Melchers and given by Eq. (5) and Eq. (7) show difficulty in complying with the existing data (Melchers, 1999).

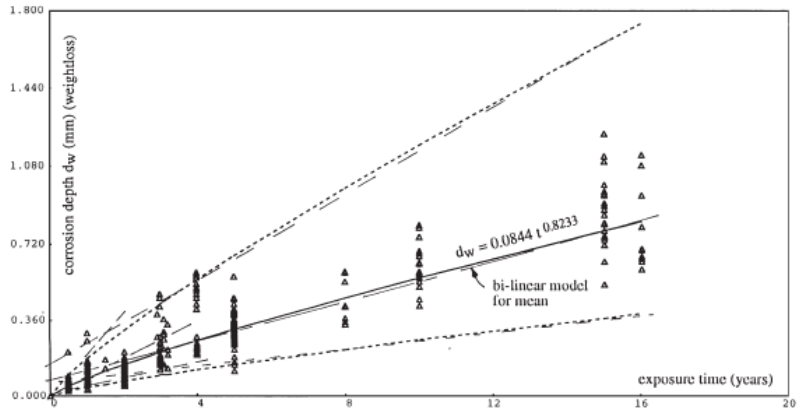

Figure 2.16: Corrosion wastage as a function of exposure time (Melchers, 1999)

Yamamoto and Ikegami (1998) suggested a corrosion model based on the assumption that general corrosion is the product of the progression of a large number of hemispherical pits. The result is a nonlinear model with a significant degree of complexity that shows the corrosion wastage to level off with time. Fitting the model to existing data didn't lead to satisfying results (Melchers, 2008).

Paik et al. (2003a) divides the corrosion wastage into three phases with coating life to be described by a lognormal distribution followed by the transition phase when the coating loses its efficiency initiating the corrosion activity. An exponential distribution is assigned to the second phase while the last phase, when corrosion progression takes place, can be represented by a concave, convex or linear curve. No clear explanation exists about which type of curve should be chosen beyond the empirical approach of fitting the measured data (Paik and Melchers, 2008). Also it is not realistic to assume that during the transition phase no corrosion damage occurs (Wang et al., 2014).

The same kind of division is followed by Garbatov and Guedes Soares (1999) in the model they suggested. The presence of the protective coating doesn't allow the corrosion process to start, defining the first phase in the model. Damage of the coating enables the corrosion progression during the second phase. The increase of thickness of the corrosion products slows down the corrosion rate, which is eventually minimized at the end of the third phase. However, there is no clear distinction between the two last phases (Melchers 2008).

The model developed by Qin and Cui (2003) uses Weibull distribution to predict the corrosion wastage in surfaces of mild steel. The suggested corrosion process shows a different pattern in which after a period of corrosion absence, an acceleration of the corrosive activity takes place until the point when general corrosion starts to appear followed by a deceleration of the process till the end of the structure's lifetime. Among the features that belong to the advantages of this model is its flexibility and the ability to describe the previous models by changing certain parametric values. However, it is difficult to come to a conclusion regarding its accuracy since an assumed set of corrosion data were used for fitting the model instead of real data (Wang et al., 2014).

Unlike the previously described models, which are based on corrosion measurements, the alternative suggestion by Melchers (2003) was a nonlinear mean value corrosion model, which consist of five phases applicable for mild steel for at-sea immersion conditions. Its development used data from coupon experiments starting from the argument that estimation of long-term corrosion wastage can be inaccurate if short-term laboratory measurements is the only source of data (Wang et al., 2014). The model focuses on the mechanisms of corrosion instead of providing a practical mean of corrosion loss prediction (Garbatov and Guedes Soares, 2008).

A summary of the advantages and disadvantages of the previously described corrosion models is presented in Table 2.3.

Table 2.3: Corrosion model review

Model	Advantages	Disadvantages
Southwell et al.	Based on a realistic source of data	Overestimation of corrosion loss in the early stages of exposure
Melchers – extension of Southwell et al	Mathematical refinement	Difficulty in complying with existing data
Yamamoto and Ikegami	Probabilistic model	Significant degree of complexity Not a good fit to existing data
Paik et al.	Practical corrosion wastage tool	No clear explanation about which curve should be chosen Unrealistic assumption of corrosion damage absence during transition phase
Garbatov and Guedes Soares	Practical corrosion wastage tool	No clear distinction between two last phases
Qin and Cui	Flexibility Ability to describe other corrosion models by parametric change	No conclusion about accuracy Fitting the model based on assumed data
Melchers	Description of actual corrosion mechanism	Complexity

2.2.4 Corrosion model selection

The description of the corrosion models of the previous chapters aimed to identify their function, the background of their development together with advantages and possible disadvantages. A common feature of most corrosion models is the complexity they can show, which is understandable since corrosion processes can be influenced by many factors and the accurate prediction of the material loss cannot be expected to be a simple task. Normally an estimation of the corrosion wastage requires knowledge of the corrosion rate of all structural members. A theoretical approach is not usually preferred because of the dependency of corrosion to several different variables and the uncertainties they can include. Statistical analysis of past data in similar cases appears to be a feasible option especially when access to long-term corrosion data in real environment hardly exists. However, the choice of a suitable corrosion model should be also governed by the objectives of every study. If the goal is to provide a mean to calculate the thickness reduction in an easy and relative accurate manner without the use of corrosion data from past measurements, then most of the above models don't appear to be a practical option to the present study. A possible solution can be found in the Paik et al model. According to Paik et al (2003a) the process of corrosion is divided in three phases that describe the coating life, the transition interval between loss of coating effectiveness, which forces the corrosion to initiate, and corrosion progression. The latter can be expressed by an initial increase of the corrosion rate followed by its decrease as the corrosion process continues or by an accelerating corrosion rate. Between these two cases a linear approximation is not excluded. The corrosion progression is described by Eq (23):

$$t_r = C_1(T - T_c - T_t)^{C_2}$$

The coefficients C_1 and C_2 are determined using statistical analysis of past data, which involves certain difficulties that stem from the way the data are collected, resulting in large scatter of the material loss measurements. Alternatively, the coefficient C_1 can be calculated regarding C_2 as a constant value, which leads to a mathematical simplification of the model but it doesn't eliminate the dependency on previous corrosion data. A range of values between 0.3-1.5 is typical for the coefficient C_2 (Paik et al., 2003a). These values correspond to a gradual decrease of the corrosion rate, which can be seen in statically loaded structures, but it may be misleading for cases where conditions promote the acceleration of the corrosion rate. Nevertheless, it has been observed that C_2 doesn't have any significant influence as the age of a ship increases. Therefore, it can be assumed that C_2=1 resulting in a constant annual corrosion rate (Paik et al., 2003a).

Having decided about the value of C_2 statistical analysis needs to be used for the calculation of the coefficient C_1 based on corrosion data from past measurements. By assuming that there is no transition time and the ship's operational profile exceeds the 25 years, the corrosion wastage can be expressed as:

$$t_r = C_1(T - T_c - T_t)^{C_2} = C_1(T - T_c) \tag{61}$$

for C_2=1 and T_t =0.

The above equation can be used for the determination of corrosion margins for the case of a ship with a service life of 25 years accepting an average coating life of 7.5 years after the statistical evaluation of the material loss data of the several structural members of the hull. The corrosion rate can be defined from the above equation in the following way:

$$C_1 = \frac{t_r}{(T - T_c)} \tag{24}$$

The total loss of the corrosion margin would reflect a situation where the ship has reached the end of its lifespan of 25 years while 50% of the margin represents 16 years of operation as it can be derived from the above equation (Ringsberg et al., 2018). The use of the corrosion allowance as it is provided by the Common Structural Rules (IACS, 2019) makes possible the calculation of the coefficient C_1. If the corrosion rate is known the thickness reduction for every time point within the service life of ship can be determined from Eq. (24). The corrosion margin is not a randomly selected figure but the product of a procedure which involved 600.000 measurements of thickness reduction of both tankers and bulk carriers with an age variation between 6 and 27 years. The statistical analysis resulted in the corrosion diminution with cumulative probability of 95% for 25 years of service, which it was followed by the definition of the corrosion margin according to the environmental conditions every structural member is exposed (Nieuwenhuijs et al., 2006). In this way the choice to use this material allowance does not violate the background of the model suggested by Paik et al., (2003a). Furthermore, the simplicity and the detachment from the direct use of thickness reduction measurements serves the needs of the present study.

2.3 Change of material properties

The correlation between corrosion and steel's mechanical properties were investigated in the study of Garbatov et al. (2014), which was based on the results from tensile tests with corroded specimens. The experimental process included the use of several girder specimens that were exposed in seawater conditions for a period of 90 days allowing the generation and growth of corrosion. Test specimens were cut off from the corroded girder in a specific shape suitable for use in tensile testing as it can be seen in Figures 2.17 and 2.18. The corrosion showed a non-uniform distribution while appeared to be in an advanced stage in many parts of the specimens whose thickness was measured 4.5 mm in parts unaffected by corrosion.

Figure 2.17:Tensile test specimen (Garbatov et al., 2014)

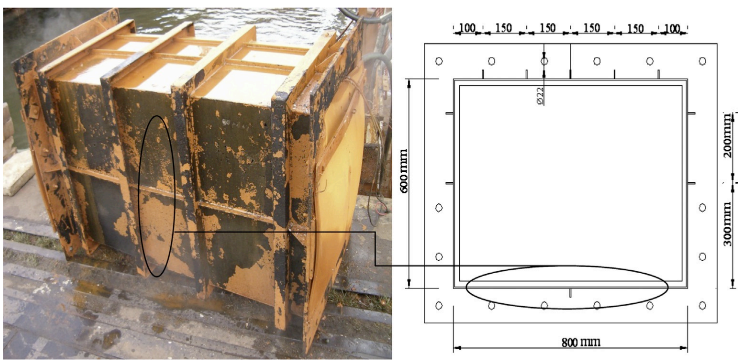

Figure 2.18:Location of test specimens in the box girder (Garbatov et al., 2014)

The severity of corrosion is quantified by the degree of degradation D which is defined by the equation:

$$D = \frac{V_o - V_c}{V_o} \times 100\% \qquad (62)$$

where the terms V_o and V_c represent the intact plate volume and the corroded volume respectively. The latter term is given by:

$$V_c = \int_l \int_b h(x, y) dx dy \qquad (63)$$

The parameters l, b in Eq. (65) are the length and breadth of the test specimen while h is its thickness.

The statistical analysis of the data which were gathered during the tensile test of the specimens led to the following expressions for Young's modulus and the yield stress as well as the construction of stress-strain curves with a variation of the degree of degradation:

$$E(D) = -1.0349D + 196, GPa \quad (64)$$

$$\sigma_{YS}(D) = -0.0229D^2 + 0.5551D + 235, MPa \quad (65)$$

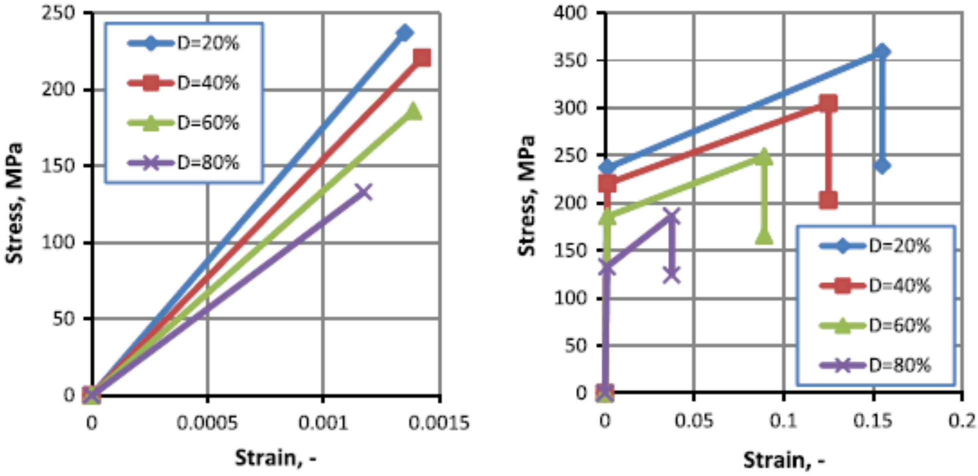

Figure 2.19:Linear elastic(left) and bilinear elastic-plastic stress-strain (right) curves (Garbatov et al., 2014)

Figure 2.19 shows a noticeable reduction of strength when the degree of degradation rises above 20%. Apart from the loss of cross section the observed strength reduction can be attributed to the change of the material properties caused by corrosion activity and to the generation of local stress concentrations due to corrosion pits (Garbatov et al., 2014).

2.4 Ship collision simulations

During the service life of a vessel accidental events such as ship-to-ship collisions may occur with severe consequences such as loss of human life, degradation of structural integrity and contamination of marine ecosystems (Youssef et al., 2014). Ship collisions can be divided in to side collisions, see Figure 2.20 and head-on collisions. In the case of side collisions, the side structure of a ship is struck by the bow of the striking ship allowing the damage in both structures to absorb most or the entire kinetic energy. However, the struck ship will probably suffer more damage in its structure due to the larger stiffness of the striking ship's bow. When the bow of a vessel strikes a rigid wall such as piers and bridge abutments the situation is defined as a head-on collision. The larger part of the kinetic energy in this case is consumed by the deformation of the bow (Paik et al., 1999). The progress of a collision is governed by an external and internal mechanism that dictate the extent of the damage. The rigid-body global motions of a ship and hydrodynamic forces constitute the external mechanism, which is defined by parameters such as the mass of both ships involved in a collision, their velocities, the point of impact at the struck ship, the collision angle of the striking ship and the hydrodynamic forces. The external mechanism controls the amount of kinetic energy that is absorbed by the structures of the struck and striking ship during a collision. The way this energy is transmitted to both structures is determined by the internal mechanism and is affected by factors such as the arrangement of the structural members of the vessels, their material properties, the bow geometry of the striking ship and the failure mode. The cargo must be also considered in the energy distribution of the collision as it can severely influence the length of the bow's penetration. In the general case of a collision between an idle ship and a striking vessel at a 90° angle, the maximum penetration can be achieved while the energy absorption will reach its largest value when the point of impact is located in the middle of the ship and not further away where part of the striking ship's energy will be lost in increasing the yaw motion of the struck ship (Karlsson, 2009).

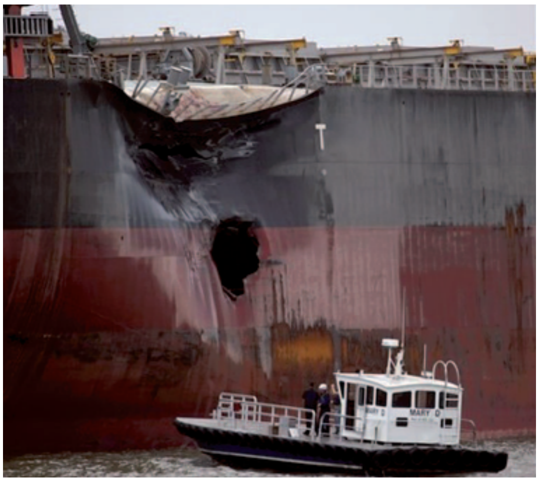

Figure 2.20:Example of side collision (Ringsberg, 2011)

The structural response during a collision, which is described by the internal mechanism can be simulated by using empirical formulae, simplified analytical methods, model experiments and non-linear Finite Element Method (FEM), see Figure 2.21 (Ozguc et al., 2005). FEM has become the primary choice in conducting and analyzing collision simulation and is classified in linear and non-linear. The use of non-linear finite element method enables the calculation of stresses and deformations of structural members of general loading and material properties that can include time-dependent loading, large deformations and materials with non-linear behavior. Complexity is a feature of non-linear analysis that is compensated by the accuracy of the results in cases when a linear approach can't be chosen (Bae et al., 2016). Modelling of the process that needs to be simulated and realistically considering all its aspects such as material failure and setting the necessary boundary conditions plays an important role in to the accuracy of the non-linear FEM. Several modelling techniques are required to properly simulate the complexity of the patterns of a structure under loading. Explicit methodology is applied for the analysis of collision or grounding, which is more suitable in dealing with non-linearity and other aspects such as contact, friction and rupture (Ozguc et al., 2005). Adopting an explicit finite element code makes possible the better use of simulation models consisting of a large number of elements accepting in the same time a reduction of the accuracy level, which can be controlled by the choice of fine mesh , element size and suitable time increment (Kitamura, 2002). Establishing the suitable strain rupture criteria is a crucial part of the FEM since it affects largely the accuracy of the calculation. Uniaxial tensile tests are used to correlate the element size and the rupture strain allowing the definition of the criterion when failure is expected (Zhang and Pedersen, 2017). Details about the use of FEM in collision simulations can be found in the work of Ehlers (2010) in which the relation between material and accuracy of the results was investigated as well as in the study of Marinatos and Samuelides (2015). The latter aimed to the derivation of a procedure for ship impact simulations, which would permit an improved description of the material response till rupture and contributed in the increase of the reliability of the results. The robustness of the applicable fracture criteria was examined by Storheim et al. (2015) attempting to identify the level of trust for each criterion when data from uniaxial tensile test are used for their calibration. Furthermore, in the study of Haris and Amdahl (2013) different collision scenarios were selected to be simulated in order to produce virtual experimental data.

The damage size was evaluated in the study of Hogström and Ringsberg (2012), which involved the investigation of the survivability of a RoPax ship during collision. Several finite element simulations were conducted to determine the influence of the following parameters:

- Material dispersion
- Failure criteria
- Bow modeling of the striking vessel
- Friction coefficient
- Speed and collision angle

Failure of the material, which leads eventually to fracture is modelled by choosing three different damage initiation criteria. The shear criterion is widely used in ship collision simulations while the FLD and FLSD criteria for multiaxial strain rate and multiaxial stress state respectively were also chosen in the study for comparison reasons. Results from the simulations led to the conclusion that an earlier damage of the material is observed when the shear criterion is applied. In addition, the FLD criterion seems to initiate the damage process faster than the FLSD criterion. It was concluded that the shear criterion appears to be more suitable for ship collision simulations.

The striking vessel can be represented by a simple conical shape or it can include a deformable bow structure with increased level of accuracy. Modelling and computational time usually enforce the adoption of a rigid bow. Comparison between a deformable and a rigid bow showed that the former causes smaller damage openings. Usually the part of bow designed to deform is responsible for any damage since its strength allows it to survive the collision while the main body of the bow is subjected to buckling and plastic deformation without breaching the outer shell in any of the involved vessels. However, the damage caused by the deformable bow appears with a larger vertical extent when an increase of the collision speed from 5 knots to 7 knots occurs. In general, the same variation of speed doubles the kinetic energy and the size of the damage opening. The change in the collision angle can't answer clearly which value leads to the larger opening size since in most of the cases an angle of 90° will cause a large damage opening while a reverse pattern is observed when the collision angle changes to 45°. Moreover, the combination of a rigid bow and an oblique collision angle will produce a large crack both in vertical and horizontal direction compared to a collision at a right angle (Hogström and Ringsberg, 2012).

Ship collision simulations involve a variation of the friction coefficient between 0.3 and 0.6. Less friction work is caused by a low value of the friction coefficient allowing larger part of the initial kinetic energy to be used for the deformation and rupture of the structure. The presence of water in the external plating below the waterline and the biological coating in the ballast tanks, which acts as lubricant combined with the roughness of most surfaces in a vessel, can alter the above range of friction coefficient to 0.1-0.6 in real conditions. The analysis of the results showed that the influence of the friction coefficient is small and is usually overshadowed by the other parameters (Hogström and Ringsberg, 2012).

The effect of corrosion in ship collision events was considered in the study of Campanile et al. (2015), which adopted a statistical approach to investigate the hull girder residual strength using three damage scenarios. The influence on the ultimate strength caused by the combined action of ship-ship collisions and material degradation due to corrosion in a series of collision simulation is the subject in the work of Ringsberg et al. (2018). The corrosion model developed by Paik et al. (2003) was chosen to express the material loss in both cases.

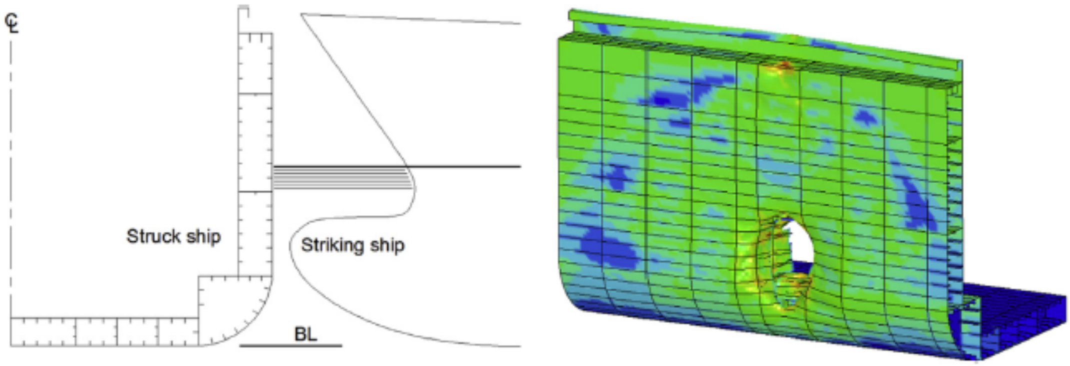

Figure 2.21:Ship collision simulation (Liu et al., 2017)

2.5 Ultimate strength assessment

The condition that is described by the failure of structural member to perform its function defines a limit state. Four types of limit states exist but only the Ultimate Limit State (ULS) serves better the purposes of a ship's ultimate strength determination. The hull girder of a vessel consists of stiffened plates and is subjected to several forces relevant to the weight of the structure and cargo. Forces from the external environment such as buoyancy and wave force must also be included. Because of the action of these forces, bending and torsional moment as well as shear force are developed in the hull girder whose ability to resist this loading combination defines its longitudinal strength. The derivation of the ultimate strength occurs according to the following criterion (ISSC, 2015):

$$\gamma_S M_S + \gamma_W M_W \leq M_U / \gamma_M \tag{66}$$

where, M_S is the maximum still water vertical bending moment, M_W is vertical bending moment due to wave action, M_U the ultimate bending moment that the hull girder can withstand while the remaining terms represent partial safety factors.

The features of the hull girder ultimate strength can be influenced by several factors such as:

- Dimensions of structural members
- Material properties
- Existing imperfections
- Type of loading – possible additional loads
- Age-related material degradation
- Accidents
- Human errors

Although all the above factors affect the magnitude of the ultimate strength, the most severe contribution must be attributed to any imperfection and more precisely to the presence of an initial deflection. If a stiffened panel is loaded in compression an initial deflection will lead to an additional bending moment, which reduces its loading capacity. The mechanism that controls the ultimate strength reduction depends not only on the magnitude but also on the shape of the existent deflection. Structural elements such as shells are more susceptible to an initial deflection compare to other elements. When a shell structure buckles, its load carrying capacity is lowered equating both buckling and ultimate strength. However, the same pattern is not observed in the case of a constraint plate structure subjected to in-plane compression, whose ability to carry loads shows an increase when elastic buckling occurs. The buckling and the ultimate strength are not the same in this case with the latter to appear when lateral deflection creates a bending moment forcing the plate structure to yield. During hogging the hull girder shows a compression of its bottom while the deck structure is loaded in tension. The maximum level of the bending moment appears when the ultimate strength of the bottom and the yield stress of the deck are reached. After yielding occurs the level of stress tends to be maintained by the deck structure. Conversely, during sagging conditions the hull girder develops a bending moment maximum value when ultimate strength is obtained by the deck, which is loaded in compression and the stress in the bottom becomes equal with the yield stress. The deck structure can't resist to any increase of the bending moment due to sagging once its ultimate strength is reached defining in this way the ultimate strength of the hull girder. Therefore, it becomes obvious the importance of the post buckling strength of a stiffened structure for the accurate calculation of the hull girders longitudinal strength (ISSC, 2015).

The assessment of the hull girder ultimate strength was first attempted by Caldwell (1965) whose work was based on the assumption that the cross-section of the structure composed by stiffened panels can be idealized by panels with equivalent thickness. The calculation of the bending moment at which the entire cross section has reached its yield stress was followed. The determination of the fully plastic bending moment was performed by considering the effect of buckling introducing a reduction factor, which it was multiplied with the yield stress (Yao, 2003). Caldwell's method was used in the study of Nishihara (1982) calculating the ultimate strength of several test girders resulting in an improved accuracy of the strength reduction factors (Yao, 1999). Further development of methods for the direct calculation of the ultimate strength was promoted by Paik and Mansour (1995) and others. These methods are applicable to relatively simple structural geometries and fail to consider the effect of post-collapse strength reduction under compressive loading (ISSC, 2015).

A simplified method was proposed by Smith (1977), which included the gradual collapse of the hull girder's structural parts during the increase of the longitudinal bending moment. According to Smith's method a division of the cross section takes place, which is represented by small elements. Several stiffeners and plating are used to formulate these element, whose average stress-average strain relationships is determined under axial loading without neglecting any buckling or yielding effect. The collapse analysis that follows assumes that the position of each plane cross-section is not affected by the deformation of the structure and each element's behavior obeys to the determined average stress-average strain relationship (Yao, 2003). Considerable efforts were made by several researchers to investigate the relationships between average stress and average strain, which is needed for the Smith's method. In the study of Gordo and Guedes Soares (1993) and Gordo et al. (1996) the above described correlation was modelled for the case of stiffened steel panels with the use of simple formulae. The same objective can be found in the work of Chen and Guedes Soares (2008), which the average stress-average strain relationship was determined for stiffened composite panels with finite element method (Chen, 2016).

The definition of the behavior of each element allows the use of an incremental process that produces the moment-curvature response when the structure is subjected to both vertical and horizontal bending moments. Two methods can be selected to carry out the previously described process: an incremental-iterative method and pure incremental method. The former adopts an iterative approach to calculate the position of the neutral axis for every curvature by determining the position in the cross-section with zero resultant force. In the latter method a small increase of the curvature is permitted for each load step. In the work of Fujikubo et al. (2013) a new approach of the second method was suggested and applied in the study of the rotation of the neutral axis in tankers and bulk carriers, which concluded the bigger importance of the neutral axis's rotation for bulk carriers compared to tankers (Guedes Soares and Santos, 2018).

According to Yao (2003) the existing methods for the calculation of the hull girder's ultimate strength can be classified in simple and advanced methods. The former is used for ultimate strength analysis while the latter for ultimate strength, failure mode and post-buckling collapse analyses. The first category includes methods such as initial yielding, elastic analysis and assumed stress distribution while progressive collapse analysis with idealized σ-ε curves, progressive collapse analysis with computed σ-ε curves, idealized structural unit method (ISUM) and non-linear finite element method (FEM) belong to the second category. These methods are briefly described in the following way:

- Initial yielding

The longitudinal strength is calculated by using the initial yield stress according to the equation:

$$M_{IY} = Z\sigma_Y \tag{67}$$

where Z and σ_Y represent the section modulus of the hull's cross section and the yield stress of the material respectively (Yao, 2003).

- Elastic analysis

This method is based on the initial yielding by replacing the yield stress term in the previous equation with the buckling strength of the stiffened panel used in the construction of the bottom or deck part of the hull girder (Yao, 2003).

- Assumed stress distribution

The method developed by Caldwell (1965) is similar with the assumed stress distribution method. Furthermore, during the calculation of the bending moment the yield stress of the element under compression is substituted by the ultimate strength under the same type of loading (Yao, 2003).

- Progressive collapse analysis with idealized/computed σ-ε curves

This type of analysis involves the application of Smith's method and includes several theoretical and empirical techniques to calculate the average stress-average strain relationships (Yao, 2003).

- Non-linear finite element method (FEM)

This method has proved to be an important tool in the derivation of the ultimate strength as it allows the consideration of parameters that can affect the load carrying capacity of the structure such as non-linear behavior of the material, the geometry of the components as well as the buckling and post-buckling response of the structure. Its ability to produce reliable results is strongly connected with the accuracy of the model that represents the real structure (Guedes Soares and Santos, 2018).

- Idealized structural unit method (ISUM)

Less modelling effort and computational time are among the advantages of this method in comparison to non-linear finite element method. This is possible by adopting a simplification of a larger structure into smaller parts allowing a faster assessment (ISSC, 2015).

Among the consequences of a ship collision, the possible reduction of the ultimate strength must be regarded as the most severe due to the collapse of the vessel that it can cause. The residual strength of the structure needs to be kept in an acceptable level to avoid any further failure. A stability assessment is necessary before any cargo transfer operation or towing of the damaged ship is attempted. The structural degradation after a collision can be expressed as parts of the hull that have been torn away, yield strength reduction of the material in the case of fire, residual stress redistribution and imperfections because of the random geometry change. Methods for the residual strength assessment of damaged vessels because of collision or grounding were developed by Paik et al. (1998) and Wang et al. (2002) who used the ultimate bending strength and section modulus for the ultimate strength estimation process. The residual strength index was introduced by Paik et al. (1998) and is defined as the ratio of the ultimate bending strength of the damaged vessel to the extreme bending moment. Dividing the residual section modulus by the minimum required section modulus, another expression of the residual strength index can be derived. The above index expressions were estimated in the study of Wang et al (2002) after the definition of the damage extent in the side and bottom of the ship for the cases of collision and grounding respectively concluding that the relations between the damage size and residual strength are not really affected by the ship's length (Mansour et al., 2008).

3 Case study-residual strength assessment

The structure of the collision simulations is described in this section focusing on the basic parameters of the case study, the finite element models that are used and the chosen corrosion model. The representation of the corroded and non-corroded material is explained as well as the function of the damage initiation and progression. An introduction to the estimation methods of the residual strength completes the current section.

3.1 Case study

The conducted simulations involve the collision between two vessels of similar size and same type. The struck ship is a coastal oil tanker of 11500 tons of deadweight (DWT) while the striking ship is a coastal product/chemical tanker whose displacement reaches 10800 tons of deadweight. The structure of the struck ship consists of longitudinally stiffened double bottom and weather deck with a transversely stiffened double side-shell. A corrugated longitudinal bulkhead is located in the center plane of its cross-section, which can be neglected in the ultimate strength assessment since its vertical corrugation has little contribution to the hull girder longitudinal strength (Ringsberg et al., 2018). Information regarding the dimensions and the structural arrangement of the struck ship can be seen in Table 3.1 and Figure 3.1.

Table 3.1: Main particulars of coastal tanker

LOA (m)	137.6
Beam (m)	21.5
Design draft (m)	7.4

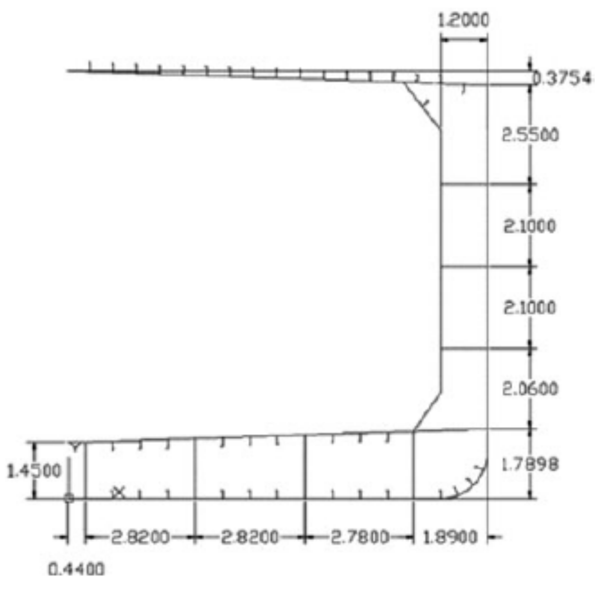

Figure 3.1: Mid-section of struck ship (Ringsberg et al., 2018)

3.2 Finite element models

The finite element models for both ships in the collision simulations were developed and used in the study of Ringsberg et al. (2018), see Figure 3.2. The generation of the models was based on the software Abaqus (Dassault Systèmes, 2014). Four-node shell elements with reduced integration (S4R) and five section points through their thickness were chosen for the creation of the mesh while the use of triangular elements (S3R) was also acceptable in some cases. The ideal size of the elements was determined during convergence analysis, which resulted in an element size of 60 mm. Parts of the models with the highest sheet thickness correspond to the element length/thickness ratio of five (Ringsberg et al., 2018).The general contact criterion in Abaqus was preferred ensuring a realistic approach regarding contact without the previous knowledge of which surfaces will eventually contact each other (Karlsson, 2009). A value for the friction coefficient of 0.3 and 0.5 was appointed to the corroded and non-corroded parts of the model respectively (Ringsberg et al., 2018).

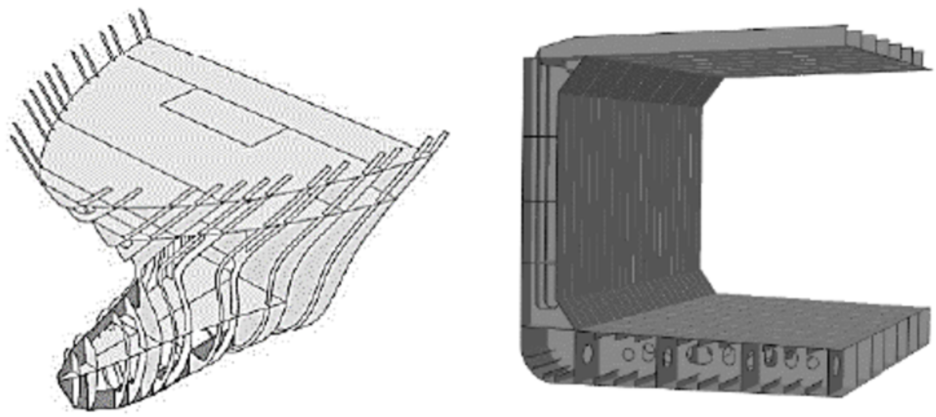

Figure 3.2:Finite element models striking ship (left) and struck ship (right) (Kuznecovs and Shafieisabet, 2017)

3.3 Corrosion model

As it has been discussed in section 2.1.4 the corrosion model that appears to be more suitable for the present study is the model developed by Paik et al. (2003a), which is mathematically expressed in the following way assuming that there is no transition time between the loss of coating's effectiveness and corrosion initiation while the service life of the vessel exceeds the 25 years:

$$t_r = C_1(T - T_c) \tag{61}$$

where t_r is the thickness reduction due to corrosion, C_1 is a coefficient that characterize the annual corrosion rate, T is the age of the vessel and T_c is the coating life with a value of 7.5 years to be a reasonable approach since it can vary between 5 and 10 years (Paik et al., 2003a). The corrosion rate which is indicated by the coefficient C_1 can be derived by Eq. (24):

$$C_1 = \frac{t_r}{(T - T_c)} \tag{24}$$

Since the total loss of the corrosion margin is expected at the end of the 25 years of service, a reduction of the corrosion margin by 50% corresponds to 16 years of service as it be calculated by Eq. (24) (Ringsberg et al., 2018).

The unavoidable material loss because of corrosive activity is dealt by adopting a corrosion addition to the ship's scantlings during the design phase. According to the net scantling approach a separation is promoted between the net thickness, which is derived by the strength requirements of the structure and the corrosion addition, which aims to compensate for the thickness reduction during the whole lifespan of the vessel. When the corrosion addition is subtracted from the gross offered thickness the net thickness is obtained according to the equation:

$$t_{off} = t_{as\ built} - t_{vol\ add} - t_c \tag{68}$$

where t_{off} is the net thickness, $t_{as\ built}$ is the actual thickness as it can be seen in a newbuilt, $t_{vol\ add}$ is the voluntary addition thickness determined by the owner of the vessel and t_c is the corrosion margin (IACS, 2019).

Each structural member is assigned with a corrosion margin that corresponds to both sides of it and is calculated in the following way:

$$t_c = Roundup_{0.5}(t_{c1} + t_{c2}) + t_{res} \tag{69}$$

where t_{c1}, t_{c2} are the corrosion margin for both sides of the part, t_{res} is reserved thickness taken as 0.5 mm and the term $Roundup_{0.5}$ dictates that the calculated value should be rounded up to the upper half millimeter. The values of the t_{c1}, t_{c2} for the case of the tanker, which serves as the struck ship can be obtain from Table 3.2 (IACS, 2019).

Table 3.2: Corrosion addition for one of a structural member-Tanker (IACS, 2019)

Compartment type	Structural member		t_{c1}, t_{c2}
Ballast water tank, bilge tank, drain storage tank, chain locker	Face plate of PSM	Within 3m below top of a tank	2.0
		Elsewhere	1.5
	Other members	Within 3m below top of a tank	1.7
		Elsewhere	1.2
Cargo oil tank	Face plate of PSM	Within 3m below top of a tank	1.7
		Elsewhere	1.4
	Inner bottom plating/bottom of tank		2.1
	Other members	Within 3m below top of a tank	1.7
		Elsewhere	1.0
Exposed to atmosphere	Weather deck plating		1.7
	Other members		1.0
Exposed to seawater	Shell plating between the minimum design ballast draught waterline and the scantling draught waterline		1.5
	Shell plating elsewhere		1.0

The term PSM that appears in Table 3.2 stands for primary structural member in the hull structure and includes floors and bottom girders, side stringers and web frames, deck transverses and deck girders, vertical webs and horizontal stringers on bulkheads (Babicz, 2015). The corrosion additions in the several structural members of a tanker's cross section are represented in Figure 3.3.

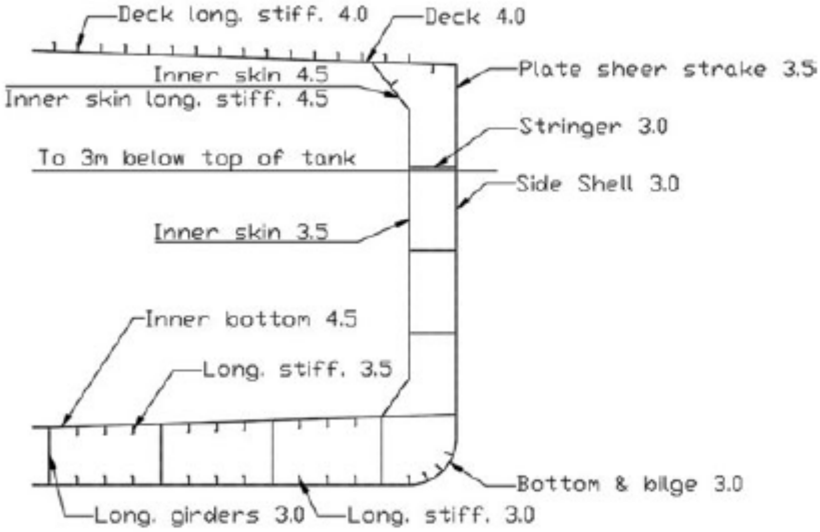

Figure 3.3: Corrosion margin (mm) for the costal oil tanker (Ringsberg et al., 2018)

3.4 Non-corroded material

The material used in the present study is a DNV Grade A (NVA) mild steel for shipbuilding applications. A nonlinear elastic-plastic constitutive material model is used to represent the material, which hasn't been subjected to any degradation of its properties due to corrosion. The isotropic hardening of the inelastic stress-strain relation is expressed by the power law according to the equation:

$$\sigma_{true} = K(\varepsilon_{true})^n \tag{70}$$

The above equation relates the true stress σ_{true} with the true strain while the remaining terms K and n are the hardening coefficient and the hardening component respectively. The Cowper-Symonds relationship is used to contemplate the influence from strain rate effects:

$$\sigma_{y,d} = \sigma_{y,s}\,(1 + (\dot{\varepsilon}/C)^{1/P}) \tag{71}$$

where $\sigma_{y,d}$ is the dynamic yield stress, $\sigma_{y,s}$ is the static yield stress, $\dot{\varepsilon}$ is the material strain rate and C, P are constants of the Cowper-Symonds relation (Ringsberg et al., 2018).

3.5 Corroded material

The influence of corrosion in the mechanical properties of steel was discussed in section 2.3, which was based on the work of Garbatov et al. (2014). Two diagrams were described that provide information about the stress and strain relationship in certain degree of degradation levels, which has been defined by the following equation:

$$D = \frac{V_o - V_c}{V_o} \times 100\% \tag{72}$$

The terms V_o and V_c are the intact plate volume and the corroded volume respectively. The finite element models of the collision simulations consist of shell elements whose two dimensions, length and breadth, are much larger than their thickness leading to the safe assumption of a constant area in the volume calculation of each element. Therefore Eq. (72) can become:

$$D = \frac{t_r}{t_{as\ built}} \times 100\% \tag{73}$$

where t_r is the thickness reduction and it is calculated by Eq. (61) while $t_{as\ built}$ is the original thickness of the plate according to Eq. (68).

The corrosion percentage is calculated by Eq. (73) using the corrosion margin of the various structural members according to IACS (2019) as the thickness reduction. The stress-strain diagrams in Figure 2.19 provide information only for 20,40,60 and 80 per cent of degree of degradation. Therefore, a division of five categories representing different levels of corrosion percentages is introduced with a difference of 20% between them corresponding to specific material models as it can be seen in Table 3.3 (Kuznecovs and Shafieisabet, 2017).

Table 3.3: Division of material models (Kuznecovs and Shafieisabet, 2017)

Corrosion percentage (D)	Material model
0~9%	NVA-Non-corroded
10~29%	NVA 20% Corroded Material
30~49%	NVA 40% Corroded Material
50~69%	NVA 60% Corroded Material
60~79%	NVA 80% Corroded Material

The calculation of the corrosion percentages using the relevant thickness reductions showed that none of the derived values were above 49%. As a result, two material models were chosen to be used:

- A minorly corroded material representing 20% of corroded steel.
- A severely corroded material representing 40% of corroded steel.

In the case of the coastal oil tanker which acts as the struck ship in the collision simulations, the distribution of the above material models was based on the calculated corrosion percentages according to Eq. (73) and can be seen in Figure 3.4. The properties of the material models of the current study are presented in Table 3.4.

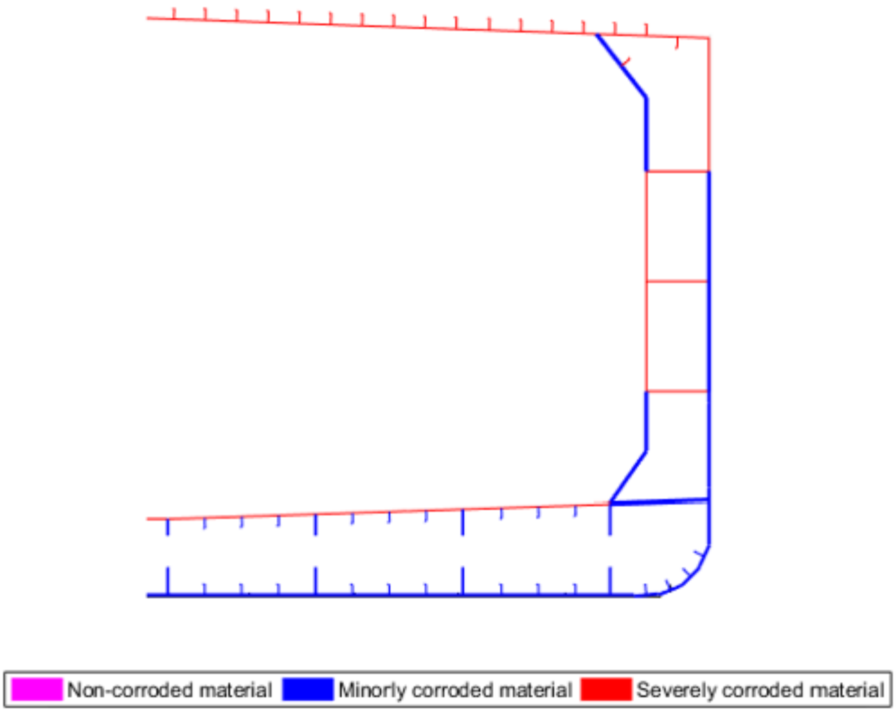

Figure 3.4: Material model distribution coastal oil tanker (Kuznecovs and Shafieisabet, 2017)

Table 3.4: Non-corroded and corroded material properties (Kuznecovs and Shafieisabet, 2017)

Parameter	NVA Non-corroded	NVA Minorly corroded	NVA Severely corroded
Young's modulus, E (GPa)	210	179	158
Poisson's ratio, v	0.3	0.3	0.3
(static) Yield stress, $\sigma_{y,s}$ (MPa)	310	310	291
Ultimate Tensile Strength σ_{TS} (MPa)	579	518	440
Hardening coefficient, K (MPa)	616	-	-
Hardening exponent, n	0.23	-	-
Necking strain ε_n (%)	23	-	-
Fracture strain ε_f (%)	35.1	24.8	20.0
Cowper-Symonds constant, C (-)	40.4	-	-
Cowper-Symonds constant, P (-)	5	-	-
DE parameters, bilinear model	(0,0), (0.02, 0.00458), (1, 0.01832)	-	-

3.6 Damage models

The degradation and failure of the material, which leads eventually to fracture, is expressed by damage models, which in the case of the non-corroded material can be divided in damage initiation (DI) and damage evolution models (DE). The former is used to describe the start of the material's failure and is indicated in Abaqus by the shear criterion, which uses the necking strain ε_n as the point of damage initiation. The latter models the progression of the damage process and is defined by a bilinear law up to the point of fracture (Kuznecovs and Shafieisabet, 2017).

The damage generation and progression of the corroded materials is modelled by the shear failure criterion neglecting the damage evolution (DE). This is justified by the lack of ductility of the corroded materials which makes difficult the observation of the necking point in tensile tests. Furthermore, the absence of data regarding the Cowper-Symonds relationship for corroded materials leads to the choice not to be considered in the current study (Ringsberg et al., 2018).

3.7 Parametric study

The ship collision simulations of the current study aim to investigate the residual strength of damaged ships considering the effect of corrosion while varying the point of impact corresponding to different draft levels of the striking ship. The corrosion influence is examined by including a non-corroded and a corroded form of the struck ship. The draft is changed resulting in four points of impact, which three of them are located between the web frames of the hull. The damage extent of a collision directly in a web frame is also included in the selected points of impact, see Figure 3.5. The collision angle between the involved vessels is chosen to be 90° in the middle of the struck ship's length since the maximum penetration and energy absorption can be achieved in this way. Furthermore, the struck ship is considered idle with a fixed position in order to avoid any external dynamic effect (Karlsson, 2009). Lastly, the collision speed of the striking vessel is 5 knots.

The parametric study also deals with different values of the friction coefficient, which is equal to 0.3 and 0.5 for the external surfaces and ballast tanks of the corroded ship respectively. The non-corroded vessel has friction coefficient equal to 0.3 (Kuznecovs and Shafieisabet, 2017). The combinations of the various parameters in the simulations can be seen in Table 3.5.

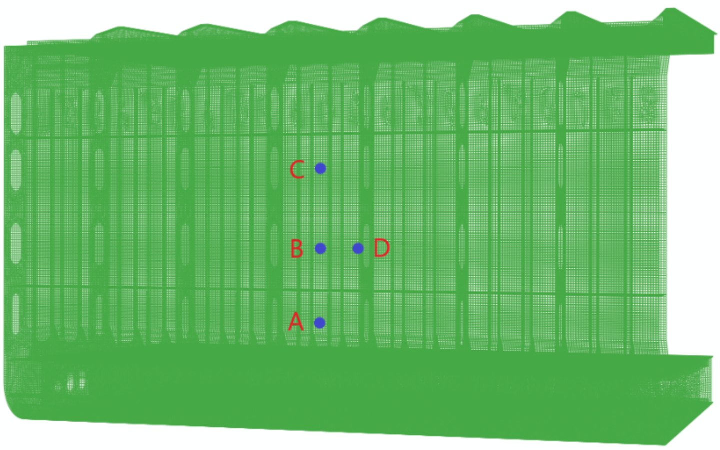

Figure 3.5: Points of impact representation

Table 3.5: Simulation parameters combination

Case	Ship Type	Velocity (Knots)	Material model (NVA)	Reduced Corrosion Margin (%)	Friction coefficient	Point of impact
T1-A	Tanker	5	Non-corroded	0	0.3	A
T1-B	Tanker	5	Non-corroded	0	0.3	B
T1-C	Tanker	5	Non-corroded	0	0.3	C
T1-D	Tanker	5	Non-corroded	0	0.3	D
T5-A	Tanker	5	Minorly & Severely corroded	100	0.3 and 0.5	A
T5-B	Tanker	5	Minorly & Severely corroded	100	0.3 and 0.5	B
T5-C	Tanker	5	Minorly & Severely corroded	100	0.3 and 0.5	C
T5-D	Tanker	5	Minorly & Severely corroded	100	0.3 and 0.5	D

3.8 Residual strength assessment

The methods that are applied for the estimation of the hull girder's residual strength are introduced in the current section. A brief description of the Smith's method is followed by a more detailed presentation of the method developed by Fujikubo et al. (2013).

3.8.1 Smith's method

The incremental-iterative method as it is referred in the Common Structural Rules (IACS, 2019) regards the hull girder as the assembly of several elements, which are composed of a stiffener and the attached plating assuming that no interaction occurs between them. The average stress-average strain relationship of each element is considered to produce the relationship between the bending moment and the curvature of the cross section under the assumption that the cross section will not deviate from its plane. The ultimate strength is obtained as the highest value of the bending moment-curvature correlation. The translation of the neutral axis as the result of gradual collapse of the elements in the cross section is also taken into account (Fujikubo et al., 2013).

The procedure which is applied to describe the progressive collapse of the hull girder under pure bending according to Smith's method can be described in the following way (Tanaka et al., 2015):

1) The entire cross section is subdivided in to several simple elements. Stiffened panels attached plating and hard corners are used to simulate the structure of each element, see Figure 3.6.

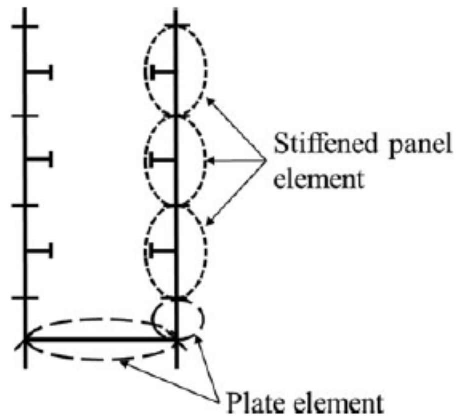

Figure 3.6:Progressive collapse analysis cross-sectional division (Tanaka et al., 2015)

2) The average stress-average strain relationship of each element is derived considering the action of tensile or compressive loading as well as the effect of buckling and yielding as it can be seen in Figure 3.7.

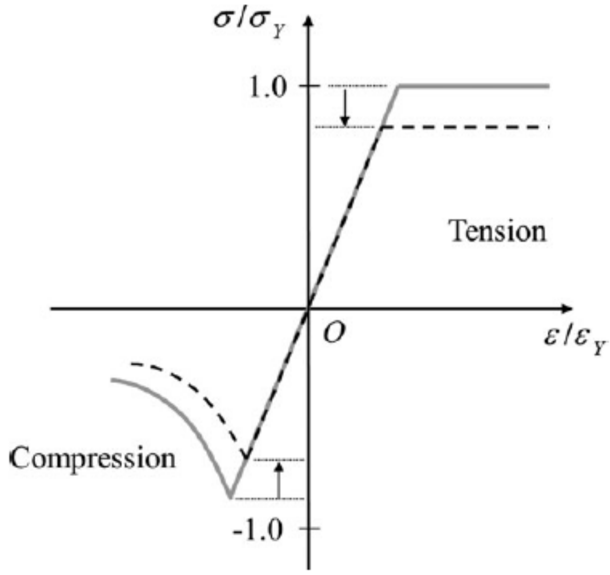

Figure 3.7:Average stress-average strain relationship/solid line (Tanaka et al., 2015)

3) The cross section is curved incrementally without neglecting the above relationship of all elements under the assumption that the cross section will remain plane. For each curvature increment the corresponding bending moment increment is calculated.

4) The addition of the curvature and bending moment increments results in the derivation of the bending moment-curvature correlation for the cross section.

3.8.2 Smith-Fujikubo method

During the progressive collapse of the cross section the neutral axis remains horizontal and is restricted to move only vertically in the case of a symmetric cross section under the effect of a vertical bending moment. The introduction of an unsymmetrical damage forces the neutral axis to rotate leading to a biaxial bending problem (Fujikubo et al., 2013). The current section focuses on the description of the methodology as it has been developed in the study of Fujikubo et al. (2013) . The Smith's method is applied for the biaxial bending problem resulting in an expression for the neutral axis. Its location and rotation are defined as a function of biaxial curvatures (Fujikubo et al., 2013). The loading case that is used for the calculation of the residual strength in the current study is also explained.

3.8.2.1 Cross-sectional force and deformation relationship

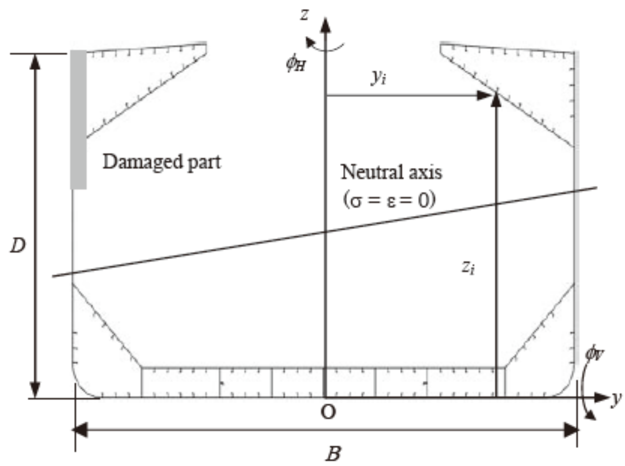

Figure 3.8: Rotation of neutral axis of an asymmetrically damaged cross section (Fujikubo et al., 2013)

The neutral axis is defined as the axis of the cross section where the bending stress and strain are equal to zero. A rotation of the neutral axis is observed when an irregular damage is introduced in the cross section as it can be seen in Figure 3.8. The location of the damage and the applied bending moment control the change of the position of the neutral axis from the horizontal plane. Using the assumption that the cross section is kept plane, the horizontal curvature Φ_H and the vertical curvature Φ_V result in the axial strain of the i-th element, which is expressed by the equation (Fujikubo et al., 2013):

$$\varepsilon_i(y_i, z_i) = \varepsilon_o + y_i\Phi_H + z_i\Phi_V \tag{74}$$

where ε_o represents the axial strain at the origin O while y_i and z_i are the horizontal and vertical coordinates of the i-th element respectively.

The average stress-average strain relationship, which is derived for each element considering the influence of buckling and yielding is described by a nonlinear function of the strain ε_i and it can be used for the calculation of the corresponding axial stress σ_i, see Figure 3.9.

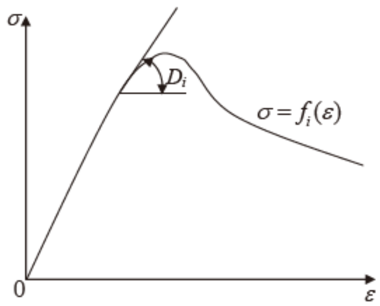

Figure 3.9: Average stress-average strain relationship (Fujikubo et al., 2013)

The nonlinear function of the average stress-average strain relationship is given by (Fujikubo et al., 2013):

$$\sigma = f_i(\varepsilon) \tag{75}$$

The integration of the axial stress σ_i over the undamaged part of the cross section leads to the derivation of the axial force P, the vertical bending moment M_H and the horizontal bending moment M_V according to the following expressions:

$$P = \sum_{i=1}^{N} \sigma_i A_i \equiv 0 \tag{76}$$

$$M_H = \sum_{i=1}^{N} \sigma_i y_i A_i \tag{77}$$

$$M_V = \sum_{i=1}^{N} \sigma_i z_i A_i \tag{78}$$

where the terms N and A_i represent the number of intact elements and the area of cross section of the i-th element respectively.

The location of the neutral axis is determined by Eq. (70) using the essential condition of zero axial force. The substitution of Eq. (74) and (75) into Eq. (76)- Eq. (78) forms a system of simultaneous nonlinear equations with the axial strain at the origin O ε_o and the curvatures Φ_H, Φ_V as independent variables. The neutral axis can be represented by a straight line in the y-z plane while its mathematical expression is (Fujikubo et al., 2013):

$$\varepsilon_o + y\Phi_H + z\Phi_V = 0 \tag{79}$$

3.8.2.2 Biaxial bending moment and curvature correlation

The solution of the previously described nonlinear system of equations is possible by adopting an incremental approach developed by Smith (1977), which allows an incremental relationship between axial stress and axial strain according to (Fujikubo et al., 2013):

$$\Delta\sigma = D_i \Delta\varepsilon \left(\because D_i = \frac{df_i}{d\varepsilon} \right) \tag{80}$$

where D_i is the tangential axial stiffness of the i-th element given by the slope of the average stress-average strain relationship as it can be seen in Figure 3.9.

The combination of Eq. (74) and Eq. (80) allows the equations Eq. (76)- Eq. (78) to be rewritten in an incremental form. Furthermore, a simplification can be possible by usage of the variables with respect to the centroidal position of the instantaneous neutral axis.

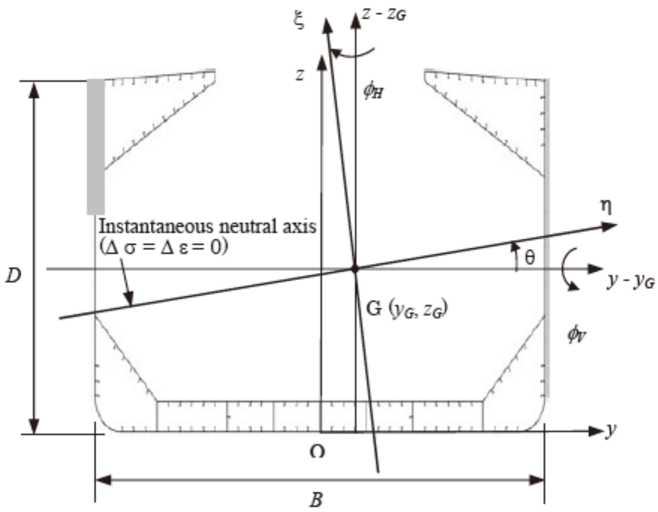

Figure 3.10:Instantaneous neutral axis for incremental analysis (Fujikubo et al., 2013)

After a series of computations, the following expression is derived:

$$\begin{Bmatrix} \Delta M_H \\ \Delta M_V \end{Bmatrix} = \begin{bmatrix} D_{HH} & D_{HV} \\ D_{VH} & D_{VV} \end{bmatrix} \begin{Bmatrix} \Delta \Phi_H \\ \Delta \Phi_V \end{Bmatrix} \tag{81}$$

The previous equation describes the correlation between the vertical and horizontal components of the biaxial bending moments and curvatures expressed in an incremental form. The tangential axial stiffness terms can be calculated in the following way (Fujikubo et al., 2013):

$$D_{HH} = \sum_{i=1}^{N} D_i (y_i - y_G)^2 A_i \tag{82}$$

$$D_{VV} = \sum_{i=1}^{N} D_i (z_i - z_G)^2 A_i \tag{83}$$

$$D_{HV} = D_{VH} = \sum_{i=1}^{N} D_i (y_i - y_G)(z_i - z_G) A_i \tag{84}$$

where the coordinates of the point G, see Figure 3.10, are provided by:

$$y_G = \left(\sum_{i=1}^{N} y_i D_i A_i \right) / \left(\sum_{i=1}^{N} D_i A_i \right) \tag{85}$$

$$z_G = \left(\sum_{i=1}^{N} z_i D_i A_i \right) / \left(\sum_{i=1}^{N} D_i A_i \right) \tag{86}$$

3.8.2.3 Biaxial bending under prescribed moment control

The loading conditions of the cross section are determined by the horizontal and vertical components of the bending moment according to the ratio $a = \Delta M_H / \Delta M_V$ while the curvature components act as controlling parameters. The incremental equation for this case and the corresponding solutions are:

$$\begin{Bmatrix} a\Delta M_V \\ \Delta M_V \end{Bmatrix} = \begin{bmatrix} D_{HH} & D_{HV} \\ D_{VH} & D_{VV} \end{bmatrix} \begin{Bmatrix} \Delta\Phi_H \\ \Delta\Phi_V^0 \end{Bmatrix} \tag{87}$$

$$\Delta M_V = \frac{\Delta M_H}{\alpha} = \frac{D_{HH} D_{VV} - D_{HV}^2}{D_{HH} - a D_{VH}} \Delta\Phi_V^0 \,, \Delta\Phi_H = \frac{\alpha D_{VV} - D_{HV}}{D_{HH} - a D_{VH}} \Delta\Phi_V^0 \tag{88}$$

The residual strength of the cross section for a prescribed ratio of $\Delta M_H / \Delta M_V$ depends on the maximum value of bending moment components since a linear correlation can be observed between them (Fujikubo et al., 2013).

4 Results and discussion

The data of the ship collision simulations are processed to produce useful information regarding the extent of the damage and the residual strength capacity of the vessel. The results are discussed and their interpretation through the available literature is followed.

4.1 Damage opening

The extent of the damage opening after collision, which is defined as the area that has been created when the velocity of the striking ship becomes zero, is presented in Figures 4.1and 4.2. The damaged areas can be derived as opening areas after projection of the deformed plates to the undistorted planes. The calculation process continues with the division of the projected area in two or more parts. The boundaries of every part and their enclosed areas are specified while the outer boundary and the total projection surface before subdivision are obtained. Finally, the damage opening is calculated by subtracting the enclosed areas of every part from the total projection area. The state of the inner and outer side-shell is demonstrated for four cases, which result from the variation of the impact point using a corroded and a non-corroded struck ship. The deformation of the outer side-shell along with the damage openings is demonstrated in Figures 4.3 and 4.4.

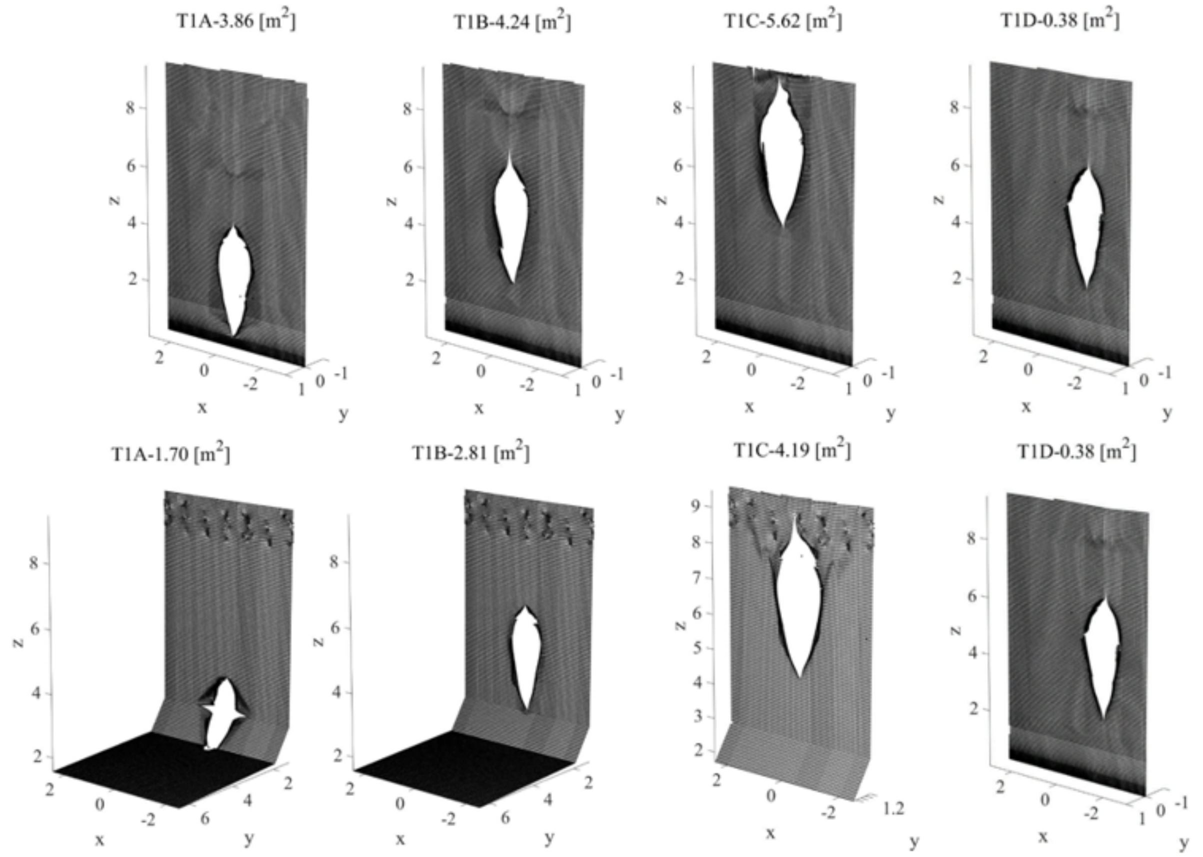

Figure 4.1: Shape and size of damage openings of outer side-shell (upper) and inner side-shell (lower) for non-corroded struck ship (T1)

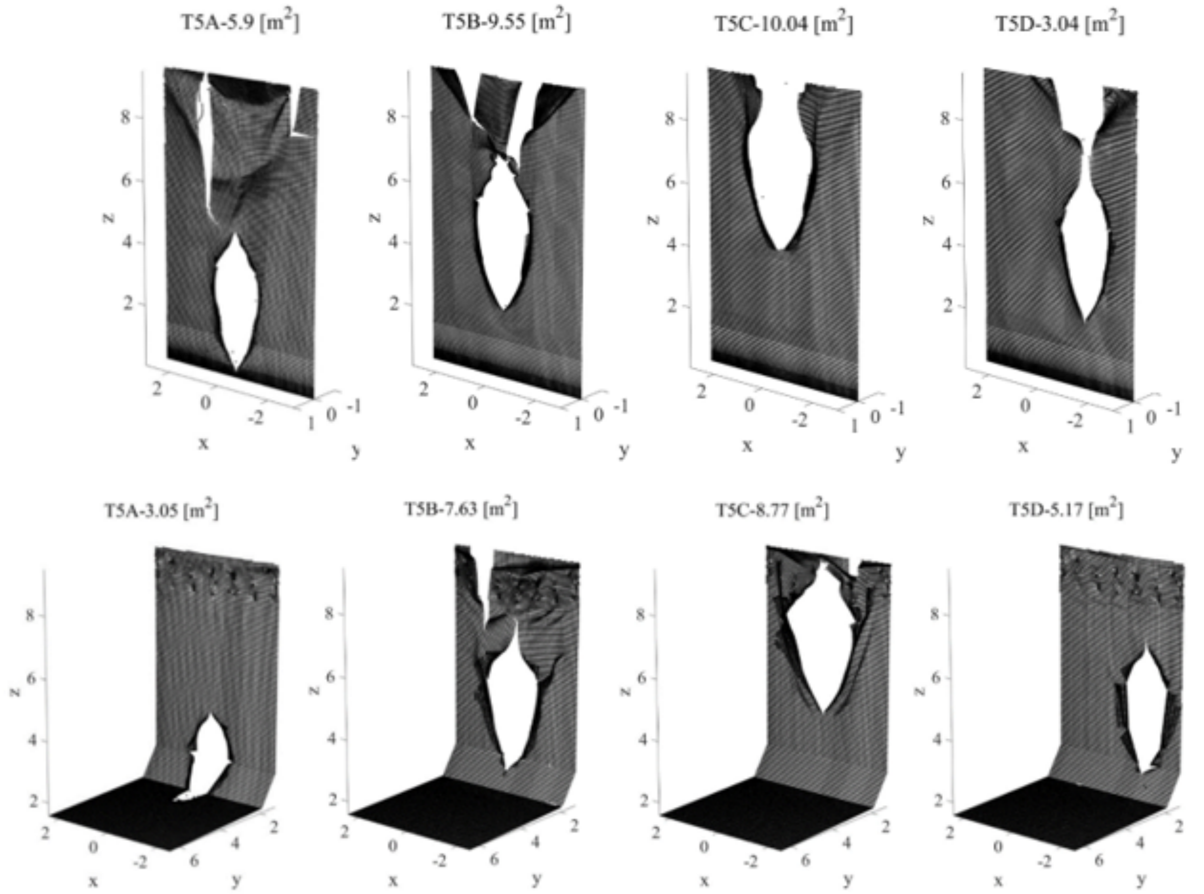

Figure 4.2: Shape and size of damage openings of outer side-shell (upper) and inner side-shell (lower) for corroded struck ship (T5)

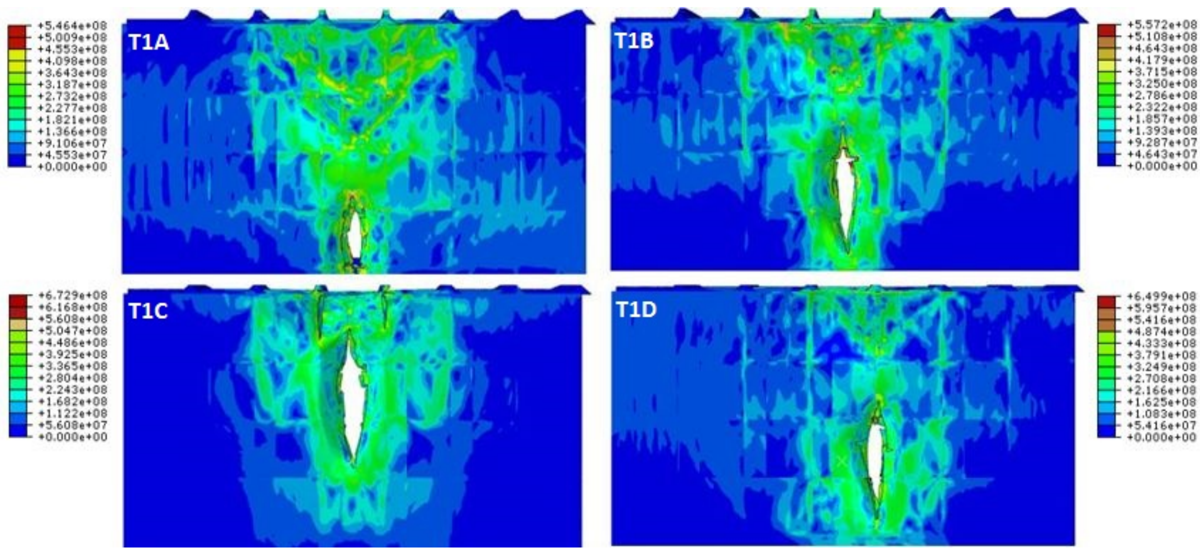

Figure 4.3: Deformation of outer side-shell (von-Mises equivalent stress [Pa]) and damage openings for T1 cases

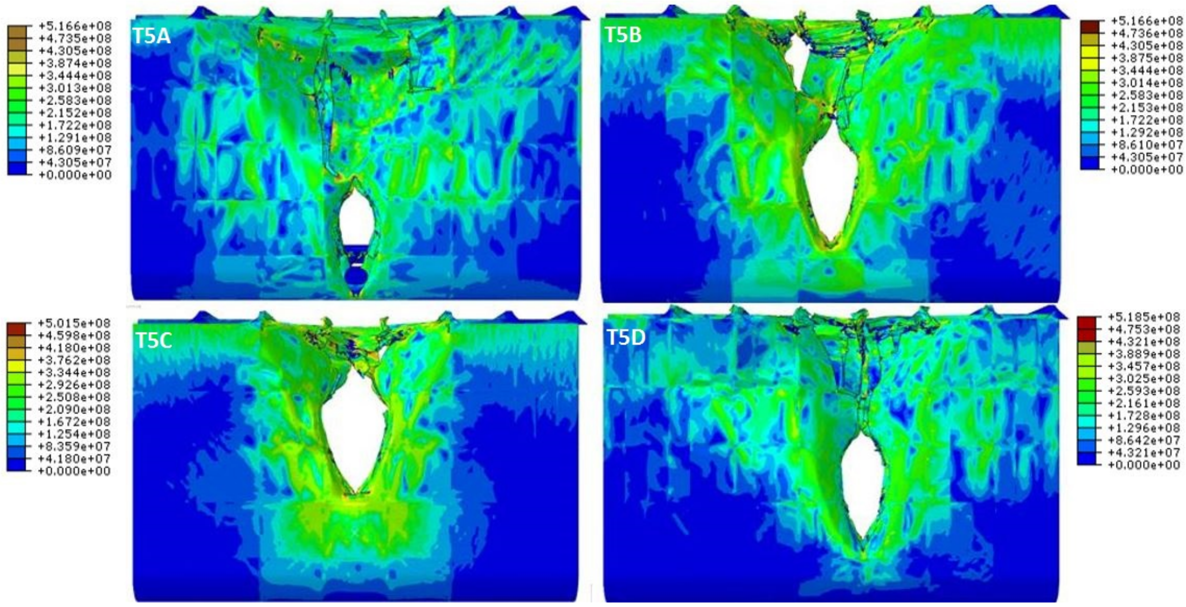

Figure 4.4: Deformation of outer side-shell (von-Mises equivalent stress [Pa]) and damage openings for T5 cases

As it can be observed in both corroded (T5) and non-corroded (T1) struck ships, the collision results in the rupture of the inner and outer side-shell of the hull. Deformations of the external parts of the hull can be observed in locations where collision of the striking ship's forecastle occurs, mainly in the areas above the damage openings. When corrosion is considered, the contact with the forecastle will result in further damage of the outer side-shell. In general, smaller openings can be observed in the inner side-shell apart from the impact case D when the collision takes place directly in to a web frame of the non-corroded hull. The size of the damage opening tends to increase as the point of impact moves upwards between the web frames. The gradual elevation of the impact point forces the forecastle to miss the hull during the collision allowing more kinetic energy to be used for rupturing the hull and resulting in larger damage openings.

The presence of corrosion leads to significant larger damage compared to the non-corroded hull. This observation can be explained by the lower yield strength of the corroded material, which doesn't allow the structure to resist the penetration of the striking vessel's bow, leading to a larger opening as the collision continues (Kuznecovs et al., 2019). The largest opening can be seen in the case T5C, for both structural parts, because of the location of the impact point less contact of the outer side-shell with the forecastle takes place. The bulbous bow of the striking ship is much more rigid than the forecastle and when the latter misses the hull of the struck ship, the energy dissipation due to plastic deformations will mainly occur in the struck hull. This fact combined with the degraded material due to corrosion results in extensive damage.

The comparison between the corroded and non-corroded hull shows that the most noticeable increase in damage opening size can be seen for the case of the collision in the web frame of the struck ship. When no corrosion effect is considered, the amount of energy that is needed to deform the web frame leads to a small opening with a value of 0.38 m^2 according to Figure 4.1 in both sides of the hull. Moreover, part of the kinetic energy of the striking ship is consumed to deform the area of the outer side-shell above the impact point because of the contact with the forecastle at the time of the collision. The corroded hull shows a significant damage for the same collision scenario, which includes not only the area where the bow penetrates but also above the impact point in the outer side-shell, which is an indication of the lower resistance to perforation due to presence of corrosion and as a result reduced fracture strain. The collision creates a damaged area with the size of 3.04 m^2 and 5.17 m^2 in the inner and outer side-shell respectively as it can be seen in Figure 4.2, which indicates the influence of corrosion in the web frame.

4.2 Residual strength analysis

The evaluation of the residual strength was carried out by the Smith method as it was described in the work of Fujikubo et al. (2013) and was presented in section 3.8.2. The calculation process was based on an in-house MATLAB code and constitutes a further development of the Smith-Fujikubo method according to the study of Kuznecovs et al. (2019) making possible the residual strength analysis of damaged ships under biaxial bending with prescribed moment control.

The Ultimate Limit State (ULS) for a certain structural condition is described by an interaction curve. It is formulated by representing both vertical and horizontal components of the bending moment in a biaxial plot for all loading directions. Degrees are used to indicate the several directions of loading with 0° and 180° to correspond to horizontal bending of the structure while hogging and sagging conditions appear at 90° and 270° respectively.

The following interaction curves were generated for the non-corroded (Figures 4.5-4.8) and the corroded struck ship (Figures 4.9-4.12) during the variation of the impact point. For comparison an interaction curve was also added that corresponds to an intact vessel with the same level of corrosion as the damaged ship.

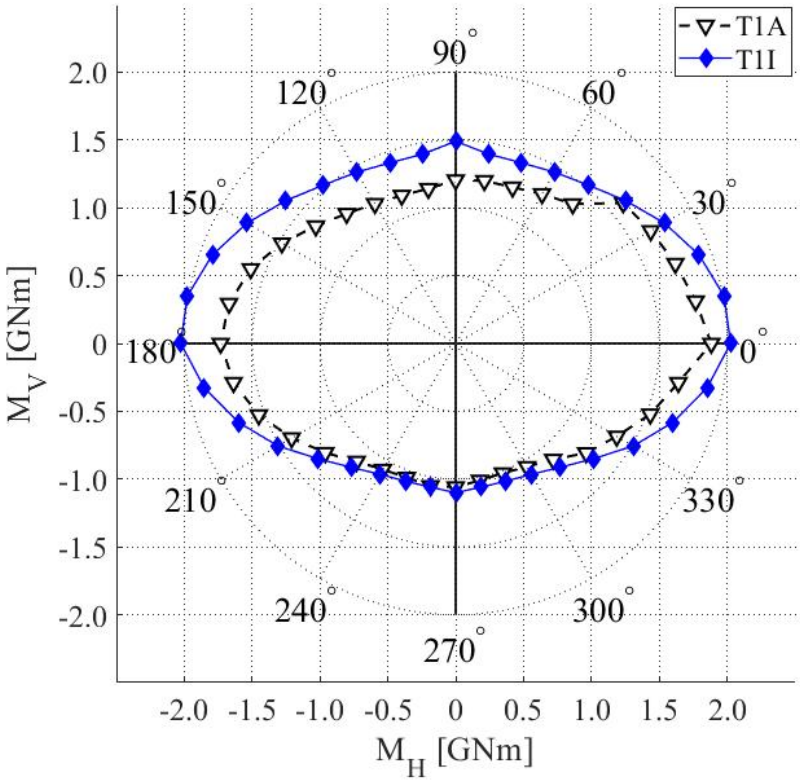

Figure 4.5: Interaction curves for non-corroded (T1) struck ship at impact point A

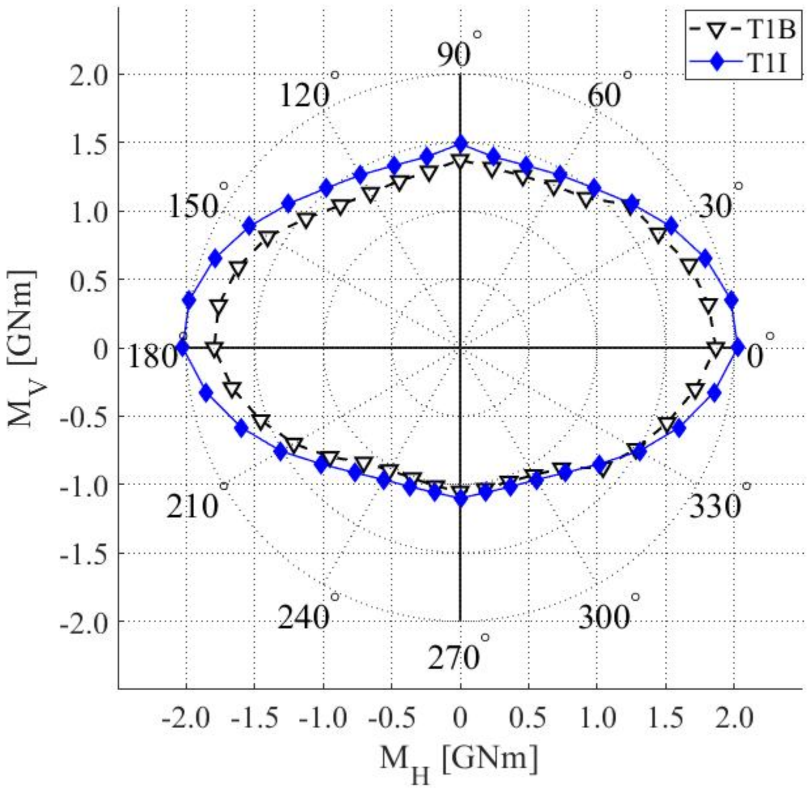

Figure 4.6: Interaction curves for non-corroded (T1) struck ship at impact point B

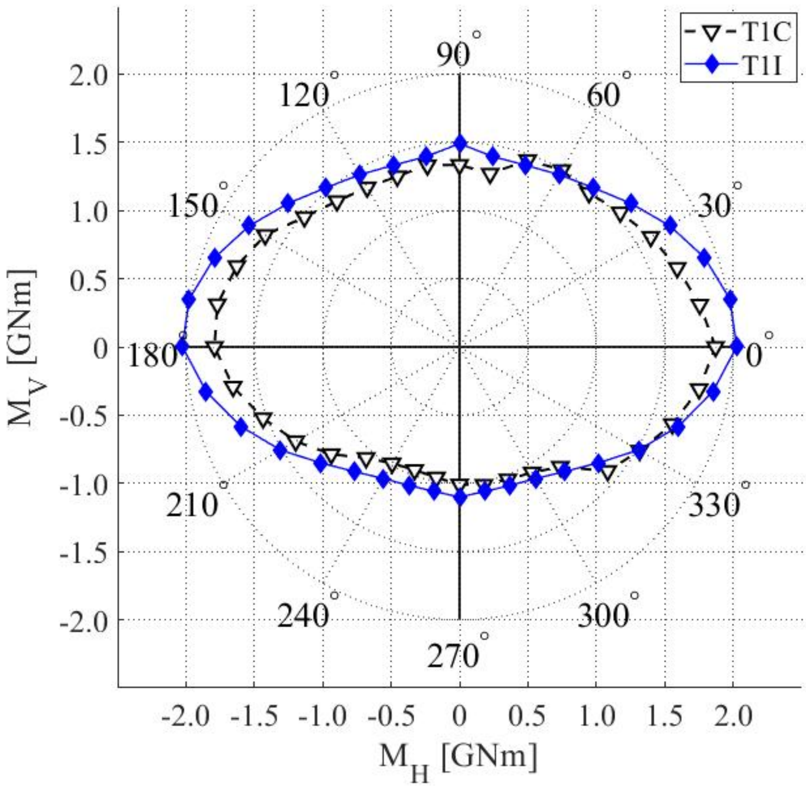

Figure 4.7: Interaction curves for non-corroded (T1) struck ship at impact point C

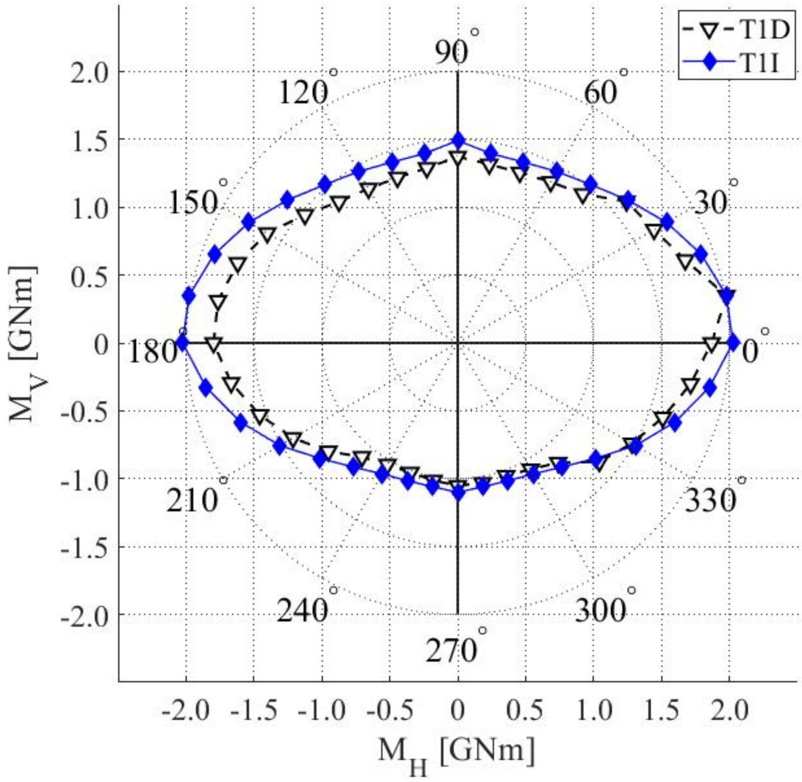

Figure 4.8: Interaction curves for non-corroded (T1) struck ship at impact point D

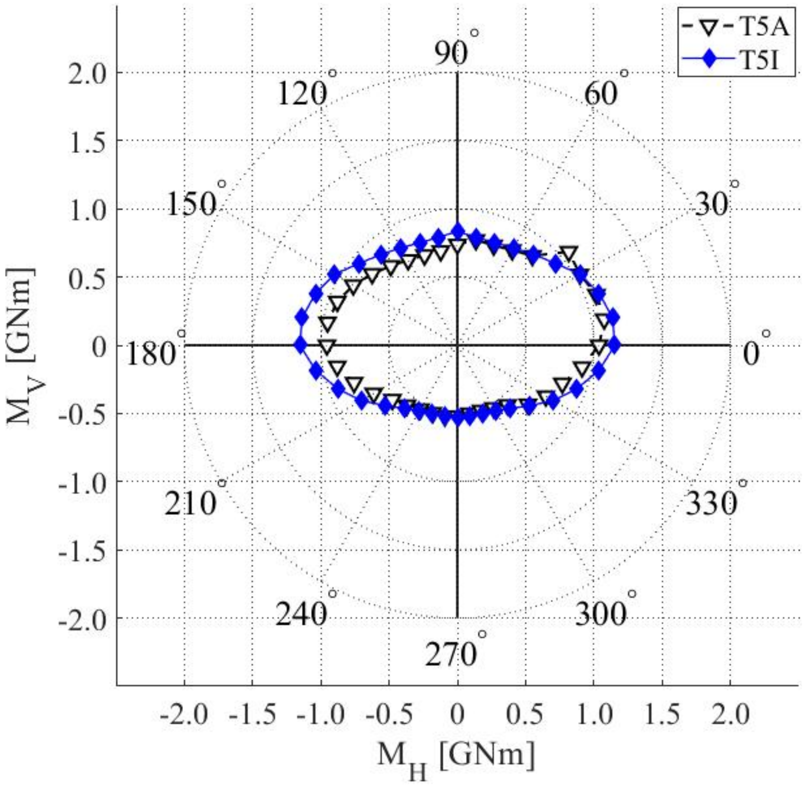

Figure 4.9: Interaction curves for corroded (T5) struck ship at impact point A

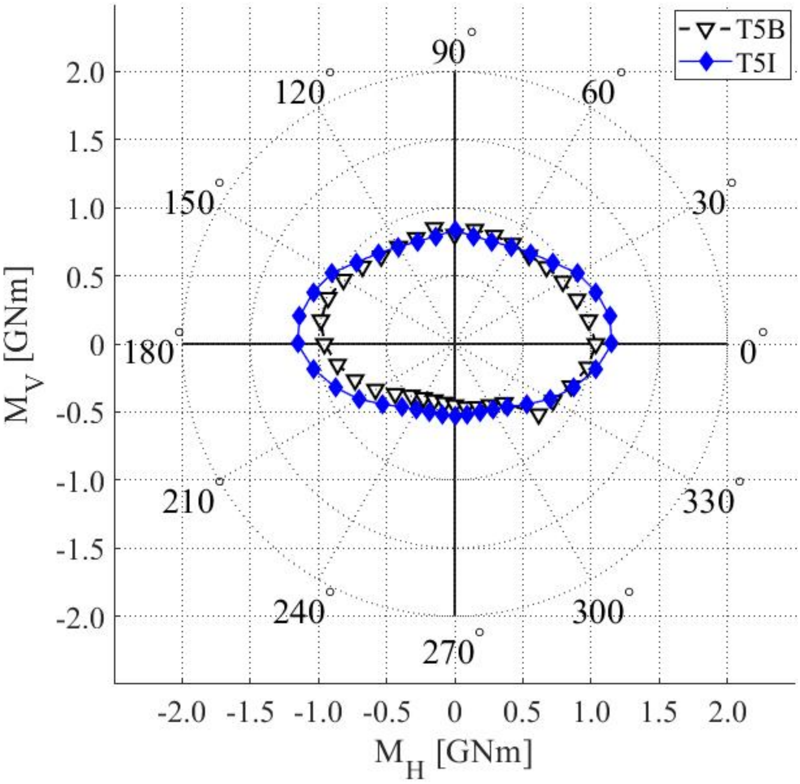

Figure 4.10: Interaction curves for corroded (T5) struck ship at impact point B

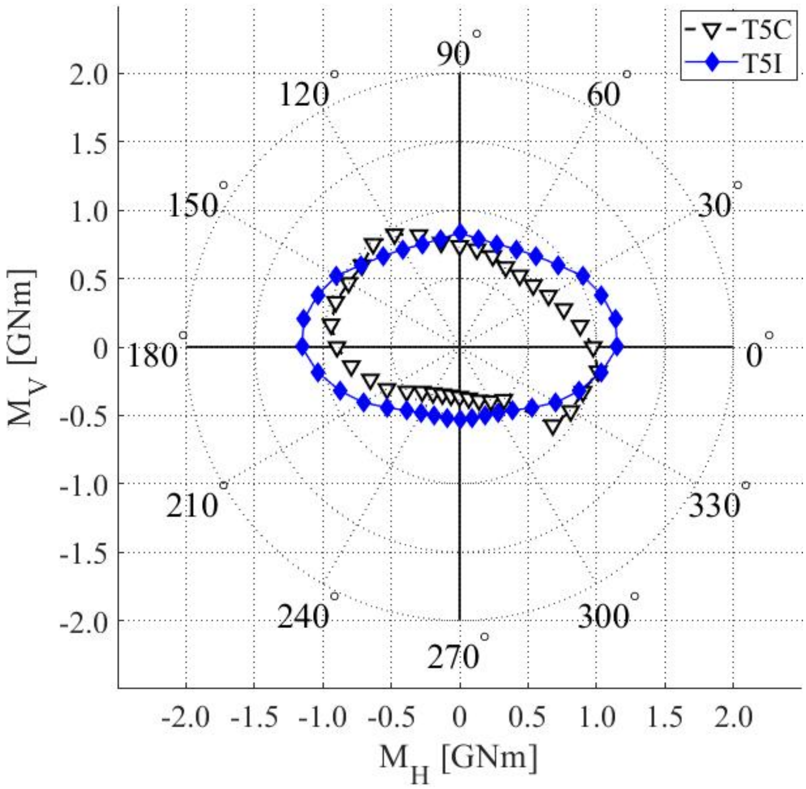

Figure 4.11: Interaction curves for corroded (T5) struck ship at impact point C

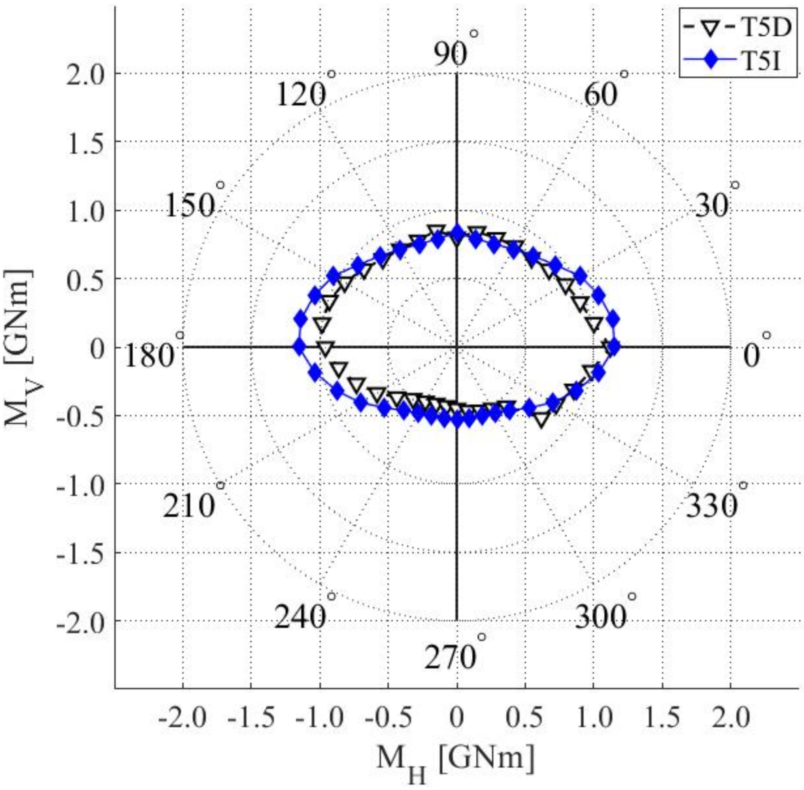

Figure 4.12: Interaction curves for corroded (T5) struck ship at impact point D

The examination of the interaction curves shows that the strength capacity of the coastal tanker in intact state (T1I) is higher in hogging than in sagging condition. This difference can be justified by the presence of more material in the structure of the double bottom, which increases its stiffness compared to a single upper deck (Kuznecovs et al., 2019). Moreover, the presence of imperfections can lead to the reduction of the ultimate strength. During hogging conditions, the deck is subjected to tension reaching first the yield stress and maintaining its loading capacity followed by the bottom, which reaches its ultimate strength under compression. The influence of initial imperfections in the yield stress is not significant, resulting in a small reduction of the ultimate strength. Under sagging bending moment, the buckling strength of the deck is reached first limiting its load carrying capacity after buckling. The stress in the deck area is redistributed but the ultimate strength of the whole section is obtained due to the large loss in the loading capacity of the buckled parts. Compressive loads seems to intensify the influence of initial imperfections compared to tensile loads making sagging conditions more suitable for the reduction of the ultimate strength than hogging (ISSC, 2015).

The ultimate strength is observed to be largest in pure horizontal bending due to the larger distance of the double sides from the centroid, which results in a bigger lever arm than the double bottom. The interaction curve of the undamaged and corroded coastal tanker (T5I) has a more horizontal shape for negative bending moments and appears smaller compared to T1I due to the larger exposure of the upper deck to corrosion than the double bottom, which results in the thickness reduction of the structural parts and a decrease in strength capacity in sagging conditions (Kuznecovs et al., 2019). In certain cases, the interaction curves between the intact and damaged struck ships seems to be intersected, which is not possible since the introduction of a damage in a ship's hull leads to lower bending moment values for each curvature. The small differences at the intersection points can be attributed to numerical errors and don't affect the general accuracy of the calculation process.

Table 4.1: Ultimate strength reduction and loading direction for each case

Case	Ultimate strength reduction (%)	Loading direction
T1A	15.6	180°
T1B	11.3	190°
T1C	11.5	190°
T1D	11.3	190°
T5A	17.2	190°
T5B	17.1	190°
T5C	26.8	30°
T5D	16.9	190°

The Table 4.1 contains information regarding the simulated cases, the reduction of the ultimate strength and the loading direction where this decrease was observed. The change in the ultimate strength value represents the largest difference between the interaction curve of an intact ship and the interaction curve, which is generated as the impact point is elevated. The intact ship can be non-corroded (T1) as well as affected by corrosion (T5).

The T1A case creates a damage opening near the bilge, which decreases the load carrying capacity by 15.6 % at 180° when the damaged area is subjected to compression. The gradual elevation of the impact point in T1B and T1C cases provides a reduction of 11.3% and 11.5% in ultimate bending strength respectively, which appears in 190° when both sections are loaded in compression. The T1D case involves the collision in to the web frame of the struck ship and creates a smaller size of opening compare to the three previous cases while the strength reduction is 11.3% at the same loading direction as the T1B and TIC. The largest change in terms of ultimate strength from the four cases for the uncorroded struck ship can be found in T1A case while all of them seem to appear during compression of the affected part. The location of the impact point in the T1A case affects mainly the structural integrity of the double bottom. The collision lowers the ultimate strength under hogging compared to the intact case but the main difference is observed when the damage area is subjected to pure horizontal bending.

The T5A case forms an opening in the bilge area of the corroded struck ship with the load carrying capacity to be reduced by 17.2 % subjecting the damaged section to compression at a loading direction of 190°. The collision at a higher point B in T5B case provides a reduction of almost the same level and identical conditions as in T5A case. The further elevation of the impact point results in 26.8% reduction of the ultimate bending strength in T5C case at 30° during tensile loading of the damaged area. The collision in the web frame of the corroded structure lowers the ultimate strength by 16.9 % at 190° under compressive loading conditions in T5D. The most noticeable difference between the four cases can be seen in T5C, which also creates the largest damage openings in all collision simulations. Moreover, the T5C case shows a reduction of the bending strength under sagging conditions in comparison to the other T5 cases, which can be attributed to the large deformed area in the deck part of the hull above the damage opening. The location of the impact point C allows the forecastle of the striking ship to cause large deformations in the deck area and as a result the load carrying capacity of the affected structural parts is lost leading to a reduction of the residual strength in sagging.

As the impact point moves higher, the size of the generated openings in the non-corroded hull increases apart from T1D case, which results in a relatively small damage due to the larger energy that is needed to deform the web frame. The reduction in bending strength doesn't show an excessive change for the various impact points and it is almost identical in terms of direction and type of loading. When corrosion is considered the damage openings tend to be increased for the elevation of the impact point from A to C and even T5D case creates a large damaged area despite the presence of the web frame. The difference in size is an indication of the corrosion influence in the yield stress of the material, which limits its ability to resist the penetration of the striking ship.

The symmetry that can be seen in the interaction curves of the intact ships (T1, T5) is lost with the introduction of damage in the hull as the impact point changes. The generated interaction curves are smaller compared to the interaction curve of the intact vessels due to the reduction of the ultimate strength, which is caused by damaging the structure of the hull. The change in the shape of the interaction curves is observed mainly for positive bending moments for the cases of the non-corroded hull (T1) as it can be seen in the Figures 4.5-4.8. The T1A case shows the most noticeable change in the shape of the interaction curve when the hull is subjected to positive bending moments. The shape of the interaction curves for the corroded hull in the T5 cases does not seem to follow a specific pattern. However, the shape of the curve appears to become smaller for sagging conditions as the impact point changes between the T5A and T5C cases. Regarding the load carrying capacity, the reduction is larger compared to T1 cases, but it appears almost the same for T5A, T5B and T5D cases. The collision at point C of the corroded hull leads to the most severe damage and the highest reduction in bending strength from all collision scenarios mainly due to the loss of a considerable part of the hull's cross section.

5 Summary and conclusions

The corrosion influence on the residual strength of damaged ships under various collision scenarios was investigated using two coastal tankers as struck and striking ships. An extensive literature study preceded the finite element simulations and aimed to identify the corrosion model, which could satisfy the needs of the current study. The advantages and the possible drawbacks of the existing corrosion models were documented leading to the selection of the model developed by Paik et al (2003a). Factors such as its simplicity and its application in the works of several researchers can be used to justify this choice. The variation of the impact point combined with a corroded and a non-corroded struck ship resulted in eight simulations cases which were conducted using the software Abaqus (Dassault Systèmes, 2014). The processing of the simulation results was performed by using an in-house MATLAB code, which enabled the formation of damage openings as well as the evaluation of the residual strength of both hulls that were involved in the collision simulations. The latter was achieved by applying the Smith-Fujikubo method as it was further developed in the study of Kuznecovs et al. (2019), which allowed the analysis of the residual strength under biaxial bending with prescribed moment control.

The simulation process involved the use of a non-corroded and a corroded hull which are indicated as T1 and T5 respectively. The location of the impact point is specified by the letters A, B, C and D. The first three represent an elevation of the impact point between the web frames of the struck ship. The point D is located at the same level as B, but the collision occurs directly in the web frame. The combination of two hulls and four impact points results in eight different simulated scenarios.

The collision in all simulated cases created a damage opening in both inner and outer side-shell of the structure. The size of these openings for the non-corroded hull (T1) showed a gradual increase during the elevation of the impact point apart from the case, which involved collision directly in the web frame (T1D) and led to an opening with a size of 0.38 m^2 in both sides of the hull. The stiffness of the structure at that point limited the size of the opening. The damage for the corroded hull (T5) was more extensive and followed the same increase pattern even for the case of the collision in the web frame (T5D), which led to considerable damage openings indicating the influence of corrosion in ship-ship collisions. The collision at the impact point C for the corroded hull (T5C) produces the most severe damage in all simulated cases creating opening with sizes of 10.04 m^2 and 8.77 m^2 for the inner and outer side-shell respectively.

The largest reduction of the ultimate strength for the non-corroded struck ship (T1) appeared for collision near the bilge area (T1A) resulting in 15.6% decrease while the remaining cases produced similar results in terms of magnitude and loading direction. The bending strength of the hull did not show any significant change as the collision occurred in a higher point. Although the corroded struck ship (T5) provided larger values of ultimate strength reduction compared to the T1 cases the most noticeable was be observed at the impact point C (T5C) contributing to a 26.8% loss of the hull's bending strength. It can be concluded that there was an undeniable influence of corrosion in the residual strength of ships involved in collisions especially when the penetration of the striking ship created damage openings with size as in T5C case.

The combination of the most crucial damage extent and the largest residual strength decrease, which occurs at the impact point C of the corroded hull (T5) seems to be the most challenging from all the collision scenarios. Moreover, the loading direction which was found to be 180° or 190° according to Table 4.1 for all the other simulated cases is changed to 30° revealing a shift in the structural response of the hull when corrosion is present, and the striking ship hits the hull at a point where most of its kinetic energy can be used to deform the structure of the struck ship.

It must be noted that the reduction of the ultimate strength under sagging and hogging conditions is not significant apart from the T1A and T5C case. If only the response of the hull under vertical bending loading is considered as in Common Structural Rules (IACS 2019) the residual strength assessment is insufficient since the largest reductions in ultimate strength were observed under pure horizontal or biaxial bending. Therefore, safer conclusions can be reached if biaxial loading is included in the residual strength calculations.

The limitations and assumptions of the current study do not seem to narrow its range of application to a large extent. They can be regarded as necessary to limit the time and complexity of the calculation process and ensure the feasibility of the study. Nevertheless, their contribution is vital in achieving the selected objectives.

6 Future work

During the completion of the current study several assumptions were made to overcome certain difficulties and simplify the processes that were followed. As a result, the scope is narrowed making the conclusions not applicable in general situations. The future work should primarily be focused on the parameters that limit the use of this study.

The ships that were used in the collision simulations were coastal tankers of similar size, which means that the derived conclusions cannot be utilized in situations involving other kind of ships. Including other types of vessels in the investigation can be part of a suggestion for future work. On the other hand, the results demonstrate the importance of generating more case study driven analyses to expand the knowledge that has been gained in the current work.

The setting of the collision simulations excluded the variation of certain parameters such as speed and collision angle. The speed of 5 knots was chosen as the speed of the striking ship because it has been established statistically to be the most common in collision incidents while the change of collision angle could increase the complexity of the calculation process. Furthermore, the struck ship was considered fixed in its position to avoid any external dynamic effect. The investigation of the influence of the above parameters as well as the motion of the struck ship in the damage extent after a collision will strengthen the applicability of the study.

The chosen corrosion model assumes that the annual corrosion rate is constant describing the corrosion wastage as a linear function of time. The need for a practical and simple way to predict the thickness reduction of the various structural members justifies the use of the model developed by Paik et al. (2003a). However, the non-linear dependence of corrosion rate has been established experimentally (Garbatov and Guedes Soares, 1999). The use of a non-linear corrosion model will be able to estimate more accurately the material loss leading to a better calculation of the ultimate strength.

The further investigation of corroded materials can be beneficial in identifying the necking point during tensile tests improving the representation of damage progression in the collision simulations. Moreover, a better knowledge of parameters such as strain rate effect and plastic hardening of corroded materials will contribute to correctly model their response in a simulated collision.

7 References

Babicz, Jan. 2015. *WÄRTSILÄ ENCYCLOPEDIA OF SHIP TECHNOLOGY*. *Wärtsilä Corporation*. https://doi.org/10.1007/978-1-4614-9610-6.

Bae, Dong Myung, Aditya Rio Prabowo, Bo Cao, Ahmad Fauzan Zakki, and Gunawan Dwi Haryadi. 2016. "Study on Collision between Two Ships Using Selected Parameters in Collision Simulation." *Journal of Marine Science and Application* 15 (1): 63–72. https://doi.org/10.1007/s11804-016-1341-2.

Bertin, Ricardo, João Abdalla Filho, and Roberto D. Machado. 2019. "Stress Analysis of Corrosion Pits Present on Curved and Plane Surfaces Considering Plasticity." In *Mecánica Computacional; Volume XXIX. Number 79. Computational Methods for the Analysis and Design of Offshore Systems and Structures (A); 7685-7697*.

Bhandari, Jyoti, Faisal Khan, Rouzbeh Abbassi, Vikram Garaniya, and Roberto Ojeda. 2015. "Modelling of Pitting Corrosion in Marine and Offshore Steel Structures – A Technical Review." *Journal of Loss Prevention in the Process Industries* 37 (September): 39–62. https://doi.org/10.1016/j.jlp.2015.06.008.

Boulougouris, Evangelos, and Apostolos Papanikolaou. 2013. "Risk-Based Design of Naval Combatants." *Ocean Engineering* 65 (June): 49–61. https://doi.org/10.1016/j.oceaneng.2013.02.014.

Caldwell JB. 1965. "Ultimate Longitudinal Strength." *Trans RINA*, no. 107: 411–430.

Campanile, A., V. Piscopo, and A. Scamardella. 2015. "Statistical Properties of Bulk Carrier Residual Strength." *Ocean Engineering* 106 (September): 47–67. https://doi.org/10.1016/j.oceaneng.2015.06.060.

Chen, Nian-Zhong. 2016. "Hull Girder Reliability Assessment for FPSOs." *Engineering Structures* 114 (May): 135–47. https://doi.org/10.1016/j.engstruct.2016.02.016.

Chen, Nian-Zhong, and C. Guedes Soares. 2008. "Ultimate Longitudinal Strength of Ship Hulls of Composite Materials." *Journal of Ship Research* 52 (3): 184–93.

Cicek, Volkan. 2017. *Corrosion Engineering and Cathodic Protection Handbook*. Hoboken, NJ, USA: John Wiley & Sons, Inc. https://doi.org/10.1002/9781119284338.

Daidola, J, J Parente, and I. Orisamolu. 1997. "Residual Strength Assessment of Pitted Plate Panels." *Report SSC-394, Ship Structure Committee*.

Dassault Systèmes. 2014. "Manual Abaqus 6.14." Documentation. 2014.

Ehlers, Sören. 2010. "The Influence of the Material Relation on the Accuracy of Collision Simulations." *Marine Structures* 23 (4): 462–74. https://doi.org/10.1016/j.marstruc.2010.12.002.

Fujikubo, Masahiko, Muhammad Zubair Muis Alie, Kentaro Takemura, Kazuhiro Iijima, and Saori Oka. 2013. "Residual Hull Girder Strength of Asymmetrically Damaged Ships." *Journal of the Japan Society of Naval Architects and Ocean Engineers* 16 (0): 131–40. https://doi.org/10.2534/jjasnaoe.16.131.

Garbatov, Y., and C. Guedes Soares. 2008. "Corrosion Wastage Modeling of Deteriorated Bulk Carrier Decks." *International Shipbuilding Progress* 55 (1–2): 109–25. https://doi.org/10.3233/ISP-2008-0041.

Garbatov, Y., C. Guedes Soares, J. Parunov, and J. Kodvanj. 2014. “Tensile Strength Assessment of Corroded Small Scale Specimens.” *Corrosion Science* 85 (August): 296–303. https://doi.org/10.1016/j.corsci.2014.04.031.

Gordo, J M, and C Guedes Soares. 1993. “Approximate Load Shortening Curves for Stiffened Plates Under Uniaxial Compression.” In *Proc. Integrity of Offshore Structures - 5*, 189–211. https://doi.org/10.13140/RG.2.1.3643.2801.

Guedes Soares, C. 1988. “Uncertainty Modelling in Plate Buckling.” *Structural Safety* 5 (1): 17–34. https://doi.org/10.1016/0167-4730(88)90003-3.

Guedes Soares, Carlos, and T.A. Santos. 2018. “Maritime Technology and Engineering III.” In *Maritime Technology and Engineering III*. https://doi.org/10.1201/9781315374956.

Haris, Sabril, and Jorgen Amdahl. 2013. “Analysis of Ship-Ship Collision Damage Accounting for Bow and Side Deformation Interaction.” *Marine Structures* 32: 18–48. https://doi.org/10.1016/j.marstruc.2013.02.002.

Hogström, Per, and Jonas W. Ringsberg. 2012. “An Extensive Study of a Ship’s Survivability after Collision - A Parameter Study of Material Characteristics, Non-Linear FEA and Damage Stability Analyses.” *Marine Structures* 27 (1): 1–28. https://doi.org/10.1016/j.marstruc.2012.03.001.

Hogström, Per, and Jonas W. Ringsberg. 2013. “Assessment of the Crashworthiness of a Selection of Innovative Ship Structures.” *Ocean Engineering* 59: 58–72. https://doi.org/10.1016/j.oceaneng.2012.12.024.

IACS. 2015. “IACS Recommendation 87 - Guidelines for Coating Maintenance & Repairs for Ballast Tanks and Combined Cargo/Ballast Tanks on Oil Tankers.”

IACS. 2019. “Common Structural Rules for Bulk Carriers and Oil Tankers.”

Incaz, Serap, and Pinar Özdemir. 2018. “International Convention On Civil Liability For Oil Pollution Damage (CLC), 1969 And Its Applications, Oil Spill Along The Turkish Straits Sea Area; Accidents, Environmental Pollution, Socio-Economic Impacts And Protection Edited By.” In , 416–23.

ISSC. 2015. “Report of Committee III.1: Ultimate Strength.” In *Ships and Offshore Structures XIX*, 279–349. CRC Press. https://doi.org/10.1201/b18898-6.

Karakasnaki, Maria, Periklis Vlachopoulos, Angelos Pantouvakis, and Nancy Bouranta. 2018. “ISM Code Implementation: An Investigation of Safety Issues in the Shipping Industry.” *WMU Journal of Maritime Affairs* 17 (3): 461–74. https://doi.org/10.1007/s13437-018-0153-4.

Karlsson, Ulf B. 2009. “Improved Collision Safety of Ships by an Intrusion-Tolerant Inner Side Shell.” *Marine Technology and SNAME News* 46 (3): 165–73.

Kee Paik, Jeom, Sung Kyu Kim, and Sang Kon Lee. 1998. “Probabilistic Corrosion Rate Estimation Model for Longitudinal Strength Members of Bulk Carriers.” *Ocean Engineering* 25 (10): 837–60. https://doi.org/10.1016/S0029-8018(97)10009-9.

Kitamura, O. 2002. “FEM Approach to the Simulation of Collision and Grounding Damage.” *Marine Structures*. https://doi.org/10.1016/S0951-8339(02)00010-2.

Kuznecovs, Artjoms, Jonas W. Ringsberg, Zhiyuan Li, and Erland Johnson. 2019. "Ultimate and Residual Strength Analyses of a Double-Hull Oil Tanker Subjected to Biaxial Bending – a Comparison between a Modified Smith-Fujikubo Method and Finite Element Analyses." *Ocean Engineering*.

Kuznecovs, Artjoms, and Roozbeh Shafieisabet. 2017. "Analysis of the Ultimate Limit State of Corroded Ships after Collision [MSc Thesis Report X-17/376]." Gothenburg: Department of Mechanics and Maritime Sciences,Chalmers University of Technology.

Lister, Jane. 2015. "Green Shipping: Governing Sustainable Maritime Transport." *Global Policy* 6 (2): 118–29. https://doi.org/10.1111/1758-5899.12180.

Liu, B., R. Villavicencio, S. Zhang, and C. Guedes Soares. 2017. "A Simple Criterion to Evaluate the Rupture of Materials in Ship Collision Simulations." *Marine Structures* 54: 92–111. https://doi.org/10.1016/j.marstruc.2017.03.006.

Mansour, Alaa; Liu, Donald. 2008. *Principles of Naval Architecture Series - Strength of Ships and Ocean Structures*. Jersey City, N.J: Society of Naval Architects and Marine Engineers.

Marinatos, J. N., and M. S. Samuelides. 2015. "Towards a Unified Methodology for the Simulation of Rupture in Collision and Grounding of Ships." *Marine Structures* 42: 1–32. https://doi.org/10.1016/j.marstruc.2015.02.006.

Melchers, R. E. 2010. "Pitting Corrosion of Mild Steel in Marine Immersion Environment—Part 1: Maximum Pit Depth." *Corrosion* 60 (9): 824–36. https://doi.org/10.5006/1.3287863.

Melchers, R. E., and R. J. Jeffrey. 2008. "Probabilistic Models for Steel Corrosion Loss and Pitting of Marine Infrastructure." *Reliability Engineering and System Safety* 93 (3): 423–32. https://doi.org/10.1016/j.ress.2006.12.006.

Melchers, Robert E. 1999. "Corrosion Uncertainty Modelling for Steel Structures." *Journal of Constructional Steel Research* 52 (1): 3–19. https://doi.org/10.1016/S0143-974X(99)00010-3.

Melchers, Robert E. 2003. "Probabilistic Models for Corrosion in Structural Reliability Assessment—Part 2: Models Based on Mechanics." *Journal of Offshore Mechanics and Arctic Engineering* 125 (4): 272. https://doi.org/10.1115/1.1600468.

Melchers, Robert E. 2008. "Development of New Applied Models for Steel Corrosion in Marine Applications Including Shipping." *Ships and Offshore Structures* 3 (2): 135–44. https://doi.org/10.1080/17445300701799851.

Melchers, Robert E. 2018. "Progress in Developing Realistic Corrosion Models." *Structure and Infrastructure Engineering* 14 (7): 843–53. https://doi.org/10.1080/15732479.2018.1436570.

Nakai, Tatsuro, Hisao Matsushita, Norio Yamamoto, and Hironori Arai. 2004. "Effect of Pitting Corrosion on Local Strength of Hold Frames of Bulk Carriers (1st Report)." *Marine Structures* 17 (5): 403–32. https://doi.org/10.1016/j.marstruc.2004.10.001.

Nieuwenhuijs, M W, J F Segretain, and P Baumans. 2006. "First Experience with Common Structural Rules for Bulk Carriers." In *Proceedings of the 17th Symposium on Theory and Practice of Shipbuilding in Memoriam Prof. Leopold Sorta (SORTA)*. Rijeka, Croatia.

Nishihara, Seiichiro. 1982. *Analysis of Ultimate Strength of Stiffened Rectangular Plate (2nd Report)*. *Journal of the Society of Naval Architects of Japan*. Vol. 1982. https://doi.org/10.2534/jjasnaoe1968.1982.157.

Ozguc, Ozgur, Purnendu K. Das, and Nigel Barltrop. 2005. "A Comparative Study on the Structural Integrity of Single and Double Side Skin Bulk Carriers under Collision Damage." *Marine Structures* 18 (7–8): 511–47. https://doi.org/10.1016/j.marstruc.2006.01.004.

Paik, J. K., J. M. Lee, and M. J. Ko. 2003b. "Ultimate Compressive Strength of Plate Elements with Pit Corrosion Wastage." *Proceedings of the Institution of Mechanical Engineers, Part M: Journal of Engineering for the Maritime Environment* 217 (4): 185–200. https://doi.org/10.1177/147509020321700402.

Paik, J. 2004. "Ultimate Shear Strength of Plate Elements with Pit Corrosion Wastage." *Thin-Walled Structures*, May. https://doi.org/10.1016/s0263-8231(04)00042-4.

Paik, Jeom K., Jae Myung Lee, Young Park, Joon Sung Hwang, and Chang Wook Kim. 2003a. "Time-Variant Ultimate Longitudinal Strength of Corroded Bulk Carriers." *Marine Structures* 16 (8): 567–600. https://doi.org/10.1016/j.marstruc.2004.01.003.

Paik, Jeom K., and Alaa E. Mansour. 1995. "A Simple Formulation for Predicting the Ultimate Strength of Ships." *Journal of Marine Science and Technology* 1 (1): 52–62. https://doi.org/10.1007/BF01240013.

Paik, Jeom Kee, Jang Young Chung, I H Choe, A K Thayamballi, and Preben Terndrup Pedersen. 1999. *On the Rational Design of Double Hull Tanker Structures Against Collision*. *HHI Engineering Review*. Vol. 25.

Paik, Jeom Kee, and Do Kyun Kim. 2012. "Advanced Method for the Development of an Empirical Model to Predict Time-Dependent Corrosion Wastage." *Corrosion Science* 63: 51–58. https://doi.org/10.1016/j.corsci.2012.05.015.

Paik, Jeom Kee, and Robert E. Melchers. 2008. *Condition Assessment of Aged Structures*. *Condition Assessment of Aged Structures*. https://doi.org/10.1533/9781845695217.

Paik, Jeom Kee, Anil K. Thayamballi, and Soo Hong Yang. 1998. "Residual Strength Assessment of Ships after Collision and Grounding." *Marine Technology and SNAME News* 35 (1): 38–54.

Peng, Yue, Master of Science, and Maritime Affairs. 2011. "An Analysis of the Implementation and Future Development of Imo Goal-Based Standards." World Maritime University.

Qin, Shengping, and Weicheng Cui. 2003. "Effect of Corrosion Models on the Time-Dependent Reliability of Steel Plated Elements." *Marine Structures* 16 (1): 15–34. https://doi.org/10.1016/S0951-8339(02)00028-X.

Ringsberg, Jonas W. 2011. "Characteristics of Material, Ship Side Structure Response and Ship Survivability in Ship Collisions." *Ships and Offshore Structures* 6 (1–2): 5. https://doi.org/10.1080/17445302.2011.553090.

Ringsberg, Jonas W., Zhiyuan Li, Erland Johnson, Artjoms Kuznecovs, and Roozbeh Shafieisabet. 2018. "Reduction in Ultimate Strength Capacity of Corroded Ships Involved in Collision Accidents." *Ships and Offshore Structures* 13: 155–66. https://doi.org/10.1080/17445302.2018.1429158.

Smith, C. S. 1977. “Influence of Local Compressive Failure on Ultimate Longitudinal Strength of a Ship’s Hull.” *Proceedings of the 1st International Symposium on Practical Design of Ships and Other Floating Structures* P: 73–79.

Soares, Guedes, and Y. Garbatov. 1999. “Reliability of Maintained, Corrosion Protected Plates Subjected to Non-Linear Corrosion and Compressive Loads.” *Marine Structures* 12 (6): 425–45. https://doi.org/10.1016/S0951-8339(99)00028-3.

Southwell, C.R., C.W. Hummer, and A.L. Alexander. 1965. “Corrosion of Metals in Tropical Environments- Aluminum and Magnesium.” *Materials Protection*.

Storheim, Martin, Jørgen Amdahl, and Ingo Martens. 2015. “On the Accuracy of Fracture Estimation in Collision Analysis of Ship and Offshore Structures.” *Marine Structures* 44: 254–87. https://doi.org/10.1016/j.marstruc.2015.09.006.

Tanaka, Yoshiteru, Hiroaki Ogawa, Akira Tatsumi, and Masahiko Fujikubo. 2015. “Analysis Method of Ultimate Hull Girder Strength under Combined Loads.” *Ships and Offshore Structures* 10 (5): 587–98. https://doi.org/10.1080/17445302.2015.1045271.

Tscheliesnig, Peter. 2006. “Acoustic Emission Testing (AT) for the Detection of Corrosion Attack on Ships (Oil Tankers).” *TÜV Austria*.

Uğurlu, Özkan, Ercan Köse, Umut Yıldırım, and Ercan Yüksekyıldız. 2015. “Marine Accident Analysis for Collision and Grounding in Oil Tanker Using FTA Method.” *Maritime Policy and Management* 42 (2): 163–85. https://doi.org/10.1080/03088839.2013.856524.

UN. 2016. “Sustainable Development Goals: Exploring Maritime Opportunities.” DNV GL AS.

Wang, Ge, Yongjun Chen, Hanqing Zhang, and Hua Peng. 2002. “Longitudinal Strength of Ships with Accidental Damages.” *Marine Structures* 15 (2): 119–38. https://doi.org/10.1016/S0951-8339(01)00018-1.

Wang, Ge, Ai Kuo Lee, Lyuben Ivanov, Thomas J. Lynch, Chris Serratella, and Roger Basu. 2008a. “A Statistical Investigation of Time-Variant Hull Girder Strength of Aging Ships and Coating Life.” *Marine Structures* 21 (2–3): 240–56. https://doi.org/10.1016/j.marstruc.2007.10.002.

Wang, Yan-Wu, Yi-Fei Wang, Xiao-Ping Huang, and Wei-Cheng Cui. 2008b. *Simplified Maximum Pit Depth Model of Mild and Low Alloy Steels in Marine Immersion Environments*. *Chuan Bo Li Xue/Journal of Ship Mechanics*. Vol. 12.

Wang, Yikun, Julian A. Wharton, and R. Ajit Shenoi. 2014. “Ultimate Strength Analysis of Aged Steel-Plated Structures Exposed to Marine Corrosion Damage: A Review.” *Corrosion Science* 86: 42–60. https://doi.org/10.1016/j.corsci.2014.04.043.

Yamamoto, N., and K. Ikegami. 1998. “A Study on the Degradation of Coating and Corrosion of Ship’s Hull Based on the Probabilistic Approach.” *Journal of Offshore Mechanics and Arctic Engineering* 120 (3): 121. https://doi.org/10.1115/1.2829532.

Yang, Hong Qi, Qi Zhang, San Shan Tu, You Wang, Yi Min Li, and Yi Huang. 2016. “A Study on Time-Variant Corrosion Model for Immersed Steel Plate Elements Considering the Effect of Mechanical Stress.” *Ocean Engineering* 125: 134–46. https://doi.org/10.1016/j.oceaneng.2016.08.005.

Yao, Tetsuya. 1999. “Ultimate Longitudinal Strength of Ship Hull Girder: Historical Review and State of the Art.” *International Journal of Offshore and Polar Engineering* 9 (1): 1–9.

Yao, Tetsuya. 2003. “Hull Girder Strength.” *Marine Structures* 16 (1): 1–13. https://doi.org/10.1016/S0951-8339(02)00052-7.

Youssef, S. A.M., Y. S. Kim, J. K. Paik, F. Cheng, and M. S. Kim. 2014. “Hazard Identification and Probabilistic Scenario Selection for Ship-Ship? Collision Accidents.” *Transactions of the Royal Institution of Naval Architects Part A: International Journal of Maritime Engineering* 156 (PART A1): 61–80. https://doi.org/10.3940/rina.ijme.2014.al.277.

Yuan, X. X., D. Mao, and M. D. Pandey. 2009. “A Bayesian Approach to Modeling and Predicting Pitting Flaws in Steam Generator Tubes.” *Reliability Engineering and System Safety* 94 (11): 1838–47. https://doi.org/10.1016/j.ress.2009.06.001.

Zhang, Shengming, and Preben Terndrup Pedersen. 2017. “A Method for Ship Collision Damage and Energy Absorption Analysis and Its Validation.” *Ships and Offshore Structures* 12: S11–20. https://doi.org/10.1080/17445302.2016.1254584.

Zheng, Shuqi, Yameng Qi, Changfeng Chen, and Shengyi Li. 2012. “Effect of Hydrogen and Inclusions on the Tensile Properties and Fracture Behaviour of A350LF2 Steels after Exposure to Wet H 2S Environments.” *Corrosion Science* 60: 59–68. https://doi.org/10.1016/j.corsci.2012.04.012.